



HAL
open science

Light-seeking navigation in zebrafish larva : from behavior to neural circuits

Sophia Karpenko

► **To cite this version:**

Sophia Karpenko. Light-seeking navigation in zebrafish larva : from behavior to neural circuits. *Neurons and Cognition [q-bio.NC]*. Université Paris sciences et lettres, 2020. English. NNT : 2020UP-SLT019 . tel-03810431

HAL Id: tel-03810431

<https://theses.hal.science/tel-03810431>

Submitted on 11 Oct 2022

HAL is a multi-disciplinary open access archive for the deposit and dissemination of scientific research documents, whether they are published or not. The documents may come from teaching and research institutions in France or abroad, or from public or private research centers.

L'archive ouverte pluridisciplinaire **HAL**, est destinée au dépôt et à la diffusion de documents scientifiques de niveau recherche, publiés ou non, émanant des établissements d'enseignement et de recherche français ou étrangers, des laboratoires publics ou privés.



THÈSE DE DOCTORAT
DE L'UNIVERSITÉ PSL

Préparée à Paris Sciences et Lettres,
Laboratoire Jean Perrin, CNRS-Sorbonne Université

**Naviguer avec la lumière :
du comportement aux circuits neuronaux chez la larve de
poisson zèbre**

Soutenue par

Sophia KARPENKO

Le 11 décembre 2020

École doctorale n°474

**Frontières de l'innovation
en recherche et éducation**

Spécialité

Frontières du vivant

Composition du jury :

Laurent BOURDIEU IBENS, ENS-CNRS	<i>Président</i>
Elena DREOSTI University College London	<i>Rapportrice</i>
Philippe VERNIER Université Paris-Saclay, CNRS	<i>Rapporteur</i>
Elim HONG IBPS, Sorbonne Université, INSERM	<i>Examinatrice</i>
Antoine WYSTRACH Université de Toulouse, CNRS	<i>Examineur</i>
Georges DEBREGÉAS Sorbonne Université-CNRS	<i>Directeur de thèse</i>

Acknowledgements

Merci à Georges de m'avoir tant appris et donné liberté, confiance et soutien pour grandir pendant ces années.

Merci aux poissons et autres membres (d'hier et d'aujourd'hui) du Laboratoire Jean Perrin et de l'IBPS. Sous cette bannière, en particulier :

Merci à Geoffrey. Merci à Guillaume, à Julie, à Thomas. Merci à Hugo, Nicolas, Maryam, Benjamin, Sharbat, Natalia, Hippolyte, Tom, Ghislaine, Volker et Raphaël.

Merci à Marie-Nicole, Malika et Anissa pour leur appui et leur bienveillance. Merci à Stéphane et à Alex de rendre possible toutes nos manips sur le *zebra*.

Merci aussi à Didier, pour ses encouragements permanents.

Merci à mes ami·e·s non-cité·e·s par discrétion, pour les moments d'évasion et les distractions nécessaires.

Merci à mes ancien·ne·s et actuel·le·s coloc·s de m'avoir et de continuer à me supporter.

Merci à dzɔ:

Полине - *check*. И, конечно же, огромное спасибо Маме и Папе - за всё.

She was getting a little giddy with so much floating in the air,
and was rather glad
to find herself walking again in the natural way. ¹

¹*Through the looking glass*, L. Carroll.

Light-seeking navigation in zebrafish larvae: from
behavior to neural circuits

Sophia Karpenko

2020

Contents

Résumé en langue française	ii
Chapitre 1 : Introduction générale	ii
Chapitre 2 : La larve de poisson-zèbre comme organisme modèle en neuro- sciences	iii
Chapitre 3 : Réorientation vers la lumière, en nage libre	iv
Chapitre 4 : Réorientation virtuelle vers la lumière	v
Chapitre 5 : Circuits neuronaux responsables de la réorientation vers la lumière	vi
Chapitre 6 : Discussion	vi
1 Introduction	2
1.1 Navigating the environment	2
1.1.1 A navigational toolbox	2
1.1.2 Describing sensory-guided navigation	5
1.2 From single-cell to systems neuroscience	7
1.2.1 The Neuron Doctrine	8
1.2.2 Emergent properties from neural networks	8
1.2.3 Tackling the complexity of an information-processing system	9
1.3 Virtual reality systems to understand behavior	10
1.3.1 Human cognitive neurosciences explored by VR	10
1.3.2 In model animals	11
2 The zebrafish larva: a model in systems neurosciences	16
2.1 A model animal in systems neuroscience	16
2.2 Locomotor repertoire description	17
2.3 Visually guided behaviors	19
2.3.1 Visual ecology	19
2.3.2 Eye movements	19
2.3.3 Diversity of visually guided behaviors	21
2.4 Functional anatomy of the visual system of larval zebrafish	22
2.4.1 Eyes structure	22
2.4.2 Downstream: ganglion cell projections	26

3	Freely swimming light-seeking reorientation	28
3.1	Light-seeking behavior in zebrafish: state of the art	28
3.1.1	Light adaptation	29
3.1.2	Tropo-phototaxis	30
3.1.3	Temporal phototaxis or klino-phototaxis	31
3.2	Navigation dynamics of zebrafish larva under a light gradient	33
3.2.1	Spontaneous navigation	33
3.2.2	Orientalional light-seeking behavior	35
3.3	Article: From behavior to circuit modeling of light-seeking navigation in zebrafish larvae	39
4	Interlude: Head-fixed virtual orientation of zebrafish larva to a light source	40
4.1	Spontaneous dynamics	40
4.1.1	Methods: monitoring of head-fixed dynamics	40
4.1.2	Results	43
4.2	Virtual orientation towards light	44
4.2.1	Gaze orientation bias	44
4.2.2	Methods: closed-loop with feedback on tail-bouts	46
4.2.3	Results	46
4.3	Discussion	50
5	Neural circuit underlying orientational phototaxis	52
5.1	Light-sheet imaging with visual stimulation	52
5.1.1	Fluorescence Calcium imaging	52
5.1.2	2P Light-sheet imaging	56
5.1.3	2P Light-sheet imaging in zebrafish	57
5.2	Neuronal correlates of zebrafish larva phototaxis	59
5.2.1	The saccadic circuit	59
5.2.2	Global responses to stereovisual contrast	61
5.2.3	Responses of the ARTR to illumination changes	65
5.3	Virtual phototaxis under a microscope	68
5.3.1	Methods	70
5.3.2	Results	70
6	Conclusions and perspectives	79
6.1	Zebrafish and light	79
6.2	Structures implicated in zebrafish light-seeking behavior	81
6.3	Outlooks in neuroscience	82
	Bibliography	84

Résumé en langue française

Pour leur survie et leur développement, les organismes motiles (les animaux, entre autres) échantillonnent les signaux sensoriels présents dans leur milieu pour naviguer vers des environnements plus favorables, c'est-à-dire où ils sont susceptibles d'éviter les prédateurs, trouver de la nourriture ou rencontrer des partenaires. Comprendre la relation entre un comportement à l'échelle de l'organisme - en l'occurrence la navigation - et la dynamique sous-jacente des circuits de neurones à l'échelle du cerveau chez les vertébrés est un défi central dans les neurosciences, auquel ce travail vise à contribuer.

Chapitre 1 : Introduction générale

Dans un premier chapitre introductif je développe quelques questions qui se posent dans les neurosciences actuelles et l'approche que nous prenons, dans notre équipe, pour y répondre.

La navigation exige, en effet, que perception sensorielle et action motrice soient coordonnées au sein d'une même boucle de rétroaction, appelée boucle sensorimotrice. Cette boucle sensorimotrice est formalisée comme étant le mécanisme de base de la navigation, présent chez un grand nombre d'organismes (des unicellulaires aux vertébrés), impliquant des sens comme la vision, l'audition, l'olfaction, la proprioception, etc. et générant des comportements assez divers, comme l'approche et l'évitement, l'interaction sociale ou la reproduction.

En particulier, il peut être intéressant d'essayer de comprendre la navigation d'un organisme par rapport à un stimulus en particulier. Les comportements de taxie et de kinésie en sont des exemples : la taxie consiste en une orientation directe de l'organisme vers la source du stimulus qui l'intéresse, alors que la kinésie est un mouvement biaisé par la concentration du stimulus, mais sans que l'organisme en infère directement l'orientation. Les deux stratégies résultent en des trajectoires biaisées vers la source du stimulus.

La question du sujet d'étude étant posée, j'essaye ensuite de mettre en perspective la façon dont on peut l'aborder. Une approche pertinente me semble être celle proposée par les neurosciences des systèmes, qui envisagent le cerveau non pas comme une col-

lection d'activités de neurones individuels, mais comme un système avec des propriétés émergentes, c'est-à-dire, un système dans lequel "le tout est plus que la somme de ses parties". De ce point de vue, il est important d'essayer d'étudier le fonctionnement du système, ici le cerveau, dans son entièreté de façon la plus naturaliste possible.

Une façon d'étudier une boucle sensorimotrice dans son ensemble, tout en étant capable de contrôler un maximum les stimuli que reçoit le sujet, est de recourir à la réalité virtuelle. La réalité virtuelle est une technique de simulation d'un environnement interactif dans lequel le sujet peut être immergé, recréant ainsi virtuellement une boucle sensorimotrice. Cette technique a permis d'effectuer des recherches autour des questions de la représentation de l'espace, l'intégration de stimuli multiples ou la gestion d'interactions sociales chez l'humain, et aussi chez nombre d'organismes modèles (le rat, la souris, la drosophile, le poisson-zèbre). Un des avantages de la réalité virtuelle, c'est la possibilité pour le sujet de rester immobile tout en ayant l'illusion de se mouvoir, grâce à un retour visuel et/ou proprioceptif.

Chapitre 2 : La larve de poisson-zèbre comme organisme modèle en neurosciences

Dans un second chapitre introductif, je présente l'organisme modèle auquel nous nous intéressons : la larve de poisson zèbre. Ayant une accessibilité unique pour l'imagerie fonctionnelle à l'échelle du cerveau entier ainsi qu'une large palette de comportements innés, c'est un organisme idéal pour étudier une boucle sensorimotrice.

Et en effet, depuis les quelques années que la larve de poisson-zèbre s'est établie comme un organisme modèle en neurosciences, des mutants et des lignées transgéniques ont été développés afin de rendre le poisson-zèbre encore plus transparent et d'obtenir une expression de rapporteurs calciques dans leurs neurones. Ces rapporteurs calciques sont des molécules qui fluorescent au contact du calcium, dont la concentration augmente fortement lorsque les cellules sont actives, rendant ainsi possible l'observation *in vivo* par imagerie optique de l'activité neuronale à l'échelle du cerveau entier, avec une résolution au neurone unique.

La boucle sensorimotrice choisie, en l'occurrence, est la navigation guidée par la lumière - aussi appelée phototaxie. Celle-ci permet à la larve de poisson-zèbre de naviguer vers et de rester dans les zones illuminées - là où se trouvent des algues unicellulaires photosynthétiques dont elle se nourrit. Ce comportement est permis par le système visuel de l'animal, développé dès 3 jours après fertilisation, notamment via les cônes sensibles à la lumière bleue.

Chapitre 3 : Réorientation vers la lumière, en nage libre

Le troisième chapitre de ce manuscrit est majoritairement consacré aux travaux que nous avons publiés dans cet article.

Afin de décrire comment un stimulus extérieur (ici la lumière) peut biaiser une boucle sensorimotrice qui a sa dynamique propre, nous nous sommes d’abord attachés à décrire la dynamique de nage spontanée de la larve de poisson-zèbre, en l’absence d’une source de lumière fluctuante. Puis, en considérant la lumière comme un perturbateur qui aurait tendance à biaiser la nage dans une direction, nous voulions voir quel effet elle aurait sur la nage spontanée.

Description de la nage spontanée. Sous des conditions d’illumination stable et uniforme, la nage spontanée de la larve de poisson-zèbre est saccadée : elle effectue des mouvements de queue discrets, à une fréquence d’une fois par seconde, qui la propulsent soit vers l’avant, soit la font tourner (à droite ou à gauche). A chaque mouvement, elle a donc le choix soit d’aller vers l’avant, soit de tourner, avec une probabilité de 0.5 pour chacune des options. Ce choix peut être modélisé par une chaîne de Markov à deux états - “tourner” et “aller tout droit”. Les mouvements de réorientation successifs ont tendance à être orientés dans la même direction : lorsque le mouvement précédent était orienté vers la gauche, le mouvement suivant, s’il est réorientationnel, aura une probabilité de 0.8 d’être dans le même sens. Ce deuxième choix peut donc également être modélisé par une chaîne de Markov, avec un état “gauche” et un état “droite”, avec une probabilité de transition entre les deux états de 0.2.

Nage en présence d’un gradient lumineux. En condition de variation lumineuse, on sait que la larve de poisson-zèbre est capable de distinguer la direction d’un gradient lumineux en comparant l’intensité lumineuse reçue sur chacun de ses deux yeux. En revanche, il n’était pas certain qu’elle soit capable d’intégrer les changements d’intensité globaux au cours du temps, et ainsi inférer la direction dans laquelle se trouve la source lumineuse sans information spatiale instantanée.

Nous voulions donc caractériser la réponse du poisson-zèbre à des changements lumineux soit de contraste soit de lumière globale, avec des variations faibles et lisses d’intensité lumineuse. Ceci a été réalisé en utilisant une expérience de réalité virtuelle où le stimulus est uniquement fonction de l’orientation du poisson par rapport à une source lumineuse virtuelle.

Dans des conditions où un contraste est imposé à l’animal, la probabilité de transition entre états “gauche” et “droite” est impactée : lorsqu’un contraste est dirigé vers la gauche (intensité gauche > intensité droite) et que le mouvement précédent était vers la gauche, cette probabilité de transition est diminuée, au contraire si le mouvement précédent était vers la droite, elle est réduite, favorisant légèrement le côté le plus lumineux et permettant à l’animal de se réorienter en moyenne pour rééquilibrer le

contraste sur ses deux yeux.

Dans une situation où l'information spatiale directe est absente, mais que l'intensité lumineuse globale change au cours du temps, c'est la probabilité d'effectuer un mouvement de réorientation (versus un mouvement vers l'avant) qui est impactée : plus l'animal a subi une grande décroissance lumineuse lors de son mouvement précédent, plus le mouvement suivant aura de chances d'être un mouvement de réorientation, qui plus est de large amplitude. Il semblerait donc que l'animal n'intègre pas les variations lumineuses dans le temps (au-delà du battement précédent), mais que cette stratégie lui permette tout de même de trouver les zones plus illuminées.

Les informations lumineuses spatiale et temporelle agissent donc de concert sur deux paramètres différents régissant la nage spontanée de la larve du poisson-zèbre.

Chapitre 4 : Réorientation virtuelle vers la lumière

Dans un quatrième chapitre, il s'agit de faire la transition entre la nage libre et la possibilité d'observer les processus en jeu au niveau neuronal. Il s'agissait de voir s'il était possible d'observer les mêmes dynamiques comportementales chez un animal partiellement immobilisé (figé dans une goutte de gel d'agarose, avec les yeux et la queue libérés).

Nous avons pu montrer, que malgré une grande diminution de la fréquence de battements de queue (de 1Hz on passe à 0.03Hz), une bonne partie des caractéristiques de nage peuvent être retrouvées. En effet, la deflection de la queue étant une mesure indirecte de la réorientation réelle qu'aurait eu le poisson en nage libre, il est possible de recréer une trajectoire angulaire virtuelle en observant la dynamique des battements de queue. Leur distribution apparait bimodale (ainsi que l'est la distribution des angles de réorientation en nage libre), et la corrélation entre directions de mouvements de réorientation successifs apparaît également, bien qu'atténuée par la plus faible fréquence d'événements de nage.

Il nous a également été possible de laisser naviguer la larve avec une source lumineuse virtuelle, de façon à reproduire les expériences du chapitre 3 mais chez l'animal fixe, en rétroagissant en boucle fermée sur les mouvements de queue de l'animal pour réajuster l'orientation de la source virtuelle par rapport à l'animal. Nous avons pu montrer que l'animal est capable de se réorienter pour faire face à une source lumineuse virtuelle en comparant le contraste reçu sur son oeil gauche et son oeil droit, et également augmenter la probabilité d'effectuer un mouvement de nage de réorientation ainsi que son amplitude, s'il a subi une décroissance lumineuse au mouvement précédent. Les deux stratégies de recherche de zones illuminées présentées dans le chapitre précédent sont donc reproductibles - à quelques éléments près - chez un animal maintenu par l'abdomen.

Chapitre 5 : Circuits neuronaux responsables de la réorientation vers la lumière

La dernière partie du projet se concentre sur le circuit neuronal qui sous-tend le comportement de phototaxie.

Je me suis spécifiquement penchée sur un circuit nommé ARTR (pour Anterior Rhombencephalic Turning Region), connu pour être impliqué dans la sélection de l'orientation à chaque mouvement de nage. Par ailleurs, ce circuit présente des dynamiques spontanées oscillatoires : les deux paires de noyaux symétriques ont une activité anti-phasique (lorsque le côté gauche est actif, le côté droit ne l'est pas et l'animal aura tendance à faire un mouvement vers la gauche). Cette dynamique interne peut être biaisée par une source lumineuse: un flash lumineux du côté gauche (droit), alors que l'animal est passif, entraîne une augmentation de l'activité du côté gauche (droit, respectivement) du réseau.

J'ai utilisé la technique développée dans le chapitre précédent en combinaison avec un microscope à feuille de lumière 2 photons, pour interroger expérimentalement l'ARTR en laissant la possibilité à la larve de poisson-zèbre de bouger ses yeux et sa queue. Pour maximiser la réponse et en simplifier l'interprétation, les stimuli visuels présentés étaient simples : des grands changements de contraste dans une direction aléatoire, délivrés au moment d'un mouvement de queue. Les deux résultats principaux observés ont été que (i) l'activité de l'ARTR est renforcée lors d'un mouvement de queue, et de façon asymétrique lors d'un mouvement de réorientation (le côté gauche est renforcé lorsque le mouvement est vers la gauche), ce qui indique un mécanisme de copie efferente. Et (ii) la réponse à un changement de contraste qui a lieu lorsque l'animal est passif est absente lorsque ce changement a lieu lors d'un mouvement propre de l'animal. Ceci semble indiquer qu'il y aurait un mécanisme de suppression ou d'inhibition des entrées visuelles lors d'un mouvement propre. Ce mécanisme peut être expliqué par un modèle de contrôle moteur, où la copie efferente permet de prédire les conséquences d'un mouvement moteur volontaire, et si la prédiction correspond au retour sensoriel, l'effet du mouvement volontaire est annulé.

Chapitre 6 : Discussion

Dans le travail présenté dans ce manuscrit, nous avons pu mettre en évidence une boucle sensorimotrice simple : la navigation de la larve de poisson-zèbre, qui est autonome en soi, mais qui peut également être biaisée par un stimulus lumineux. Nous l'avons décrite avec un modèle simple à deux chaînes de Markov, chacune régissant le basculement entre les états "aller vers l'avant" ou "tourner", ainsi que "gauche" et "droite". Les probabilités de transition au sein des deux chaînes peuvent être modulées par des variations temporelles ou spatiales de la lumière. Comme ce comportement s'est avéré observable chez un animal partiellement immobilisé, nous avons pu com-

mencer à étudier la dynamique des réseaux neuronaux sous-jacents en boucle fermée, en observant comportement et activité neuronale en même temps. Ceci nous a permis de mettre en lumière des mécanismes rappelant la copie efferente et la suppression sensorielle, en accord avec les modèles de contrôle moteur.

Nous avons fait en sorte d'observer des réponses à des changements lumineux faibles, car les changements abrupts pourraient provoquer des comportements de fuite impliquant des réseaux neuronaux distincts qui court-circuitent le mode "exploratoire" que l'on peut observer en nage spontanée et phototactique.

Le circuit sur lequel nous nous sommes penchés semble central dans la boucle sensorimotrice considérée, car ayant une dynamique spontanée mais répondant également à la lumière. Mais cette région fait évidemment partie d'un circuit plus large, avec, sans doute, une région d'intégration multisensorielle en amont, et une région en aval qui serait un générateur de mouvements de queue.

Je termine ce manuscrit par une ouverture sur l'évolution actuelle du domaine des neurosciences. La métaphore actuelle utilisée pour décrire le fonctionnement d'un cerveau est celle de l'ordinateur : la métaphore computationnelle. Mais il se pourrait que cette métaphore ne soit pas adaptée pour en saisir la complexité : peut-être ne résout-il pas de problèmes et n'implémente-t-il pas des fonctions, mais a une toute autre façon de représenter son environnement, générer des prédictions et des comportements. Toute la problématique me semble aujourd'hui être là : trouver une métaphore et un cadre théorique adéquats pour la description de ce système, et trouver les liens entre l'échelle macroscopique (le comportement) et l'échelle microscopique (l'activité de neurones) du cerveau.

Chapter 1

Introduction

“Oh my ears and whiskers, how late it’s getting!”

The White Rabbit.¹

1.1 Navigating the environment

The ability to navigate their environment is one of the defining features of animals (with few exceptions). It is through navigation that animals exploit their milieu for foraging and explore their surroundings to find mates or a new habitat. This ability to navigate is thus indispensable for their survival.

Navigational tasks are performed by animals in a huge variety of environments over various spatial and temporal scales. A migrating bird, the homing honeybee, the transporting dung beetle or the running *E. coli* travel distances differing by several orders of magnitude (even relatively to their body size), for different lengths of time, and various purposes.

How, despite the complexity of the surrounding world, animals manage to find their way to survive and thrive is an engaging question.

1.1.1 A navigational toolbox

The process an animal implements to solve a navigational problem may be decomposed as follows (see figure 1.1): (1) sample available external cues using its sensors, (2) integrate them with respect to its internal state, and (3) trigger an adequate motor response. These steps form a sensorimotor loop - as each motor response brings about potentially new cues and/or updates the internal state. In this conception of a sensorimotor loop, the agent is embodied and situated within its environment, which puts two

¹*Alice’s Adventures in Wonderland*, L. Carroll.

main physical constraints on the system: the non-randomness of perceived information sequences (*information self-structuring*) and the continuity of the environment (teleportation is not possible). This idea of embodiment has recently been developed in the field of robotics, in order to build bio-inspired adaptive and autonomous machines (Lungarella & Sporns, 2005; Pfeifer et al., 2007).

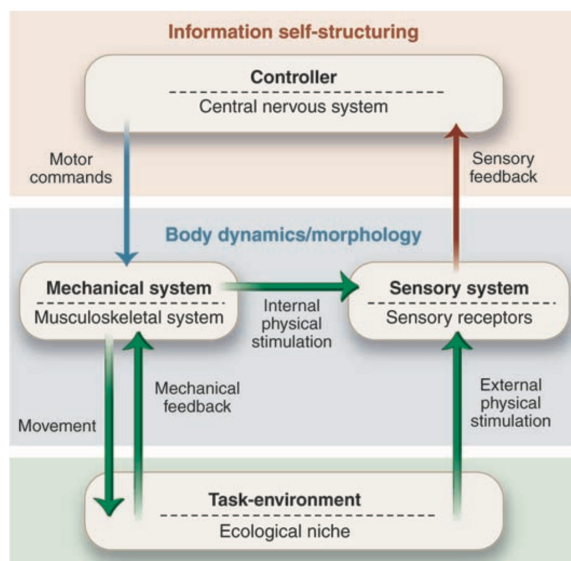


Figure 1.1: The sensorimotor loop from Pfeifer et al. (2007)

In many cases, it is known which cues are relevant for specific tasks animals perform: some birds sense or even see the earth’s magnetic field to migrate long distances (Heyers et al., 2007; Mouritsen, 2018; Wiltschko & Wiltschko, 2019), honeybees use landmarks to return home (Pahl et al., 2011), dung beetles follow the milky way at night to move away from the dung pile (Dacke et al., 2013), *E. coli* climb sugar gradients to find food. As a single cue type does not encompass the whole world, other cues may play a role to form a complete representation of the surroundings: birds also use olfaction during their flight, bees perform path integration from visual motion accumulation, dung beetle also check the moonlight to orient and *E. coli* is repelled by alcohol. Crucial or vital stimuli might override less important ones, some might act in synergy, others cancel themselves out.

Given the variety of environments as well as the diversity of sensory cues used for navigation, it seems *a priori* unlikely that animals rely on a unique, universal behavioral strategy for these navigation tasks. Nevertheless, as noted by Wiener et al. (2010), in their synthesis on animal navigation,

Some fundamental processes may have been conserved by evolution, and others may have evolved convergently in different taxa [...]. Evidence [...] suggests that the more complex and recent processes are, in many (if not

all) cases, synthesized from the older and simpler processes.

Wiener et al. (2010)

In that scope, studying “simple” forms of navigation might be key to gain insight into fundamental processes, not only to understand the mechanism itself - how it is implemented and hardwired in a given organism - but also to include it within a more general comparative or even evolutionary approach.

Apart from cue-combination, another layer of complexity may be added to the cognitive system itself. This has been formalized by the “Navigation toolbox” from Wiener et al. (2010): behavioural complexity grows with the ability of a cognitive system to represent maps (figure 1.2).

Level	Level 1 Sensorimotor toolbox	Level 2 Spatial primitives	Level 3 Spatial constructs	Level 4 Spatial symbols (uniquely human)
Elements	Vision Audition Olfaction Touch Kinaesthetic Proprioception Magnetic cues Thermoreception ...	Landmarks Terrain slope Compass heading Local heading Panorama Boundaries Posture Speed Acceleration ...	Cognitive Map Self localization Goal localization Frames of reference	External maps Wayfinding signage Human language
		Contextual Information (e.g., motivations, odor)		
	▼	▼	▼	▼
Behaviour supported	e.g. Taxes, Kineses	e.g. View-matching Beacon navigation	e.g. Cogn. mapping Path planning	Communicating spatial information

Figure 1.2: The navigation toolbox from Wiener et al. (2010)

With the hope of breaking down the process to its essential elements, in this work, the spotlight will be drawn on Level 1 *the sensorimotor toolbox*, presented as the most basic level of navigation. Despite its simplicity the sensorimotor loop supports a wide range of behaviours “such as approach and avoidance(...), mating, predator avoidance, tool use, or social interaction” (Wiener et al., 2010). Particularly of interest for the following work are taxes and kineses, which are innate locomotor responses to a given stimulus (phototaxis for light, chemotaxis for an odour...) resulting in approach or avoidance responses.

Chemotaxis has been extensively studied, especially in bacteria (Adler & Tso, 1974; Berg & Brown, 1972; Celani & Vergassola, 2010; Macnab & Koshland, 1972; Mello & Tu, 2007; Yuan et al., 2010), more recently in multicellulars like *C. elegans* or drosophila larva, but is also displayed by amoeba or single cells of multicellular organisms. An even broader variety of organisms display phototaxis: archaeobacteria, uni- and pluri-cellular algae, amoebzoa, animals like platynereis, drosophila larva or zebrafish larva. In fact, this behaviour seems to have such an evolutionary advantage, that phototaxis alone has evolved independently 8 times in eukaryotes (Jékely, 2009). This evolutionary diversity implies also a strategic diversity: all organisms do not perform phototaxis in the same fashion (they have different receptors, different trajectory shapes,..), and makes it all the more interesting to observe convergences.

1.1.2 Describing sensory-guided navigation

Taxes and kinesis differ from one another by the direction of short-term movements with respect to the source or gradient.

The authors of *The Orientation of Animals* (Fraenkel & Gunn, 1961), summarised it as follows:

“The term **taxis** is today used for **directed orientation** reactions. (...) **We use the word only for reactions in which the movement is straight towards or away from the source of stimulation.** (...) Undirected locomotory reactions, in which the speed of movement or the frequency of turning depend on the intensity of stimulation, we call **kinesis.**” “Thus, positive and negative phototaxis mean respectively movement **straight towards** or **straight away** from the light.”

The Orientation of Animals, (Fraenkel & Gunn, 1961).

Within taxes, it is possible to distinguish two categories, now based on stimulus sampling: klinotaxis and tropotaxis. These two behaviours can be segregated either by receptor type, or more accurately by the involved gradient-sensing strategy, summarised in figure 1.3, borrowed from Gomez-Marin & Louis (2012). Tropotaxis involves a simultaneous comparison of stimulus intensity, requiring two spatially segregated receptors; whereas klinotaxis is a temporal comparison which can be performed using one single sensor (but not necessarily), but requires some basic form of memory.

In summary, the distinction between taxis and kinesis is based on the gradient climbing strategy: if the movement is directed towards the stimulus, parallel to the gradient - it is a taxis; if the movement is undirected but its speed (ortho-) or rate of turning (klino-), like *E. coli*, varies with stimulus intensity - it is a kinesis. Within a taxis, the difference is based on the sampling strategy: an instantaneous spatial comparison using at least two distinct receptors of the same type is termed tropotaxis, whereas a comparison of the stimulus intensity at two different time points is called klinotaxis.

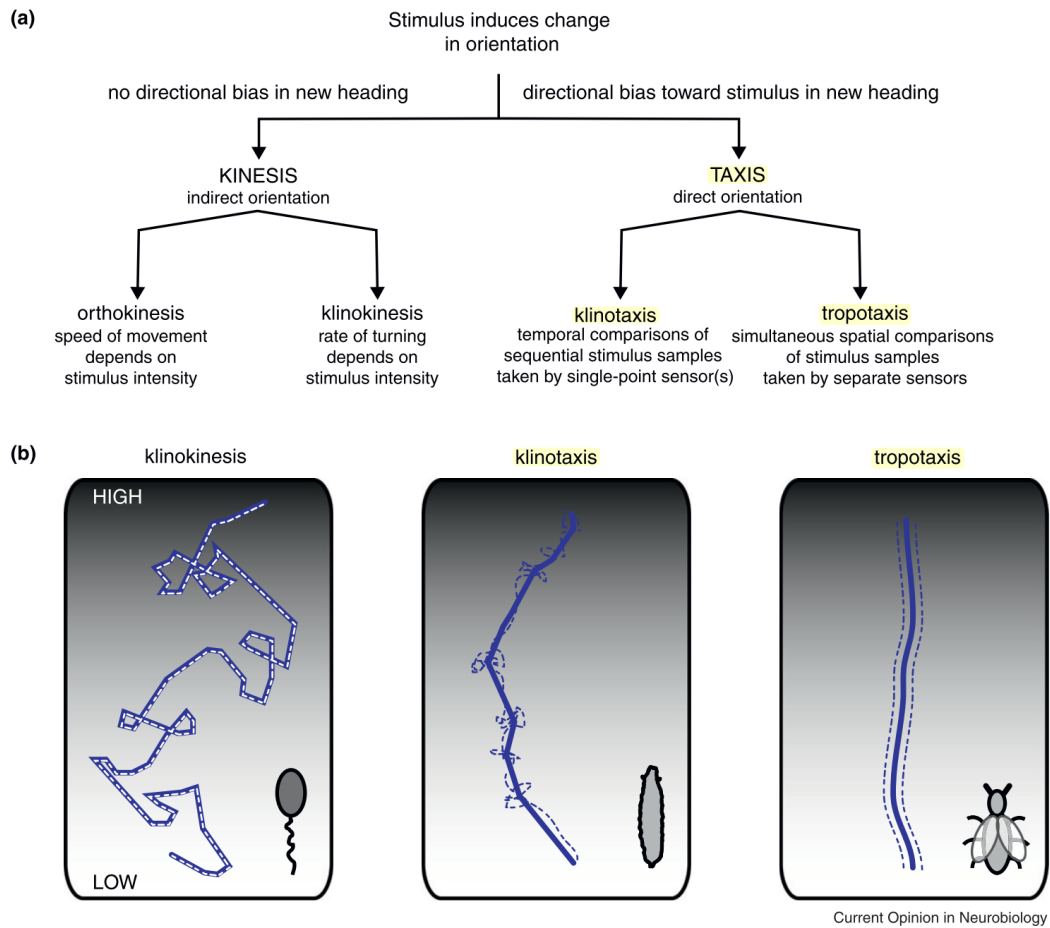


Figure 1.3: Classification of navigational strategies from Gomez-Marín & Louis (2012)

Taxis and kinesis strategies are sometimes discussed in terms of efficiency with regards to the resulting aggregation, or speed of aggregation around a stimulus.

“It has [...] been shown that although kinesis can result in aggregation, they do so by means of an inefficient and devious method. Taxes [...] can produce aggregation too, but much more efficiently. They result in the animal moving directly towards or away from the source of stimulation. When a single light acts as the stimulus, the animal either moves straight forward, with its body axis in line with the light rays, or locomotion is along this line in general, slightly complicated by regular symmetrical deviations. The kind of reaction in which these regular deviations are a necessary part of the orientation mechanism is here named klinotaxis.”

The Orientation of Animals, (Fraenkel & Gunn, 1961).

Considering efficiency as a parameter to be optimized implicitly assumes that the animal pursues one and only one goal, which is finding the stimulus source. This can be true in some special cases, but in a multi-modal and changing environment, we might expect a need for trade-off-like responses to different stimuli, where high efficiency is not necessarily optimal. Indeed, efficiency may get one stuck in a dead-end when facing novel (or unusual) situations - as exemplified by the moth trapped spiraling around a street light (Hsiao, 1973) - or trapped in a local maximum, with no opportunity of exploring beyond and pursuing a global maximum (trade-off between exploring and exploiting one's environment).

In recent studies, however, the question of multisensory integration and its trade-offs has started to be addressed, taking into account environment complexity. New approaches focus on the diversity of an animal's response to a stimulus as a function of its internal state arguing that the behavioral response to a stimulus is often non-deterministic (Scholz et al., 2017; Tsai & Chou, 2019). Some consider behavioral switches within spontaneous behavior, as for example the alternation between exploration and exploitation behaviors of an environment; or the optimality of a searching or foraging strategy (Sims et al., 2019; Viswanathan et al., 1999).

Many stimuli can indeed be interpreted not as cues that the animal has to robustly and infallibly follow, but rather as hints pointing towards more favorable environments.

All in all, recent studies have taken on the importance of grasping the whole biological system embodied within its complex multimodal environment.

1.2 From single-cell to systems neuroscience

“As always in science, the state of knowledge depend[s] on the state of development of the instruments.”

Foundations of the neuron doctrine, (Shepherd, 2015).

1.2.1 The Neuron Doctrine

The classical neuroscience approach is deeply grounded on the *Neuron doctrine* (Shepherd, 2015). It emerged in the late 19th century, following the founding anatomical observations Ramon y Cajal did using Golgi's staining (Golgi, who incidentally was a great objector of this idea). It establishes the neuron as a fundamental unit of the nervous system: anatomical, physiological, genetic, and metabolic as summarized by Waldeyer in 1891, who coined the term "neuron" in his review. As the Neuron Doctrine spread, advances in imaging and electrophysiology techniques during the 20th century corroborated it even more (in the 1950s, the electron microscope proved the discontinuity of synapses, the microelectrode enabled the understanding of a neuron's electrical activity, etc.). It was completed with the idea of the neuron as an informational unit (Warren McCulloch and Walter Pitts, 1943), a paradigm shaping much of research present and past.

Research through the prism of the Neuron Doctrine has thus been the study of the activity of individual neurons. This brought about the foundational research on the neuron as a perceptual unit: for example, stimulus-response of single neurons, like the study of receptive fields (Spillmann, 2014). With accumulating knowledge, it became possible to connect the individually studied neurons within a network - for example the different computational layers of a sensory system (for the visual system: photoreceptors, ganglion cells, the visual cortex) - to understand the operations performed by neuronal assemblies from layer to layer.

Most - if not all - of this grounding work was the investigation of a static response in an *open-loop* configuration: the stimulus does not update according to the reaction of the organism (from *in vitro* studies to *in vivo* on paralyzed animals). This means that the sensorimotor loop mentioned previously is broken: the input from the chosen stimulus can be measured but the response may be incomplete. This brings up the question of whether we can understand a sensory system without its closed sensorimotor loop. Can we properly understand how a cognitive system processes information in isolation from its natural closed-loop context ?

1.2.2 Emergent properties from neural networks

Step by step, from single neurons to subnetworks, recent advances in neuroscience, genetics, recording (multiple electrodes, EEG) and imaging techniques (fluorescence imaging, fMRI) have made it possible to investigate the entire nervous system as a whole, its structure and namely its dynamics *in vivo*. This is the area of systems neuroscience. *In vivo* spontaneous dynamics, their modification by a sustained stimulus or their bias by an acute stimulation can be observed. They can even be integrated in a closed sensorimotor loop by updating the stimulus according to the motor response.

With this approach emerged the idea of the nervous system as a complex system, meaning that collective dynamics are fundamentally different from and cannot be explained

by the sum of single-cell responses. An eloquent example might be the one of place cells in the hippocampus. They were initially found to be firing only in a particular place-field, *i.e.* a specific region of the environment, thus the firing of a single cell was thought to provide information on the animal's location in space, making the hippocampus “a spatial map” (O'Keefe et al., 1971). Further studies have shown phenomena of place field remapping even within the same environment: the place-cell's activity was no longer specific. And it is now known, that place cells are actually multisensory: they convey not only spatial visual information, but also olfactory, vestibular and information on self-motion (Jeffery, 2007).

One could see emergent properties neurosciences as being a natural development of the neuron doctrine, but some argue the necessity of a complete paradigm shift. As we still lack a unified theory of brain function, instead of following Cajal who considers brain circuits as “*impenetrable jungles where many investigators have lost themselves*” (1923), Yuste suggests that “perhaps one reason for our limited success as a field is the possibility that the neuron doctrine has become an obstacle to further advances and may need to be superseded as a paradigm in order to create a general theory of brain function” (Shepherd, 2015, pp. xxxiii–xxxvi).

A final ironical remark of Shepherd's Neuron Doctrine of 1991 is worth mentioning:

“The present generation of neural networks represents a view of nervous organization that harkens back to that of Golgi: the view that the complex interconnectedness of networks is more important than the details of neuronal structure and function.”

1.2.3 Tackling the complexity of an information-processing system

In the complex system framework of neuroscience, an interesting conceptual contribution was made by David Marr in 1982 to the description of the visual system.

“Almost never can a complex system of any kind be understood as a simple extrapolation from the properties of its elementary components (...) If one hopes to achieve a full understanding of a system as complicated as a nervous system (...) then one must be prepared to contemplate different kinds of explanation and different levels of description that are linked, at least in principle, into a cohesive whole, even if linking the levels in complete detail is impractical.”

(Marr, 1982, pp. 19–20)

Marr proposed a “three-level” analysis to fully understand a system carrying out an information-processing task:

- a computational level: what is the problem the system is trying to solve ?

- an algorithmic level: how it is being solved (“software”)
- an implementational level: the architecture underlying it (“hardware”)

There is a “one-to-many” mapping from the computational level to the algorithmic level, as well as from the algorithmic level to the implementational level. For one description of the computation behind a particular information processing task, there are several algorithms for solving it, and many different ways in which they each can be physically implemented.

1.3 Virtual reality systems to understand behavior

To try to get some insight into how the brain accomplishes a sensorimotor task at these different levels, bearing in mind the idea of interacting, even manipulating the sensorimotor loop without disrupting it, an interesting approach can be virtual reality.

Virtual reality is the simulation of an interactive environment in which the subject can be embedded, recreating the sensorimotor loop. Virtual navigation is possible by providing sensory (most of the time visual) and sensible (within the virtual environment) feedbacks to motor actions in a continuous closed-loop. A cue at time t generates a new updated environment at $t + dt$, dt being preferentially smaller than the subject’s preception time. The feedback update is parametric: the subject’s movements map to trajectories in parameter space, and correspond to updates of the virtual world.

In contrast with open-loop systems where conditions are presented independently of the animal’s response to stimuli, in this paradigm both are locked on one another: a stimulus might trigger a motor action, which in turn triggers the sampling of an updated or novel stimulus.

1.3.1 Human cognitive neurosciences explored by VR

First applications of VR were made in industry (automobile, aviation, military sectors). It spread to academic research for use in behavioral studies in the early 90s, and was very quickly applied to medical training, namely surgery. Today it is used as a tool for training for example in medicine (Bernardo, 2017; Izard et al., 2018), but also as possible therapy for mental disorders or phobias (Riva et al., 2019), as a tool for data visualization (El Beheiry et al., 2019), or entertainment, brain-machine/computer interfaces and also in research in the fields of neuroscience and psychology (Bohil et al., 2011). It is on the latter that I will focus on here.

The first steps of VR for humans were imperfect: “immersion” triggered number of side-effects from visual deficits (Mon-Williams et al., 1993), to dizziness, headaches or nausea (Regan, 1995). These side-effects have been termed “cybersickness”. It can be explained by the incongruity between sensory inputs: visual information provides users with the sense of motion which is not matched by vestibular feedback. Also by the

lag in the closed-loop, between timing of tracked movements and the generated virtual environment update, which has been very much improved lately (Harris et al., 2019).

Bohil et al. (2011) detailed the advances made in cognitive neurosciences thanks to virtual reality experiments. I will explore some of the presented elements here.

Spatial cognition and navigation. The maze experiment in which humans navigate a virtual radial maze reveals evidence for hippocampal activity (as expected from animal studies), but also evidence of frontal cortex activity, suggesting the additional contribution of working memory circuits. Some insights were also made as to strategies for path learning in a virtual environment: ‘spatial’ learners rely on landmarks (patterns on the walls) to build a cognitive map whereas ‘response’ learners remember a series of turns at each decision point. The second strategy is argued to be a non-spatial one, as it wouldn’t rely on the necessity of forming a cognitive map. Studies also revealed human place-cell activity specifically related to navigation (invasive recording from medial temporal lobe and frontal lobe of hippocampus as well as EEG).

Multisensory integration. Experiments involving the *body-transfer illusion* provided some eloquent insights into stimulus and timing constraints for multisensory integration. The body-transfer illusion is the illusion of owning a third person’s body or body part, which can be induced by concomitant visual and for example tactile stimulation. It has been shown, that first person visual perspective is key for creating the illusion, whereas timing of visuo-tactile stimuli is secondary.

Social neuroscience. Combined with imaging, VR unraveled the implications of different brain regions in theory of mind (empathizing with others through their facial expressions), mentalizing (interpret the intentions of others enabling one to anticipate another’s behavior); replication of the obedience study of Milgram (with results suggesting that observing a virtual other in distress creates personal discomfort for the observer, rather than empathy for the virtual character); etc.

1.3.2 In model animals

The first studies to demonstrate locomoting animals interacting with a virtual visual environment involved insects in the 1980s. In rodents, body tethered rats have been first put on a trackball for effective maneuvering by Hölscher et al. (2005).

As VR is a very interesting system not only enabling the control of the sensorimotor loop, but also offering the possibility of partially immobilizing an animal in order to combine behavioral studies with neural recordings. It has been widely developed for model systems such as mice, flies, zebrafish and worms.

1.3.2.1 Within the sensorimotor loop

Measuring motor output. A first step towards the generation of an embodied experience is to effectively and quantitatively measure motor outputs which will be used

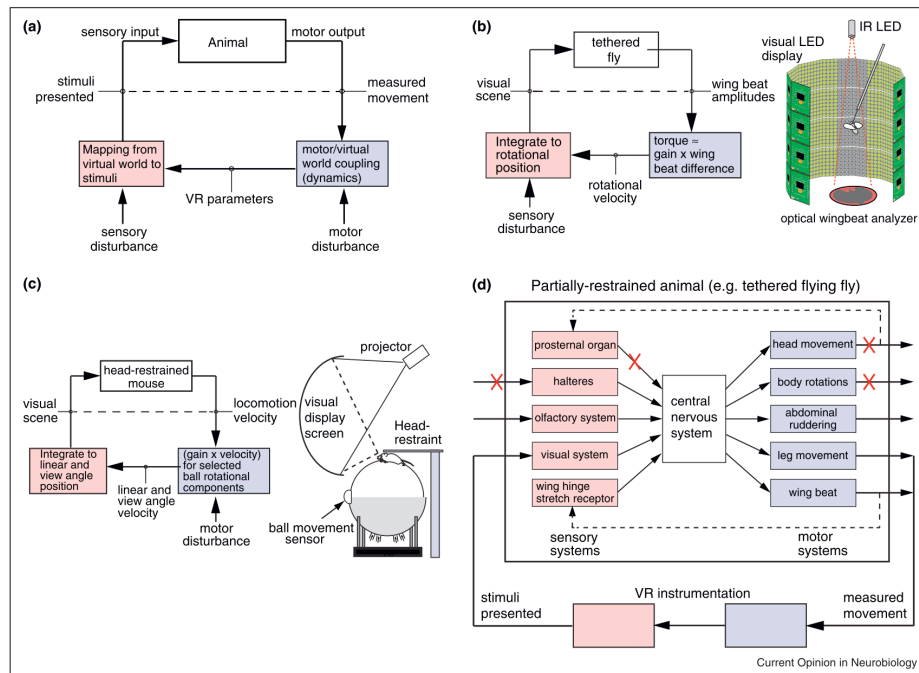


Figure 1.4: Virtual reality systems from Dombeck & Reiser (2012)

to navigate in the virtual world (figure a). In some cases it may be quite challenging.

Take the fly for example (see figure b): its wingbeats were recorded with an electromechanical torque meter in the early experiments (Götz, 1968), and with optical wing tracking more recently (Currier & Nagel, 2018; Maimon et al., 2010; Shiozaki et al., 2020). But getting an effective readout of the complete movements wingbeats would generate has not yet been done. Reorientation, *i.e.* its torque can be assessed (Currier & Nagel, 2018; Shiozaki et al., 2020), but navigation in two dimensions, yet alone three has not yet been achieved.

These challenges explain why many research on the fly has been done with it walking on a tracking ball (Fisher et al., 2019; Haberkern et al., 2019; Vishniakou et al., 2019), although this behavior is less often displayed than flying. The tracking ball, or treadmill is also a widely used option for head-restrained rodents (see figure c). With this method, navigation in a virtual 2D environment can be easily recorded, for studies spanning from navigation or spatial learning memory to sensory processing and decision making (Thurley & Ayaz, 2017).

In head-restrained zebrafish, optical tracking of tail movements may be done, with different ways of quantifying tail deflection (curvature, displacement) (Bianco et al., 2011; Jouary et al., 2016; Kist & Portugues, 2019; Wolf et al., 2017). Also ‘fictive swims’ recordings can be done using electrodes placed on bundle of motor neuron axons (Vladimirov et al., 2014).

Shaping the stimulus. VR implementation is obviously highly dependent on the stimulated sensory system, namely on its perception of space and time. The spatial resolution and extent of the stimulus should be adapted to the sensor’s acuity and broadness. Similarly for temporal resolution, the update lag dt should be shorter than the animal’s reaction time, or even perception time. Taking the example of vision, reaction times are about 100ms in rodents and 80ms in flies. Rodents are very sensitive to light, have a low visual acuity and a large field of view while flies have an even lower visual acuity but a larger sampling of the visual space. Thus the developed VR techniques are different: dim projectors with a panoramic but low-resolution display for rodents and arrays of LEDs that update faster for flies.

Zebrafish have reaction times spanning from tens (for acoustic or mechanically-elicited startle responses, (McClenahan et al., 2012) to hundreds of milliseconds or even seconds (for OMR see Portugues & Engert (2011)), and a wide visual field ($\sim 300^\circ$ horizontally). Thus for visually-guided behaviors classical projectors (with a 60Hz refreshing rate) - or sometimes LEDs - are generally sufficient, with a panoramic or spherical screen.

An important issue in shaping the sensory input of a motor output is to consider the gain of the function transforming one into the other (see figure 1.3.2.1, “motor disturbance” box): $output = input \times gain + offset$. Adjusting the gain can be done by setting it such that a mean movement in the virtual setup would trigger a displacement of a mean value close to what the animal would experience in a naturalistic setting. It has also been shown that some animals - and specifically of interest to me, zebrafish larvae - are able to adapt their behavior to compensate for a high or a low gain (Portugues & Engert, 2011).

Engaging in the feedback loop. Another issue worth considering, is whether the animal is engaged: is it in the loop ? In some cases it might be obvious from the behavior, as the desert ant which performs path integration in a virtual environment and reproduces its homing behavior successfully (Dahmen et al., 2017). If not, a technique for testing it is to apply a disturbance signal, like for example a drift, which the animal, if it is engaged in the feedback loop, will be able to compensate in order to maintain a straight trajectory (Heisenberg & Wolf, 1988).

In settings where the animal is partially fixed (head-fixed for example), engaging in the loop is more challenging than in freely moving conditions. But it has become possible to compare the recorded neural circuitry in both settings. This has for example been done for hippocampal place cells in head fixed mice navigating along a virtual linear track (Dombeck et al., 2010; Harvey et al., 2009). These studies found that several key features of virtual place cells were highly similar to those measured in place cells in freely moving rodents.

1.3.2.2 Discussion on VR systems for neuroscience

Advantages of VR. A great advantage of VR for neurosciences is to simulate an interactive environment for naturalistic behaviors to take place while brain activity can be monitored via imaging or direct recording (Gray et al., 2002). Multisensory inputs are possible to assess inhibition, synergy or linearity with a maximal control over the presented stimulation and of the perceived sequence of stimuli received by the animal, as it is recorded. VR also provides an assessment of the role of feedback from motor events during the simulated experience and how it can shape neuronal dynamics (Maimon et al., 2010; Saleem et al., 2013).

Moreover unnatural couplings may be established between the animal’s movement and the virtual world: unrealistic combinations of stimuli (contradictory or decoupled) can be presented to get insight into how conflicts might be resolved (Heisenberg & Wolf, 1988; Major et al., 2004), or a discontinued parameter space for a virtual teleportation (Stowers et al., 2017), etc.

VR enables the simulation of an entire natural task environment in order to elicit the full range of behavioral possibilities. And as emphasized by Krakauer et al. (2017), “study of the neural implementation of behavior is best investigated” after the detailed analysis of tasks and of the behavior they elicit: “behavioral work provides understanding, whereas neural interventions test causality”.

Indeed, it has been shown that in general, activity levels, tuning, sensitivity and neural encoding are modulated by the behavioral state of the animal, and overall general activity increases with locomotion (Maimon et al., 2010; Niell & Stryker, 2010; Saleem et al., 2013). So if one really aims at deciphering the neural code - if there is one - closed-loop paradigms will be informative.

Combining closed-loop paradigms and imaging techniques in zebrafish larva has been on the rise for the past ten years. It has been used for the investigation of eye position and velocity control (Brysch et al., 2019), motor adaptation (Ahrens, Huang, et al., 2013), visually guided and goal-directed navigation (Kist & Portugues, 2019; Robson, 2013), prey-capture (Bianco et al., 2011; Mearns et al., 2020), decision-making or evidence accumulation (Bahl & Engert, 2019; Dragomir et al., 2019; Mu et al., 2019) and even social behavior in adult zebrafish (Huang et al., 2020).

The importance of closed-loop paradigms has incidentally recently been demonstrated even at the level of the brain: glial cells have been shown to accumulate evidence that an action is futile (absence of feedback), thus eventually suppressing this behavior (Mu et al., 2019).

Limitations of VR. Needless to say, as in any system, there are still some drawbacks even in closed-loop VR systems. Some feedback loops are still broken, namely due to restraint. It may disrupt the control mechanisms of head and eye position for head-fixed animals (Zeil et al., 2008). A particular concern is about the lack of vestibular

input, which can trigger mismatches between visual and (the absence of) vestibular stimulation (Minderer et al., 2016). Restraint can especially be an issue for studying motor control and locomotion. Tethered flying flies, walking flies and rodents tend to change their gait as compared to when freely-moving. Flies pitch down excessively and mice rotate much more while walking.

Still, these experiments seem to bear some interesting information, with results comparable to freely moving systems. These limitations may be overcome through habituation to head restraint, or training to recover a more natural locomotion gait.

If there are quirks in the closed-loop resulting in an ‘unnatural feedback’, different responses might be expected from the animal (Heisenberg & Wolf, 1988; Major et al., 2004), hence, emphasizing the importance of studying the behavior in freely moving conditions beforehand.

Chapter 2

The zebrafish larva: a model in systems neurosciences

An excellent model vertebrate for studying exploratory or goal-directed navigation, offering the possibility of a “brain-wide” approach is the zebrafish larva. It enables the combination of behavioral studies with brain-scale functional imaging at cellular resolution, sometimes even in freely moving animals (Kim et al., 2017). In this second introductory chapter, I will present the larval zebrafish model, the navigation problems it has to solve in its environment and the solutions it has developed on the levels of “software” and “hardware” implementation (algorithms and functional anatomy) to tackle these problems.

2.1 A model animal in systems neuroscience

After some early developmental studies in the late 1930s (ref. . **On the early development - bipolar differentiation and cleavage - of the zebra fish, *Brachydanio rerio***), the zebrafish *Danio rerio* was durably introduced into the laboratory by George Streisinger in the 1970s for the study of genetics and neural system development. It rapidly grew as a model animal in developmental biology and genetics. Indeed, it has a rapid and external development, a great genetic malleability, high physiological and genetic homology to mammals. It has eventually reached the field of systems neuroscience in the last two decades. (Stewart et al., 2014)

Zebrafish undergo a rapid development: a larva hatches at most 72 hours after its egg has been fertilized. The larval stage is considered to span the 3 to 30 dpf period, during which the zebrafish continuously grows and develops. Over this period of time, its brain grows from 100,000 neurons up to 10,000,000 neurons in the adult.

Adding to its advantages as a model for genetics and developmental biology, zebrafish larva has gained popularity in neuroscience research thanks to some morphological

and anatomical traits - they are small, optically transparent and their small brain is composed of around 100 000 neurons at this stage (about a thousand times less than mice, still enough to subserve complex behaviors) - which enable the optical recording of almost their entire brain activity *in vivo*.

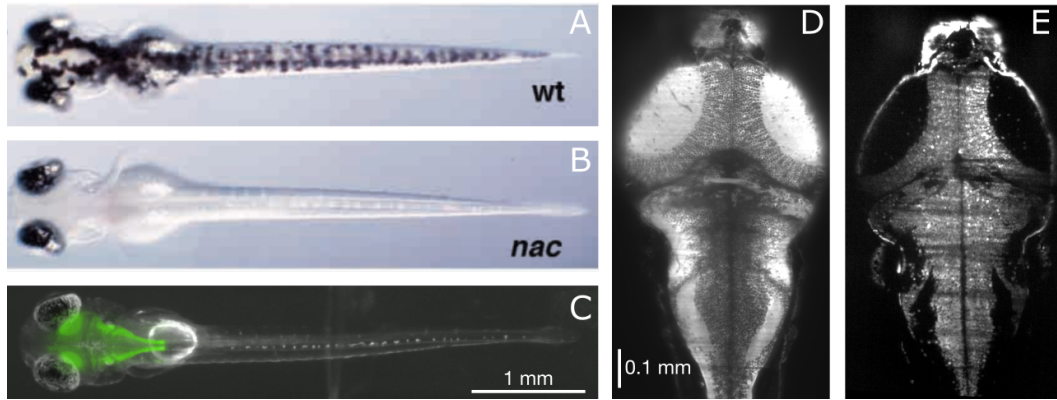


Figure 2.1: Wild-type, mutant and transgenic lines of zebrafish larva. Dorsal views of (A) wild-type, (B) nacre (from Lister et al. (1999)), (C) pan-neural GCaMP5 expressing larva illuminated by a light-sheet. (D-E) Microscopic view of brains of two larvae expressing GCaMP respectively in the neurons' cytosol and in the nucleus.

This was possible through the development of a diversity of different zebrafish lines: mutants that are more transparent than wild types (*nacre* mutation, see figure 2.1), or transgenic lines that express Genetically Encoded Calcium Indicators (GECIs), the most widely used in neuroscience being the GCaMP family (a fusion of green fluorescent protein GFP, calmodulin, and the peptide sequence M13) (see part on calcium imaging). Gcamp binds to calcium (Ca^{2+}), inducing a conformational change that increases its quantum fluorescence efficiency. As intra-cellular calcium is released in neurons when they are electrically active, it enables one to record all active cells expressing the reporter in the brain. The optimal expression of the GCaMP reporters used today corresponds to 5 to 8 dpf (most of the studies mentioned in the following use larvae of this age), when the animal is sufficiently small and transparent for optical accessibility.

Thus, the possibility the larval zebrafish offers is to link whole-brain activity to behavior - the most complex product of a nervous system - in a vertebrate. This perspective has motivated numerous behavioral studies on this animal in recent years, starting with the description of its locomotor repertoire.

2.2 Locomotor repertoire description

Larval zebrafish swim in a “burst and glide” fashion: they propel themselves using short bursts of tail movement called swim bouts, alternating with inactive “resting” periods called interbout intervals, during which the fish only moves passively through

the water. These bouts may vary in amplitude, duration, or reorientation direction, forming the locomotor repertoire of the zebrafish larva.

First descriptions of this locomotor repertoire were obtained from manually-triggered recordings (Budick & O’Malley, 2000). Budick et al had then already described two main navigation patterns in larval zebrafish: forward swims and reorientation turns.

A finer classification of swim types allowed to distinguish forward swims, routine turns, C-turns, J-turns, O-bends, etc. The different movements were classified based on the kinematics of the zebrafish larva when performing these different swim bouts (Kalueff et al., 2013).

Automated tracking of freely moving animals has enabled their observation for long time periods and the collection of long swimming sequences (Franco-Restrepo et al., 2019). Quantitative analyses of these swimming sequences shed light onto more subtle differences in locomotion patterns either in response to a stimulus (Liu et al., 2015; Marques et al., 2018), or in spontaneous swimming conditions (Dunn et al., 2016; Johnson et al., 2020). Classification techniques enabled an astuter differentiation of locomotory movements: these approaches lead to identify no fewer than 13 different types of bouts, 7 of which can be considered turning and 6 forward (see figure 2.2). They are used differentially in different contexts (for example in phototaxis, only 4 of those subtypes are used: 2 forward and 2 turns) (Marques et al., 2018).

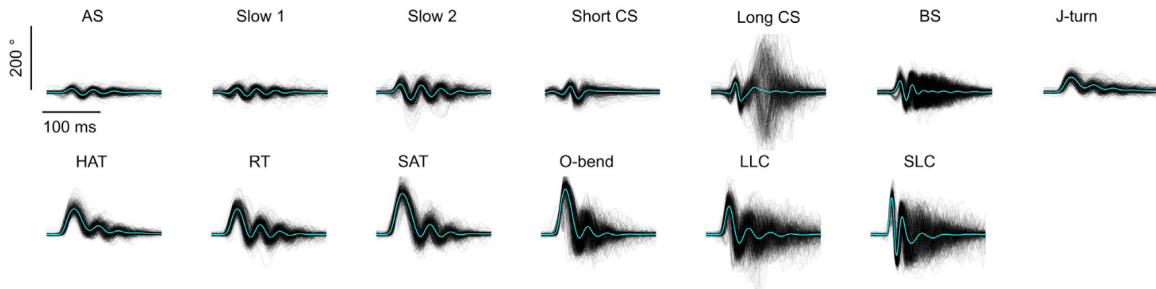


Figure 2.2: Angle of caudal tail segment versus time of one hundred bouts of each type, from automatic clustering. Cyan lines are the average of all bouts in a category. Symmetrical envelopes are forward swims, asymmetrical signals are turning movements. AS: forward approach swim; Slow 1 & 2: slow type approach swims 1 and 2; Long/Short CS: capture swims (final forward movements in hunting sequences); BS: burst type forward swims with high tail-beat frequency; J-turns: turns associated with prey orientation behavior; HAT: high-angle turns; O-bends: large turns; RT: routine turns; SLC: C-start (turning) escape swims; LLC: long latency C-starts (turns). From Marques et al. (2018)

While earlier studies were focusing on triggering a specific type of response to a well controlled stimulus, automation has enabled to loosen some constraints and keep the

animal under observation for longer periods of time, and thus have access to more naturalistic behaviors.

2.3 Visually guided behaviors

Many of the aforementioned locomotor patterns can be triggered by visual stimuli, on which the larval zebrafish heavily relies. A lot of navigation problems thus involve the visual system through so-called visually-guided behaviors. I will briefly contextualize the larval zebrafish's visual ecology to keep in mind to what environment the animal has adapted to, and review some of the visually-guided behaviors I will be referring to in this work.

2.3.1 Visual ecology

“The development, structure and function of the zebrafish visual system are shaped by its ecology.”

(Neuhauss, 2010)

The *Danio rerio* belongs to the cyprinid family, endogenous of the Indian sub-continent. It lives in shallow, shady, vegetated and slow-moving waters. It is diurnal and omnivorous. During the rainy season, adult zebrafish move from brooks to flooded areas (like rice paddy fields), where spawning occurs. There, larvae can hatch and develop in still, seasonal waters before reaching the stream (Engeszer et al., 2007).

Living in a visually complex environment with large variations of luminance levels requires a well-developed visual system, with colour perception and UV-sensitive vision for tracking otherwise translucent prey. The larva's rapid development also translates into a rapid maturation of the visual system, quickly supporting visually-guided behaviors like predator avoidance, prey capture and countercurrent swimming. This swift maturation can be interpreted as an ecological adaptation to escape predators, forage and orient itself as early as possible.

2.3.2 Eye movements

The zebrafish eye position is controlled by 6 extraocular muscles. They enable movements in the vertical (like the vestibulo-ocular reflex) as well as in the horizontal axes. As they are part of reorientation behaviors of the larva in the horizontal plane, we will consider only the latter ones. Among horizontal eye movements, controlled by 2 muscles (the medial and the lateral rectus), two main ones can be displayed spontaneously: vergence movements and saccadic eye movements.

Vergence movements occur during hunting. The larva being a prey, its eyes are located on either side of its body to increase its visual field. But as it is also a predator of



Figure 2.3: Image a zebrafish could see in its environment. From group of T. Baden, Sussex University.

small unicellular organisms (paramecia), the larva can transiently converge its eyes (total forward rotation of 35.5° instead of 18.5° of a single eye at rest, relative to the rostro-caudal axis) in order to increase the binocular overlap in front of it, probably to better evaluate the distance to the prey (Bianco et al., 2011).

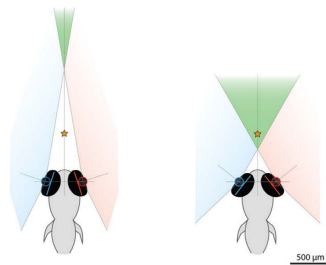


Figure 2.4: Eye vergence movement in larval zebrafish when hunting a prey. From Bianco et al. (2011)

Saccadic eye movements are a fast coordinated shift of eye position. They are robustly displayed at 4dpf. Periods of spontaneous saccades occur, depending on the behavioral state of the larva. In animals with a fovea (a central zone in the retina which has most visual acuity), saccades are the transitions between fixation times (when one looks at an object). But zebrafish lack a fovea and thus do not need to redirect their gaze from one point of interest to another. So the functional purpose of saccades is assumed to be the widening of the animal's visual field (Easter & Nicola, 1997 ; Martinez-Conde & Macknik, 2008).

Horizontal eye movements can be induced by the optokinetic response (OKR), triggered by a rotational stimulus in the horizontal plane (figure 2.5 A). It translates into slow tracking eye movements linearly following the stimulus, reset by fast high-amplitude saccades (Orger, 2016; Rinner et al., 2005).

2.3.3 Diversity of visually guided behaviors

Most visually guided behaviors are fully displayed at 96hpf (hours post-fertilization) or 4 dpf (days post-fertilization). This corresponds to the moment when the eye’s lens starts forming a sharp image on the retina and when the extraocular muscles are completely formed (Easter Jr & Nicola, 1996). Visual performance is regulated by a circadian clock and is best during day time (Fleisch & Neuhauss, 2006).

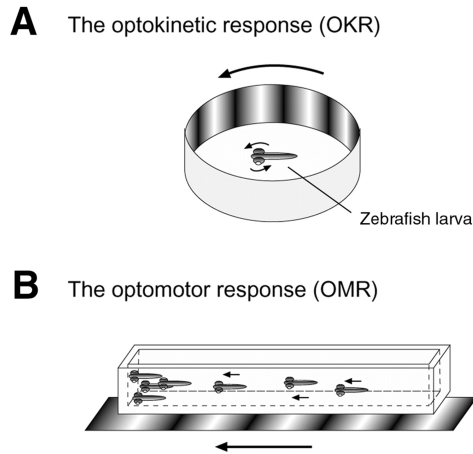


Figure 2.5: Illustration of optokinetic and optomotor responses in larval zebrafish. From Roeser & Baier (2003).

In order not to be swept away with the current, zebrafish larvae exhibit an optomotor response to whole-field visual motion: if they are carried away, larvae follow the direction of the perceived motion, in order to stabilize the surrounding visual scene. The psychophysics of this response have been well studied: motion perception is mainly driven by first-order (Fourier) signals (Orger et al., 2000) and is mediated by green and red cones in the zebrafish retina (Orger et al., 2000). The study of this response has then been completed and linked to underlying neural activity (Ahrens, Orger, et al., 2013a; Kist & Portugues, 2019; Naumann et al., 2016 ; Orger et al., 2008; Orger, 2016; Wang et al., 2019). The robustness of the response directly depends on the robustness of the visual input. Recent studies have allowed to reveal the bases of decision-making processes at a neuronal level, by describing neuronal assemblies that are able to accumulate motion-direction evidence in the context of incomplete or conflicting motion signals (Bahl & Engert, 2019; Dragomir et al., 2019).

Zebrafish larvae also display less deterministic visually-driven behaviors such as photo-

taxis, which drives the animal towards illuminated regions. It is color-specific: positive phototaxis in larval zebrafish is mediated through blue wavelengths (Orger & Baier, 2005), UV is typically avoided (Guggiana-Nilo & Engert, 2016), as well as infrared wavelengths (Hartmann et al., 2018). Situations of positive and negative phototaxis exist: the animal has to undergo a period of habituation at a high intensity to display light-seeking behavior to a slightly lower target intensity (Burgess et al., 2010). This has been termed flexible phototaxis in a recent preprint by Chen et al. (2020). Indeed, the animal, rather than seeking the highest luminance possible, rather tries to maintain environmental luminance at a set-point which depends on luminance history. Another aspect of phototaxis, is that its preference is reversed during development: larval zebrafish tend to display positive phototaxis (about 80% of individuals), while adult zebrafish seem to avoid light (Gerlai et al., 2000; Maximino et al., 2010; Oliveira et al., 2015; Serra et al., 1999), and display what is sometimes called scototaxis (attraction towards the dark). This change of behavior could be interpreted through their change of habitat from shallow waters to more deep and shady regions.

While most above described behaviors are often approximated and constrained to the horizontal plane in 2D, some do contain robust 3D components, as witnessed by the diving component of the escape response (to a looming, *i.e.* visual or auditory stimulus), which probably is an useful adaptation to escape predators from above like dragonfly larvae (Bishop et al., 2016).

2.4 Functional anatomy of the visual system of larval zebrafish

Zebrafish develop quickly: they hatch at 3 dpf and most of their organs are functional around 5 dpf to quickly support their innate behaviors (fins and tail are formed, the mouth as well as the digestive tract are open for feeding, eyes form an image on the retina,...). I will briefly review some of the developmental stages of their visual system, the hardware of their visually-guided behaviors, and namely phototaxis.

2.4.1 Eyes structure

Anterior segment

At 3 dpf the anterior segment of the eye (composed ,among others, of the lens and the cornea) is able to form a sharp image on the retina: the larval zebrafish’s eye is emmetropic. Based on the “Helmholtz hypothesis”, which states that two bright objects can be resolved by the cone mosaic only if their images illuminate separate cones that are separated by at least one unilluminated one, their visual acuity (resolution) calculated from cone density is of 2.9° . This value roughly corresponds to the behaviorally determined threshold of $3\text{--}4.5^\circ$ in 4 dpf zebrafish using near-threshold stripe sizes for triggering OKR. (Easter Jr & Nicola, 1996; Haug et al., 2010)

The horizontal visual field of each eye captures 163° of its surroundings at 4 dpf (Easter Jr & Nicola, 1996). At rest they are rotated forward by about 18.5° , the total extent of its horizontal field of view is around 300° with a small binocular overlap (Bianco et al., 2011). The vertical field of view represents at least $\sim 130^\circ$ (symmetric relatively to the coronal plane of the zebrafish body) (Zimmermann et al., 2018).

Retina

The zebrafish possesses a canonical vertebrate retina, composed of cone and rod photoreceptors. All have specific spectral sensitivities, but rods are responsible for what is called scotopic vision (under low luminance levels) and cones are known to mediate color vision: the zebrafish is *tetrachromat* with four types of cone cells. The peak sensitivities of the different opsins are the following:

- rods: 501–503 nm
- cones:
 - UV 360–361 nm
 - SWS (short wavelength-sensitive) cone (blue) 407–417 nm;
 - MWS (medium-) cone (green) 473–480 nm;
 - LWS (long-) cone (red) 556–564 nm.

UV-cones are the first to develop on the retina (4dpf), followed by S, M and finally L cones. Rods are the last to appear on the retina and though they appear to be functional at 5dpf, their patterning on the retina seems to constantly evolve through the larval stage (Raymond et al., 1995; Saszik & Bilotta, 1999; Venkatraman et al., 2020).

In a recent paper, Zimmermann et al. (2018) explore how the visual system of the zebrafish larva has effectively adapted to the visual naturalistic scenery of its environment. Indeed, photoreceptors are not uniformly distributed throughout the retina (first shown by Raymond et al. (1995), not cited in Zimmermann et al. (2018) or Dehmelt et al. (2019))

It is argued, that in a naturalistic environment there is little color above the animal, thus the retinal structure collecting light from above is mainly achromatic (rods and terminals of achromatic bipolar cells). The lower visual field and the horizon being color-rich, cones are more dense and sensitive in the upper and medial part of the retina. And finally, a “high-gain UV system” collects information from above the frontal horizon, a zone they called the “strike zone”, likely supporting prey capture of UV-scattering prey.

Phototaxis is performed through blue cones (Orger & Baier, 2005). We can note that those are more densely located around the horizontal plane of the retina which probably enables an accurate appreciation of the surrounding illumination.

The retina also contains non-visual opsins which could play a role in circadian rhythmicity, light adaptation or body color adaptation. To be able to function over 10 log

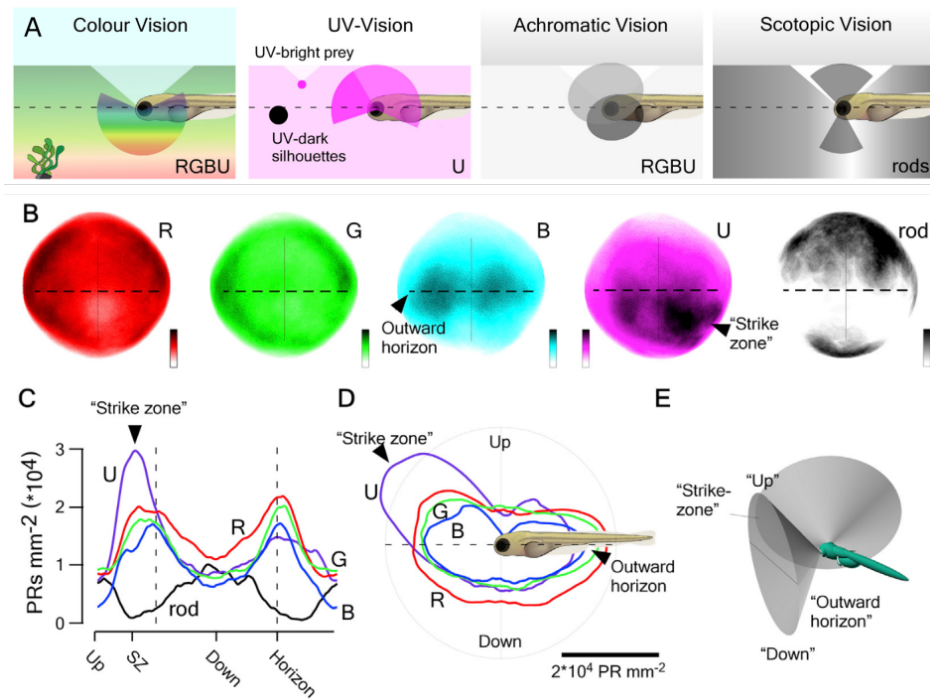


Figure 2.6: Chromatic and achromatic naturalistic vision in zebrafish larvae. (B) Photoreceptor density distribution throughout the retina, for red (R), green (G), blue (B), UV (U) cones and rods. (C-D) Distribution of cone and rod densities as a function of azimuth. (E) Model of zebrafish visual field. From Zimmermann et al. (2018)

units of light intensity and protect its photoreceptors, the entire retina morphologically adapts to light or dark. These changes operate through the migration of melanosomes and positional changes of photoreceptor cells: rods are shaded, whereas cone tips exposed. (Neuhauss, 2010; Nilsson, 2009)

Inner retina

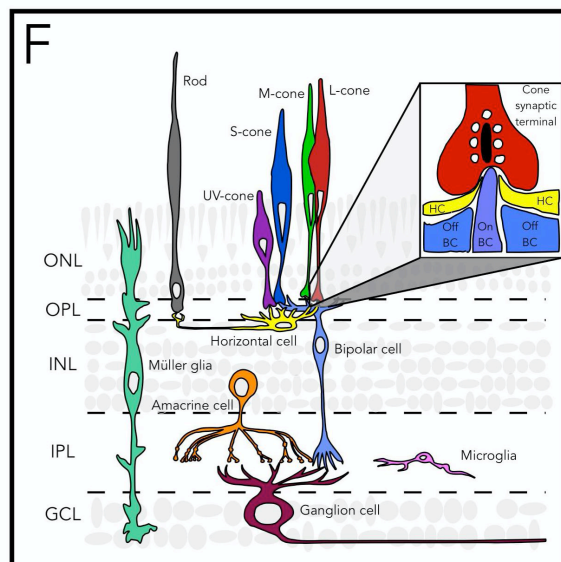


Figure 2.7: Diagram of the vertebrate retina and the retinal cells. Inset highlights the synapse between cones and horizontal and bipolar cells, where the cone synaptic terminal contains synaptic vesicles attached to the synaptic ribbon (black). In close apposition to the ribbon, the dendrites on On-bipolar cells (On-BCs) invaginate into the synaptic terminal and are flanked by two horizontal cell (HC) processes. Off-bipolar cells make more basal contacts in close proximity but not apposed to the synaptic ribbon. Different cellular layers: outer nuclear layer (ONL); outer plexiform layer (OPL); inner nuclear layer (INL); inner plexiform layer (IPL); ganglion cell layer (GCL);. From Angueyra & Kindt (2018)

In the inner retina, bipolar cells transmit visual information from the photoreceptors to ganglion cells, which in their turn project mainly to the optic tectum in a contralateral manner (forming a complete optic chiasm). Horizontal cells integrate inputs from multiple photoreceptors and increase contrast sensitivity through lateral inhibition by projecting on neighboring photoreceptors. Amacrine cells functionally structure the inner retina horizontally by being the post-synaptic connection of bipolar cells and projecting onto bipolar and ganglion cells.

The flow of information thus follows photoreceptors -> bipolar cells -> ganglion cells where horizontal and amacrine cells are regulators.

Bipolar cells. Zebrafish bipolar cells can be functionally subdivided into ON-type,

OFF-type and ON/OFF-type (Emran et al., 2007). The ON-type are active with light onset, whereas OFF-type are activated upon light decrement. Some bipolar cells are wavelength-selective, others are not, forming the achromatic visual pathway (Zimmermann et al., 2018)

Ganglion cells. The retinal OFF-pathway plays a reorientation role in stereo-visual phototaxis: it drives turns away from the eye experiencing the greater reduction in light intensity - if the OFF pathway is disrupted in only one eye of the animal, turns are performed in the correct direction (towards the light spot) if it is located in the “blind” visual field. But if the light spot is in the intact visual field, turns are not biased towards the light. The retinal ON pathway, on the other hand, mediates the approach response, and is involved in increasing scoot frequency when the larva faces the light source. (Burgess et al., 2010)

It has recently been shown by Zhou et al. (2020), that retinal ganglion cells’ function is highly variable with their position within the retina, with the interesting finding, that blue-off ganglion cells (activated when blue light gets extinguished) are highly overrepresented. They speculate, that this feature could be used by a non image-forming visual pathway, and could rather serve as a blue-background estimation system (Zhou et al., 2020). Those ganglion cells are very likely to be involved in the phototactic circuit, as this behavior is mediated by blue light, through blue cones and through the ganglion OFF-pathway.

2.4.2 Downstream: ganglion cell projections

The terminal arborization of ganglion cells in the optic tectum is topographic (neighbor ganglion cells terminate neighboring in the tectum) with an inverted projection pattern (nasal axons terminate posterior in the tectum and *vice-versa*).

The zebrafish optic tectum is a homolog of the mammalian superior colliculus, located in the midbrain. Although it seems to process visual motion information with direction selectivity (Wang et al., 2019), upon laser ablation of the larval tectum, visual acuity, OMR and OKR responses remain unaffected. Only the frequency of resetting saccades during OKR decreased (Roeser & Baier, 2003). The optic tectum is thus probably not directly involved in motion detection, but mediates eye movements as does the superior colliculus. The optic tectum is also involved in binocular integration (Gebhardt et al., 2019), is required for prey capture and collision avoidance (Orger, 2016).

As brought to light in this introduction, zebrafish larva has the advantage to display a broad range of innate behaviors - many of them visually-guided - forming a rich locomotor repertoire. Also, its accessibility for anatomical studies led to a thorough description and understanding of its visual system. Thus this model animal enables the study of naturalistic goal-directed navigational processes, exploratory locomotion,

hunting behaviors, sleep, decision-making processes, etc. It is also the only vertebrate organism in which behavioral studies combined with neuronal imaging on the scale of the whole nervous system are feasible, which can provide insight into how these processes are generated within the brain.

In the following chapters I will focus on larval zebrafish's light-seeking behavior. In order to keep the stimulus continuously updated relatively to the animals motor actions, this work has been done using closed-loop paradigms.

The next chapter will be dealing with the behavioral algorithm of light-seeking behavior in free-swimming conditions. The following section will focus on the necessary transition between free-swimming to head-fixed conditions, in which the larval tail movements become a proxy to its reorientation attempts relative to a light source. And the final chapter, will deal with the neuronal underpinnings of light-seeking behavior through large-scale functional imaging in head-fixed closed-loop conditions.

Chapter 3

Freely swimming light-seeking reorientation

The following effort belongs to this framework of combining behavioral studies with large-scale neuronal recordings. It aims at contributing to it through the study of light-seeking behavior, also called phototaxis.

In this chapter I will first present the state of the art regarding light adaptation and light-seeking behavior in larval zebrafish. Starting from the hypothesis that spontaneous dynamics are only slightly biased by a smooth gradient, I will then describe the spontaneous swimming of larval zebrafish using a minimal set of parameters. I will then show how these stochastic parameters are impacted during light-seeking behavior through the identification of visual cues that are used by the animal to orient towards a light source, by disentangling the effect of contrast and global intensity changes.

3.1 Light-seeking behavior in zebrafish: state of the art

Extensive research has been devoted to the study of the response of zebrafish larvae to a luminous stimulus (Brockerhoff et al., 1995; Emran et al., 2009; Burgess2007; Horstick et al., 2017). Some specifically focused on its lightseeking behavior: in laboratory conditions, after a prior habituation phase under a uniform and constant illumination, zebrafish larvae tend to navigate towards regions of higher intensities (a behavior generically termed positive phototaxis). It has been shown that zebrafish larvae perform all three “level 1” navigational strategies with respect to light (kinesis, klino- and tropo-taxis, defined in [the section about sensory-guided navigation](#)), though the terms used may sometimes be unspecific. Where some studies have been unspecific regarding a certain strategy (Burgess et al., 2010; Hartmann et al., 2018; Zhang et al., 2017), tropophototaxis has been described by X. Chen & Engert (2014), Guggiana-Nilo &

Engert (2016), Wolf et al. (2017), klinophototaxis by X. Chen & Engert (2014), photokinesis by Fernandes et al. (2012). The larval behavioral response to light is for the most part visually mediated for the exception of photokinesis described by Fernandes et al. (2012), which may be executed with deep brain photoreceptors.

Even though all agree on the existence of a preference in zebrafish larva for dim visible light, still the complete equation of how the animal reacts and/or durably adapts its behavior with respect to light is not completely clear.

Negative phototaxis is also displayed in larval zebrafish when the presented intensity is higher than the habituation intensity (Burgess et al., 2010). More subtly, a recent study suggests that larval zebrafish use phototaxis to maintain environmental luminance at a set point that depends on luminance history, seeking an optimum rather than a maximum (Chen et al., 2020).

3.1.1 Light adaptation

Response to high-amplitude short luminance changes. In their study Burgess & Granato (2007), start by an examination of the spontaneous kinematics of larval zebrafish. They notice a bimodality in the distribution of bend amplitudes and thus head reorientations, and conclude that the spontaneous locomotion essentially comprises scoots (low amplitude reorientations) and turns (higher amplitude). The basal frequency of these locomotory movements are modulated by different luminous stimuli, a modulation that would always depend on prior adaptation (light intensity).

A short (500 ms) light flash or dark flash transiently increases turn frequencies, but not frequencies of forward swims. This increase is proportional to the difference of stimulus intensity (tested intensity - adapted intensity). Turns evoked by increases in illumination are indistinguishable from routine turns, whereas turns evoked by reductions in illumination are different from routine turns.

Non-visually mediated responses to prolonged decreases in luminance. Fernandes et al. (2012) focused on the non-visually mediated light-seeking behavior, termed dark photokinesis. They showed that enucleated fish (eyes removed) still have behavioral responses to light stimuli.

The first response is the visuo-motor response (VMR), *i.e* the heightening of basal locomotor activity in response to an abrupt decrease in illumination (lasting ~ 5 minutes followed by adaptation over 30 minutes, as activity drops back to basal rhythm (Burgess & Granato, 2007)). Larvae lacking eyes also displayed a transient period of hyperactivity upon loss of illumination, before settling into a state of low baseline activity (figure 3.1 C). Enucleated larvae show a reduced but significant tendency to swim towards a weak light stimulus, without direct orientation towards the light source (figure 3.1 A, B).

They explain this behavior as being photokinesis: a heightened locomotor activity in

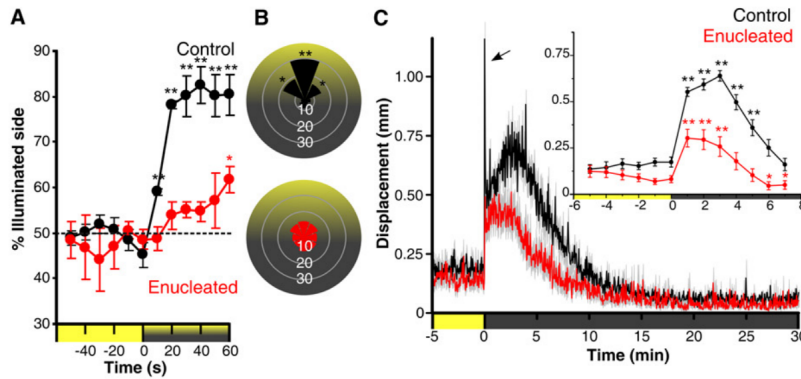


Figure 3.1: Percent of larvae observed on the illuminated side of the testing arena over time. Enucleated larvae exhibit a gradual shift to the illuminated side of the arena. (B) Larval body orientation during exposure to a phototaxis stimulus. Enucleated larvae show no bias in body orientation, where intact larvae do. (C) Locomotor activity during dark-induced VMR. Inset: enucleated larvae significantly increase activity following light extinction. From Fernandes et al. (2012)

dark areas, which drives individuals “in a non-directional, stochastic fashion” towards brighter zones, with an increase of routine turns and longer swim bouts. They also point towards a diving component in the VMR: lights extinction triggers rapid downward swims.

Another study by Horstick et al. (2017) elucidated that these deep brain photoreceptors interact with the retina to mediate two different search strategies: loss of light detected via the retina drives an initial strong local search. Then, deep brain photoreceptor signaling drives outward locomotor patterns for remote light sources. Local search activity initially masks extended search locomotor features. Local search is mediated via an increase in the frequency of turn/turn maneuver pairs and an increase in correlation of turning direction. During outward swimming, although larvae maintained an elevated rate of turns, the correlation of successive turns declined to baseline levels.

3.1.2 Tropo-phototaxis

Since zebrafish possesses two spatially separated receptors for sensing light - its eyes - it would seem straightforward that for phototaxis it uses both of them and uses the tropotaxis strategy. This has indeed been brought to light by Burgess et al. (2010) who investigated the visual pathways involved in this process.

In the study of Burgess et al. the experiment consisted in shining a light spot in the periphery of a petri dish and recording the response of all larvae in the petri dish during 5 seconds. They analyzed the proportion of either forward swims (scoots) or

turns when larvae were presented a novel light source. They observed a global increase in levels of turns and scoots during phototaxis compared to uniform illumination, with a slight increase in turn frequencies with distance to target and with angular distance to target. Turn magnitude also increases with angular distance to target and its direction is preferentially towards the light source. Scoot frequency increases when angular distance to target decreases

Note that the way a frequency is defined here is the mean percentage of larvae initiating a scoot or a turn during a 400 ms recording window. The inactive larvae are termed to be in “stationary phase”. The analysis is “instantaneous”: whole trajectories of individuals are dismissed, only movement type and orientation in a certain time window are analyzed. And this particular experiment might involve both tropo- and klino-phototaxis strategies, as perceived contrast as well as global illumination vary hand in hand with distance and orientation to the light spot.

A few years later, X. Chen & Engert (2014) worked at disentangling both possibly contribution strategies by exploring two experimental paradigms. In a first setting, involving spatial or stereovisual phototaxis, a larva was tested for 15-30min in a petri dish illuminated from below by a disk of light. The result was - as expected - that the larvae stayed within the illuminated region, by assessing the spatial contrast it would perceive by approaching the border of the illuminated circle (see figure 3.2 A).

3.1.3 Temporal phototaxis or klino-phototaxis

The main aim of X. Chen & Engert (2014) was to describe the algorithm of the temporal component of larval zebrafish phototaxis. To do so, they performed a second experiment, using a “virtual circle”. When the larva crossed a virtual circular border (of shape and size similar as in the previous spatial experiment), instead of a constant and uniform illumination in the petri dish, the lights would go off (see figure 3.2 B).

This second experiment led to the description of a set of behavioral algorithms, or rules, a larva could follow to solve the particular problem of staying within a spatially delimited temporally varying illumination profile.

First, rule number I [Angle] determines the turn amplitude of a bout: a first turn after the light-to-dark transition is a large angle turn, the subsequent ones’ (at least 3) are still large but their amplitude gradually decreases.

A second rule II [Lock/Flip] sets the direction of a turn relatively to the previous one: in steady (light or dark conditions), the direction of successive turns shows a slight correlation, they are “locked”. But when crossing the border, the two turns immediately preceding and following a transition (would it be light-to-dark or dark-to-light) are generally “flipped”, which means they are anti-correlated in direction (if the preceding bout was to the left, chances are the following one will be to the right). So when the larva crosses the border, the bout following the crossing is flipped with

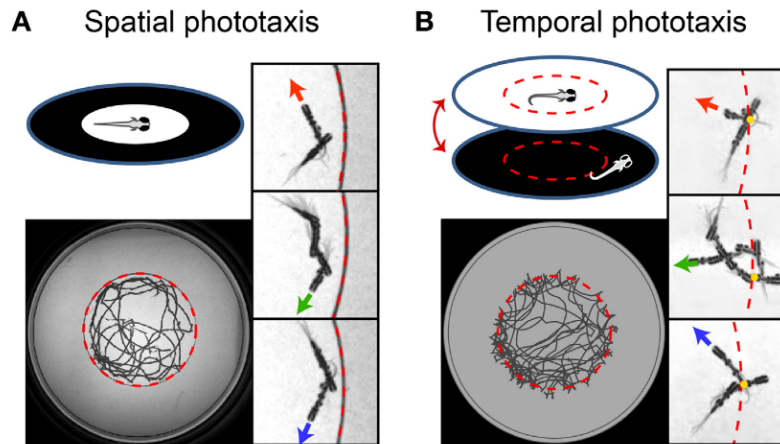


Figure 3.2: Larval zebrafish prefer light over darkness in the spatial comparison assay. (B) Temporal comparison assay: the Virtual Circle. The uniform illumination is turned off when the fish exits the virtual circle (dashed red circle, invisible to fish), and turned on again when the fish returns. From X. Chen & Engert (2014)

respect to the previous one. The second in darkness is strongly “locked” with the first one (and of high-amplitude due to rule number I) which makes the larva quickly escape the darkness. But then comes the border again, in the opposite direction this time: dark-to-light. The bout direction flips again and locks in the light. Thus this rule contributes to the fish staying close to the virtual border (as observed in experimental conditions).

Still these two rules weren’t enough to account for a very high probability of presence of the animal next to the virtual border. Thus the third rule III [Bounce] states that the cumulative angle turned over a given light interval is “flipped” in relation to the cumulative angle turned over the preceding dark interval. And a final rule IV [Efficiency] decides that the strong tendency of the fish to “flip” between the last turn in light and the first turn in dark is relaxed depending on the number of bouts executed before this transition into dark.

With this series of algorithms of turn modulation and time integration, Chen et al. were able to reproduce numerically - to some extent - their experimental data.

These rules actually require non-trivial forms of memory, as stated in their discussion. First there must be a memory of the direction of previous turn, on which locks and flips are based. They also stress that their rule III requires a memory of cumulative angle made in similar conditions (light or dark), which I would argue would not be essential if you have a lateralized circuit that is reinforced for example through efferent copy of a movement made to the same side. Then, there has to be a memory of the time since a light transition, supposed to last for several bouts (up to 10, corresponding to 10 seconds).

And finally, even though Chen et al. speculate on higher order spatial processing possibilities, since the efficiency of the fish to return to the virtual circle cannot be fully explained by the implementation of aforementioned algorithms, they note it is unlikely: “[it is] not required for the animal to form a spatial representation of the virtual circle.”

3.2 Navigation dynamics of zebrafish larva under a light gradient

This part is a rapid summary of the first section of the article *From behavior to circuit modeling of light-seeking navigation in zebrafish larvae*.

3.2.1 Spontaneous navigation

For the sake of simplicity, we decided to come down to the description of a minimal set of parameters necessary and sufficient for an accurate account of larval locomotion. As mentioned before, larval zebrafish locomotory pattern consists of series of discrete bout movements, each lasting for ~ 200 ms. Those bouts can be simply categorized as either forward (scouts) or reorienting (turns) (Budick & O’Malley, 2000; Burgess & Granato, 2007), which shows on the bimodal distribution of reorientations $\delta\alpha$ (figure 3.3 B).

At each bout, the larva has the choice between performing a forward scoot (F) or a turning bout (T), and, if it triggers a turn, the latter can be oriented either leftward (L) or rightward (R). We modeled this set of choices using a Markov model with 2 chains: a bout type chain and a side chain. The “side state” affects the fish only when it is in the “turn state” (figure 3.3 C)

While the choice between scoot and turn appears to be almost random, successive reorientations bouts on the other hand, are preferentially executed in the same direction. A change in direction occurs every 5 to 6 swim bouts (X. Chen & Engert, 2014; Dunn et al., 2016). This shows when computing the correlation C_q between reorientations of bout n and bout $n + q$: instead of dropping to 0 at the first bout, as expected if the choice of direction were random, the autocorrelation function slowly decays until bouts 7 to 8 (figure 3.3 D). This directional correlation is time-dependent, dropping to 0 for an inter-bout $\tau > 10$ secs (figure 3.3 E).

The distribution of inter-bout intervals τ being quite narrow around the mean (1 sec) and the median (<1 sec), we neglected this time-dependancy in the following analyses and were able to fit a mean probability of turning at each bout: $p_T = 0.41 = 1 - p_F$ and a mean probability of flipping directional states at each bout $p_{flip} = 0.19$ (figure 3.3 C).

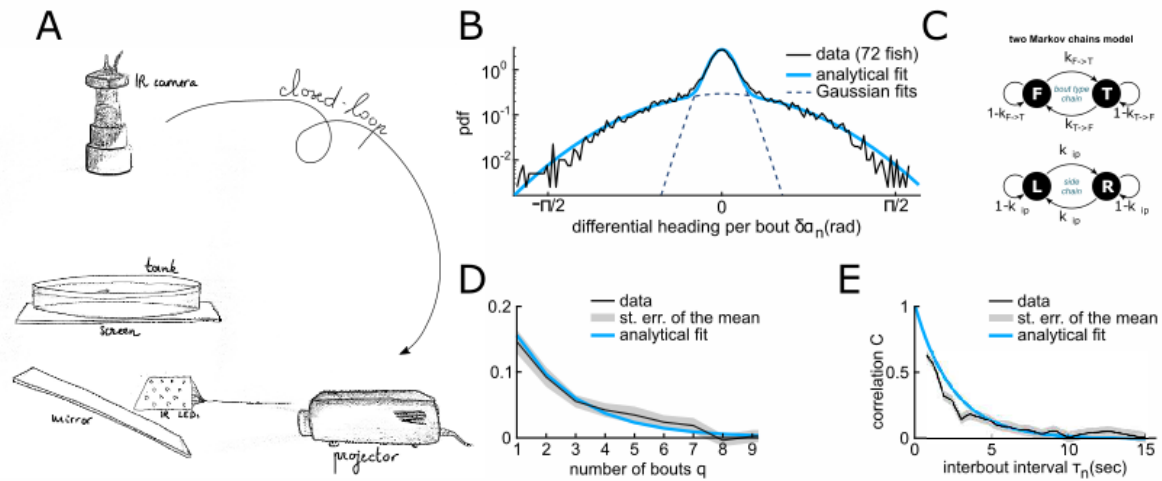


Figure 3.3: (A) Experimental setup: real-time monitoring of the larva's position and orientation using IR illumination, enables closed-loop visual stimulation using a video projector. (B) Experimental (dark) and analytical (blue) distributions (pdf: probability density function) of reorientations $\delta\alpha_n$. (C) Two independent Markov chains model for spontaneous navigation: the bout type chain controls the forward scoot (F) versus turning (T) state. The side chain controls the transitions between left (L) and right (R) headings when the animal is in the turning state, with transition rates which can be converted to the probability p_{flip} . (D) Correlation in reorientation angles C_q as a function of the number of bouts (grey) and associated fit. (E) Orientation correlation of turning bouts as a function of the time elapsed between those bouts. The blue line is the exponential fit.

3.2.2 Orientational light-seeking behavior

The previously mentioned studies set the groundwork for our approach: we wanted to understand the sequence of sensory percepts and motor actions that lead to an effective reorientation towards either a spatially or temporally defined light gradient, hypothesizing, that intrinsic spontaneous dynamics (in the absence of a cue) would be biased by the stimulus.

In order to get a better understanding of the sequence of sensorimotor events that enables a zebrafish larva to reorient with regards to a light stimulus, we decided to make two important simplifications to the problem:

- first regarding the stimulus: instead of being a light source in three-dimensional space, with gradients in all three directions, we locked the stimulus exclusively on the animals orientation (also called heading or yaw) in a closed-loop fashion. Thus the light intensity changes only when the animal reorients - reorientation being a crucial step in light-seeking behavior - but it stays unchanged upon linear displacement.
- then regarding the trajectories: instead of performing a temporal analysis, we discretized the trajectories into sequences of bouts (as we did for the description of spontaneous swimming). At each bout we know both the exact stimulus the animal experienced and its motor action with regards to the stimulus.

It is known, that in generic phototactic conditions, larvae first orient, then swim towards the light source Burgess et al. (2010). Thus they are able to perceive a spatial gradient instantaneously and align themselves to it. In such case, contrast and whole-field intensity act in synergy: aligning to and climbing the gradient implies an equalization of intensity received on left and right eye and also an increase in global perceived intensity. To be able to analyze separately the two phototaxis strategies described in the literature, we separated the contributions of contrast and whole field illumination. When investigating contrast contribution defined by $c = I_L - I_R$, where I_L and I_R are the intensities received respectively by left and right eye, the total intensity $I_L + I_R$ remains constant. And when examining the contribution of whole field intensity I , the animal's eyes receive the same amount of illumination at a time t , the gradient being solely temporal.

We also decided to avoid very abrupt light increments and decrements and thus focus on moderate gradients. This is to avoid very high amplitude responses like escape responses or VMR, which arguably are not part of phototactic behavior, even though they might participate to a light-seeking strategy in some contexts (Burgess & Granato, 2007; Fernandes et al., 2012).

3.2.2.1 In a spatial gradient

In our first experimental paradigm, we investigated how the larva reorients with respect to a visual contrast (figure 3.4 A). Note that this case presents what could be a trade-off, since equalizing the intensities of both eyes implies the reduction of the intensity received by one of the two eyes. The contrast is set to be null ($I_L = I_R$) at an angular distance to the light source $\theta = 0$ (figure 3.4 B).

We found that after a few bouts, the distribution of fish's orientations was statistically biased towards $\theta = 0$ (figure 3.4 C). This bias was mediated by a quasi-linear dependence of the mean reorientation $\langle \delta\theta \rangle$ with contrast c . This dependence is only the result of a bias in the selection of the turning bouts orientation (left vs right): the mean orientation of the turning bouts varies linearly with the imposed contrast (figure 3.4 D). The ratio of turning bouts and the variance of the two distributions do not vary with contrast (figure 3.4 E). These results indicate that stereo-visual contrast has no impact neither on bout type selection nor on bout amplitude.

With a stereo-visual gradient, the selection of the turning orientation is in competition between two distinct mechanisms: motor persistence, which favors the previous bout orientation, and stereo-visual bias, which favors the brighter side. We were able to shed some light on this interference by sorting out bouts with a 'reinforcing stimulus' where the bright side is in the direction of the previous bout, and a 'conflicting' stimulus, in which the contrast tends to evoke a turning bout in a direction opposite to the previous one. We showed that the stereo-visual contrast continuously modulates the innate motor program by increasing or decreasing the probability of flipping bout orientation p_{flip} (figure 3.4 F).

3.2.2.2 In a temporal gradient

In our second paradigm, we looked at how the larva reorients - and whether it can reorient - with respect to a temporal gradient, when direct spatial information is absent (three tested temporal gradients figure 3.5 A).

Despite the absence of any direct orientational cue, a large majority of the larvae displayed positive phototactic behavior: their orientational distribution showed a significant bias towards the virtual light source, that is the direction of maximum intensity (figure 3.5 B-D).

In this case there was no systematic bias of the reorientation bouts towards the brighter direction. Instead, the phototactic process originates from a visually driven modulation of the orientational diffusivity, as measured by the variance of $\delta\theta$: it increases in response to a decrease in relative illumination $\delta I/I$. Both the probability of turning p_T and their amplitude σ_T act in concert to produce this effect (figure 3.5 F-G).

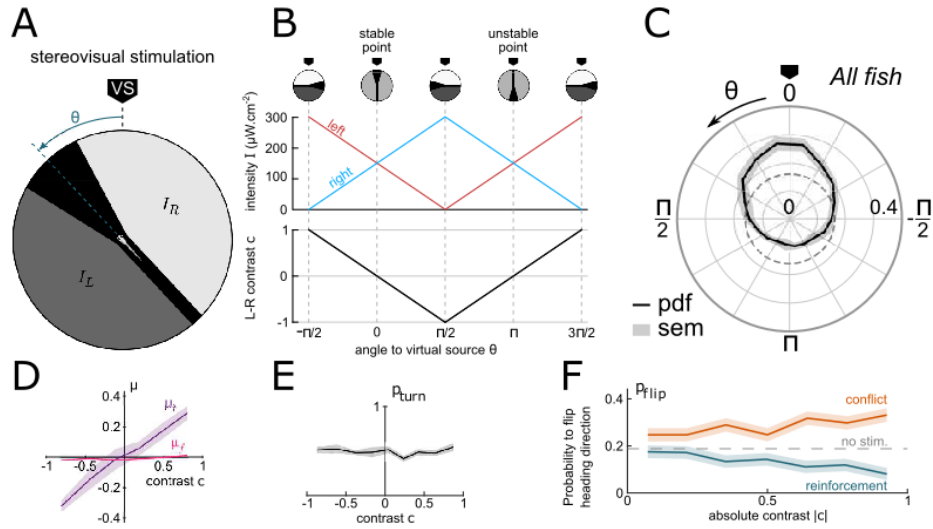


Figure 3.4: Stimulus pattern delivered to the larva. The orientation relative to the virtual source is noted θ . (B) Left and right intensities (top panel) and contrast $c = \frac{I_L - I_R}{I_L + I_R}$ (bottom panel) as a function of θ . The virtual light source is defined by a null contrast ($c = 0$) and corresponds to a stable point ($\frac{dc}{d\theta} < 0$). (C) Probability density function (pdf) of orientations for all tested fish ($N = 47$). (D) Mean and (E) relative weight of the turning distribution as a function of the contrast. For each value of the contrast, these quantities were extracted by double-Gaussian fitting of the bout angles. (F) Probability of switching direction p_{flip} as a function of the contrast, in situations of conflict or reinforcement.

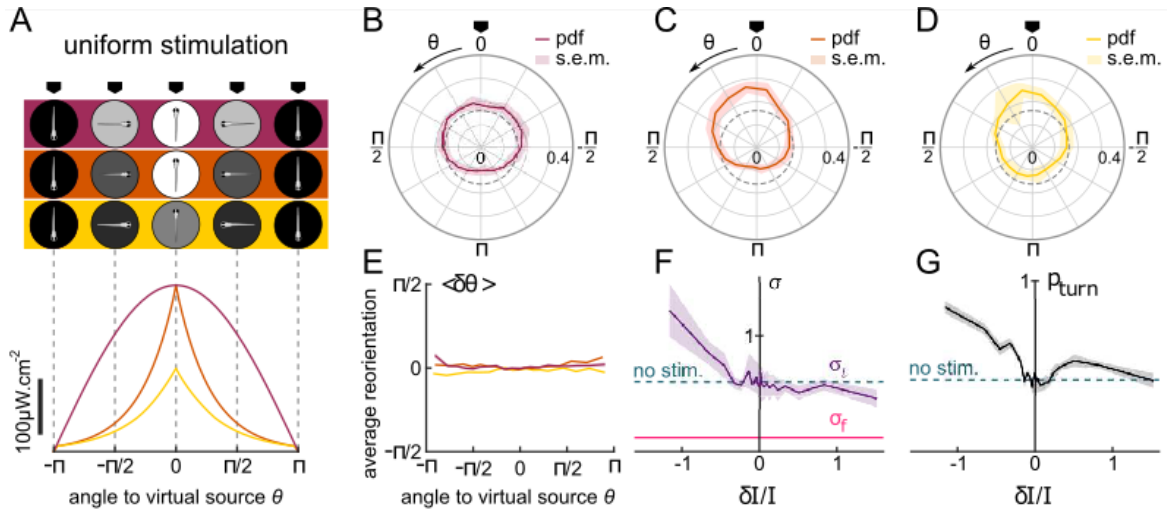


Figure 3.5: (Orientational phototaxis driven by modulation of the global illumination. Top panel : Angle-dependent intensity profiles delivered to the larva. The virtual light source is located at $\theta = 0$, defined as the point of maximum intensity. The profiles are sinusoidal (uniform 1, purple) or exponentially shaped (uniform 2 and 3 orange and yellow, respectively). (B–D) PDF of the fish orientations for the three profiles. (E) Mean reorientation per bout $\langle \delta\theta \rangle$ of all fish as a function of θ for the three profiles. No significant bias towards the source ($\theta = 0$) is observed. (F) Standard deviation σ_{turn} of turning bouts as a function of $\delta I/I$. The standard deviation of forward σ_{fwd} was fixed, and σ_{turn} was then estimated using a double-Gaussian fitting of the bout angles. (G) Probability of triggering a turning bout as a function of $\delta I/I$.

3.3 Article: From behavior to circuit modeling of light-seeking navigation in zebrafish larvae

From behavior to circuit modeling of light-seeking navigation in zebrafish larvae

Sophia Karpenko^{1,2}, Sebastien Wolf^{3,4}, Julie Lafaye¹, Guillaume Le Goc¹, Thomas Panier¹, Volker Bormuth¹, Raphaël Candelier¹, Georges Debrégeas^{1*}

¹Sorbonne Université, CNRS, Institut de Biologie Paris-Seine (IBPS), Laboratoire Jean Perrin (LJP), Paris, France; ²Université Paris Sciences et Lettres, Paris, France; ³Laboratoire de Physique de l'École Normale Supérieure, CNRS UMR 8023 & PSL Research, Paris, France; ⁴Institut de Biologie de l'École Normale Supérieure, CNRS, INSERM, UMR 8197 & PSL Research, Paris, France

Abstract Bridging brain-scale circuit dynamics and organism-scale behavior is a central challenge in neuroscience. It requires the concurrent development of minimal behavioral and neural circuit models that can quantitatively capture basic sensorimotor operations. Here, we focus on light-seeking navigation in zebrafish larvae. Using a virtual reality assay, we first characterize how motor and visual stimulation sequences govern the selection of discrete swim-bout events that subserve the fish navigation in the presence of a distant light source. These mechanisms are combined into a comprehensive Markov-chain model of navigation that quantitatively predict the stationary distribution of the fish's body orientation under any given illumination profile. We then map this behavioral description onto a neuronal model of the ARTR, a small neural circuit involved in the orientation-selection of swim bouts. We demonstrate that this visually-biased decision-making circuit can similarly capture the statistics of both spontaneous and contrast-driven navigation.

*For correspondence:
georges.debregeas@upmc.fr

Competing interests: The authors declare that no competing interests exist.

Funding: See page 16

Received: 19 October 2019

Accepted: 02 January 2020

Published: 02 January 2020

Reviewing editor: Gordon J Berman, Emory University, United States

© Copyright Karpenko et al. This article is distributed under the terms of the [Creative Commons Attribution License](https://creativecommons.org/licenses/by/4.0/), which permits unrestricted use and redistribution provided that the original author and source are credited.

Introduction

Animal behaviors are both stereotyped and variable: they are constrained at short time scale to a finite motor repertoire while the long-term sequence of successive motor actions displays apparent stochasticity. This dual characteristic is immediately visible in the locomotion of small animals such as Nematodes (*Stephens et al., 2008*), Zebrafish (*Girdhar et al., 2015*) or *Drosophila* larvae (*Gomez-Marin and Louis, 2012*), which consists of just a few stereotyped maneuvers executed in a sequential way. In this case, behavior is best described as a set of statistical rules that defines how these elemental motor actions are chained. In the presence of sensory cues, two types of behavioral responses can be distinguished. If they signal an immediate threat or reward (e.g. the presence of a predator or a prey), they may elicit a discrete behavioral switch as the animal engages in a specialized motor program (e.g. escape or hunt, *Budick and O'Malley, 2000; Fiser et al., 2004; Bianco et al., 2011; McClenahan et al., 2012; Bianco and Engert, 2015*). However, most of the time, sensory cues merely reflect changes in external factors as the animal navigates through a complex environment. These weak motor-related cues interfere with the innate motor program to cumulatively promote the exploration of regions that are more favorable for the animal (*Tsodyks et al., 1999; Fiser et al., 2004*).

A quantification of sensory-biased locomotion thus requires to first categorize the possible movements, and then to evaluate the statistical rules that relate the selection of these different actions to the sensory and motor history. Although the probabilistic nature of these rules generally precludes a

eLife digest All animals with the ability to move use sensory signals to help them navigate towards areas that seem better than their current location. Such areas might contain desirable things like food and mates, or they might allow an animal to escape from threats such as predators. But how the brain gives rise to this navigation behavior is unclear.

Karpenko et al. have now obtained insights into the underlying mechanism by studying a behavior in zebrafish larvae called phototaxis. Phototaxis is the tendency to move in response to light. The advantage of using zebrafish larvae to study this behavior is that their brains are small and semi-transparent. This makes it possible to record the activity of almost every neuron. As a result, an individual's brain activity can be mapped on to their behavior more precisely than in most other species.

To probe how visual cues influence fish behavior, Karpenko et al. exposed individual fish to a carefully controlled virtual light source and then tracked their movements with a camera. The fish used two strategies to move towards the light. They selected their next movement based partly on the difference in the amount of light reaching each of their eyes, and partly on the change in overall brightness with each swim movement. Karpenko et al. used this information to build a numerical model of fish phototaxis, and to show how a simple brain circuit could generate this behavior.

Species whose brains differ in size and structure may nevertheless develop similar strategies to perform similar tasks. By quantifying a generic behavior in a simple animal model, this study could provide insights into comparable behaviors in other species. In addition, the study suggests a simple mechanism for how animals select actions on the basis of sensory signals, which may also be relevant to other species and other tasks.

deterministic prediction of the animal's trajectory, they may still provide a quantification of the probability distribution of presence within a given environment after a given exploration time.

In physics terms, the animal can thus be described as a random walker, whose transition probabilities are a function of the sensory inputs. This statistical approach was originally introduced to analyze bacteria chemotaxis (*Lovely and Dahlquist, 1975*). Motile bacteria navigate by alternating straight swimming and turning phases, so-called runs and tumbles, resulting in trajectories akin to random walks (*Berg and Brown, 1972*). Chemotaxis originates from a chemical-driven modulation of the transition probability from run to tumble: the transition rate is governed by the time-history of chemical sensing. How this dependency is optimized to enhance gradient-climbing has been the subject of extensive literature (*Macnab and Koshland, 1972; Adler and Tso, 1974; Mello and Tu, 2007; Yuan et al., 2010; Celani and Vergassola, 2010*). More recently, similar descriptions have been successfully used to quantify chemotaxis and phototaxis in multicellular organisms such as *Caenorhabditis elegans* (*Ward, 1973; Miller et al., 2005; Ward et al., 2008*), *Drosophila* larva (*Sawin et al., 1994; Kane et al., 2013; Gomez-Marin et al., 2011; Tastekin et al., 2018*) or different types of slugs (*Matsuo et al., 2014; Marée et al., 1999*). Although the sensorimotor apparatus of these animals are very different, the taxis strategies at play appear to be convergent and can be classified based on the gradient-sensing methods (*Fraenkel and Gunn, 1961; Gomez-Marin and Louis, 2012*). Tropotaxis refers to strategies in which the organism directly and instantaneously infers the stimulus direction by comparison between two spatially distinct sensory receptors. In contrast, during klinotaxis, the sensory gradient is inferred from successive samplings at different spatial positions. This second strategy is particularly adapted when the organism has only one receptor, or if the sensory gradient across the animal's body is too small to be detected (*Humberg et al., 2018*). It requires at least a basic form of memory, since the sensory information needs to be retained for some finite period of time.

In the present work, we implement such a framework to produce a comprehensive statistical model of phototaxis in zebrafish larvae. Zebrafish larva is currently the only vertebrate system that allows in vivo whole-brain functional imaging at cellular resolution (*Panier et al., 2013; Ahrens et al., 2013*). It thus provides a unique opportunity to study how sensorimotor tasks, such as sensory-driven locomotion, are implemented at the brain-scale level.

Although adult zebrafish are generally photophobic (or scototactic, *Serra et al., 1999; Maximino et al., 2007*), they display positive phototaxis at the larval stage, from 5 days post-fertilization (dpf) on *Orger and Baier (2005)*. At this early stage, their locomotion consists of a series of discrete swimming events interspersed by ~ 1 s long periods of inactivity (*Girdhar et al., 2015*). Previous studies have shown that, when exposed to a distant light source, the first bouts executed by the fish tend to be orientated in the direction of the source (tropotaxis) (*Burgess et al., 2010*). Furthermore, *Chen and Engert (2014)* have shown, using a virtual reality assay, that zebrafish are able to confine their navigation within a bright region in an otherwise dark environment even when deprived from stereovisual contrast information. This latter study thus established that their phototactic behavior also involves a spatio-temporal integration mechanism (klinotaxis).

From a neuronal viewpoint, recent calcium imaging experiments identified a small circuit in the rostral hindbrain that plays a key role in phototaxis (*Ahrens et al., 2013; Dunn et al., 2016; Wolf et al., 2017*). This region, called ARTR (anterior rhombencephalic turning region) or HBO (hindbrain oscillator), displays pseudo-periodic antiphase oscillations, such that the activity of the left and right subpopulations alternate with a ~ 20 s period. This alternation was shown to set the coordinated direction of the gaze and tail bout orientation, thus effectively organizing the temporal sequence of the successive reorientations. It was further shown that this circuit oscillation could be driven by whole-field illumination of the ipsilateral eye, such as to favor the animal's orientation towards a light source (*Wolf et al., 2017*).

In the present study, we aim at quantifying the statistical rules that control the larva's reorientation dynamics in the presence of a continuous angular gradient of illumination (orientational phototaxis). Using a virtual-reality closed-loop assay, we quantify how swim bouts selection is statistically controlled by the light intensity received on both eyes prior to the bout initiation, or the change in illumination elicited by the previous swim bout. Our experimental configuration allows us to disentangle the contribution of the two aforementioned strategies: tropotaxis and klinotaxis. From the analysis of this short-term behavior, we built a minimal Markov model of phototaxis, from which we compute the long-term distribution of orientations for any angular profile of illumination. This model offers explicit predictions of the statistics of the fish orientation that quantitatively compare with the experimental observations. We further expand on a recent rate model of the ARTR circuit to propose a functional neuronal model of spontaneous navigation and contrast-biased orientation selection. We demonstrate that the statistics of turn orientation can be fully understood by assuming that this self-oscillating circuitry, that selects the orientation of turning bouts, integrates stereovisual contrast in the form of incoming currents proportional to the visual stimulus.

Results

Kinematics of spontaneous navigation as a first-order autoregressive process

Zebrafish larvae aged 5–7 dpf were placed one at a time in a Petri dish (14 cm in diameter). Their center-mass position and body axis orientation were tracked in real time at 35 frames/s (*Figure 1A–B*). This information was used to deliver a body-centered visual stimulus using a video-projector directed onto a screen supporting the Petri dish.

Prior to each phototactic assay, the larva was allowed an ≈ 8 min-long period of spontaneous exploration under uniform and constant illumination at maximum intensity $I_{max} = 450 \mu W.cm^{-2}$. Such pre-conditioning phases were used to promote light-seeking behavior (*Burgess and Granato, 2007*), while enabling the quantification of the basal exploratory kinematics for each fish.

Larval zebrafish navigation is comprised of discrete swim bouts lasting $\approx 100ms$ and interspersed with 1 to 2s-long inter-bout intervals (τ_n) during which the fish remains still (*Dunn et al., 2016*). Each bout results in a translational motion of the animal and/or a change in its body axis orientation, and can thus be automatically detected from kinematic parameters. As we are mostly interested in the orientational dynamics, we extracted a discrete sequence of orientations α_n measured just before each swimming event n (*Figure 1B–C*) from which we computed the bout-induced reorientation angles $\delta\alpha_n = \alpha_{n+1} - \alpha_n$.

Although the complete swim bouts repertoire of zebrafish larvae is rich and complex (*Johnson et al., 2019*), the statistical distribution of the reorientation angles $P(\delta\alpha_n)$ in such unbiased

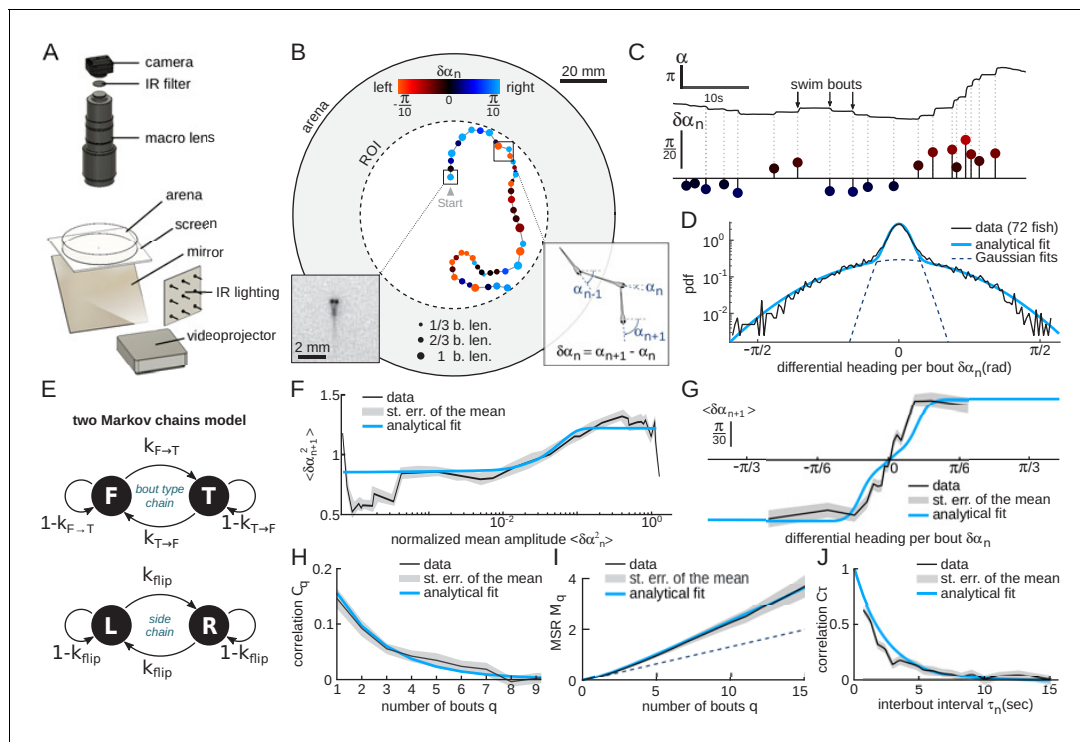


Figure 1. Kinematics of spontaneous navigation. $N = 75$ fish, $n = 16, 147$ bouts, mean of 7 trajectories per fish. (A) Experimental setup: real-time monitoring of the larva's position and orientation using IR illumination, enables closed-loop visual stimulation using a video projector. (B) Typical trajectory of a 6 days old larva in the region of interest (ROI) of the arena under constant, uniform illumination. Each point indicates the fish position at the onset of a swim bout. Dots' size and color encode the bout distance and bout reorientation angle, respectively. Insets: blow-up of an example frame (left) and definition of the reorientation angle $\delta\alpha_n$ at bout index n (right). b.len: body length. (C) Time-sequence of the fish body orientation α (top). Swim bouts elicit rapid re-orientations. The angular dynamics can thus be represented as a series of discrete reorientation events of various amplitudes $\delta\alpha_n$ (color code as in (B)). (D) Experimental (dark) and analytical (blue) distributions (pdf: probability density function) of reorientations $\delta\alpha_n$. The two normal distributions used in the fit with **Equation A1**, weighted by p_{turn} and $1 - p_{turn}$, are also displayed in dashed blue lines. (E) Two independent Markov chains model for spontaneous navigation: the *bout type chain* controls the forward scoot (F) versus turning (T) state, with transitions rates $k_{T \rightarrow F}$ and $k_{F \rightarrow T}$. The *side chain* controls the transitions between left (L) and right (R) headings when the animal is in the turning state, with transition rate k_{flip} . (F) Mean squared reorientation amplitude of bout $n + 1$ as a function of the squared amplitude of bout n (grey), and its associated analytical fit (blue, Appendix From behavior to circuit modeling of light-seeking navigation in zebrafish larvae **Equation A5**). (G) Average reorientation of bout $n + 1$ as a function of the reorientation at bout n (grey), and its associated analytical fit (blue, **Equation A11**). (H) Correlation in reorientation angles C_q as a function of the number of bouts (grey) and associated fit (blue, **Equation A14**). (I) Mean square reorientation (MSR) M_q as a function of the number of bouts, and associated fit (blue, **Equation A17**). The dotted line is the linear extrapolation of the first two data points and corresponds to the diffusive process expected for a memory-less random walk (no correlation in bout orientation). (J) Orientation correlation of turning bouts (thresholded at 0.22rad) as a function of the time elapsed between those bouts. The blue line is the exponential fit. Data from this and the following figures are available at **Karpenko (2019a)** (copy archived at https://github.com/elifesciences-publications/programs_closed-loop_phototaxis).

conditions can be correctly captured by the weighted sum of two zero-mean normal distributions, $P(\delta\alpha_n) = p_{turn}\mathcal{N}(0, \sigma_{turn}^2) + p_{fwd}\mathcal{N}(0, \sigma_{fwd}^2)$, reflecting the predominance of only two distinct bouts types: turning bouts (standard deviation $\sigma_{turn} = 0.6$) and forward scoots ($\sigma_{fwd} = 0.1$) (**Figure 1D**). This bimodal distribution is consistent with the locomotor repertoire of larvae described by **Marques et al. (2018)** during spontaneous swimming and phototactic tasks. In the absence of a visual bias, the turning bouts and forward scoots were found to be nearly equiprobable, $p_{turn} = 1 - p_{fwd} = 0.41$.

Successive bouts were found to exhibit a slightly positive correlation in amplitude (**Figure 1F**). This process can be captured by a two-state Markov-chain model that controls the alternation between forward and turning bouts, while the amplitude within each population is randomly sampled from the corresponding distribution (**Figure 1E**). Within this scheme, we analytically derived the dependence in the amplitude of successive bouts and thus estimated the forward-to-turn and turn-to-forward transition rates, noted $k_{f \rightarrow t}$ and $k_{t \rightarrow f}$ (all analytical derivations are detailed in Appendix

From behavior to circuit modeling of light-seeking navigation in zebrafish larvae). We found that $k_{f \rightarrow t}/p_{turn} = k_{t \rightarrow f}/p_{fwd} \approx 0.8$. This indicates that the probability to trigger a turn (*resp.* forward) bout is decreased by only 20% if the previous bout is a forward (*resp.* turn) bout. For the sake of simplicity, we ignore in the following this modest bias in bout selection and assume that the chaining of forward and turning bout is memory-less by setting $k_{f \rightarrow t} = p_{turn}$ and $k_{t \rightarrow f} = p_{fwd}$. We checked, using numerical simulations, that this simplifying assumption has no significant impact on the long-term navigational dynamics: the results presented in the following, notably the diffusion coefficient, remain essentially unchanged when this small correlation in bout type selection is taken into account.

In line with previous observations (Chen and Engert, 2014; Dunn et al., 2016), we also noticed that successive turning bouts tended to be oriented in the same (left or right) direction (Figure 1G). This orientational motor persistence was accounted for by a second Markov chain that set the orientation of turning bouts, and was controlled by the rate of flipping direction noted k_{flip} (Figure 1E bottom). Notice that, in contrast with the model proposed by Dunn et al. (2016), although the orientational state is updated at each bout, it only governs the direction of turning bouts. When a forward bout is triggered, its orientation is thus unbiased.

This model provides an analytical prediction for the mean reorientation angle $\langle \delta\alpha_n \rangle_{\delta\alpha_{n-1}}$ at bout n following a reorientation angle $\delta\alpha_{n-1}$ at bout $n - 1$. This expression was used to fit the experimental data (Figure 1G) and allowed us to estimate the flipping rate $p_{flip} = 0.19$ (99% confidence bounds ± 0.017). We further computed the autocorrelation function of the reorientation angles and the Mean Square Reorientation (MSR) accumulated after n bouts (Figure 1H–I). Both were consistent with their experimental counterparts. In particular, this model quantitatively captures the ballistic-to-diffusive transition that stems from the directional persistence of successive bouts (Figure 1I). As a consequence, the effective rotational diffusivity at long time $D_{eff} = 0.3rad^2$ is about twice as large than the value expected for a memory-less random walk (i.e. with $p_{flip} = 0.5$, see dashed line in Figure 1I).

In this discrete Markov-chain model, time is not measured in seconds but corresponds to the number of swim bouts. It thus implicitly ignores any dependence of the transition rates with the interbout interval. We examined this hypothesis by evaluating the correlation in bouts orientations as a function of the time elapsed between them. To do so, we first sorted the turning bouts by selecting the large amplitude events ($|\delta\alpha| < 0.22rad$). We then binarized their values, based on their leftward or rightward orientation, yielding a discrete binary signal $s(t_n) = \pm 1$. We finally computed the mean product $\langle s(t_n)s(t_p) \rangle$ for various time intervals $\Delta t = t_p - t_n$. The resulting graph, shown in Figure 1J, demonstrates that the correlation in orientation of successive bouts decays quasi-exponentially with the inter-bout period. This mechanism can be captured by assuming that the orientation selection at each bout is governed by a hidden two-state continuous-time process. The simplest one compatible with our observations is the telegraph process, whose transition probability over a small interval dt reads $k_{flip}dt$, and whose autocorrelation decays as $\exp(-2k_{flip}t)$. Setting $k_{flip} = p_{flip}/median(\tau_n) = 0.2s^{-1}$, this model correctly captures the τ_n -dependence of the orientational correlation of bouts.

In the two following sections, we use the discrete version of the Markov-chain model to represent the fish navigation, and investigate how the model parameters are modulated in the presence of a virtual distant light source. We then go back to the underlying continuous-time process when introducing a neuronal rate model for the orientation selection process.

Contrast-driven phototaxis can be described as a biased random walk

We first examined the situation in which the perceived stereo-visual contrast is the only cue accessible to the animal to infer the direction of the light source (tropotaxis regime). The visual stimulus consisted of two uniformly lit half-disks, each covering one visual hemifield. The intensity delivered to the left and right eyes, noted I_L and I_R respectively, were locked onto the fish's orientation θ relative to the virtual light source (Figure 2A): the total intensity ($I_L + I_R$) was maintained constant while the contrast $c = I_L - I_R$ was varied linearly with θ , with a mirror symmetry at $\pi/2$ (Figure 2B). This dependence was chosen to mimic the presence of a distant source located at $\theta = 0$ for which the contrast is null.

The orientation of the virtual source in the laboratory frame of reference was randomly selected at initiation of each assay. After only a few bouts, the animal orientation was found to be statistically

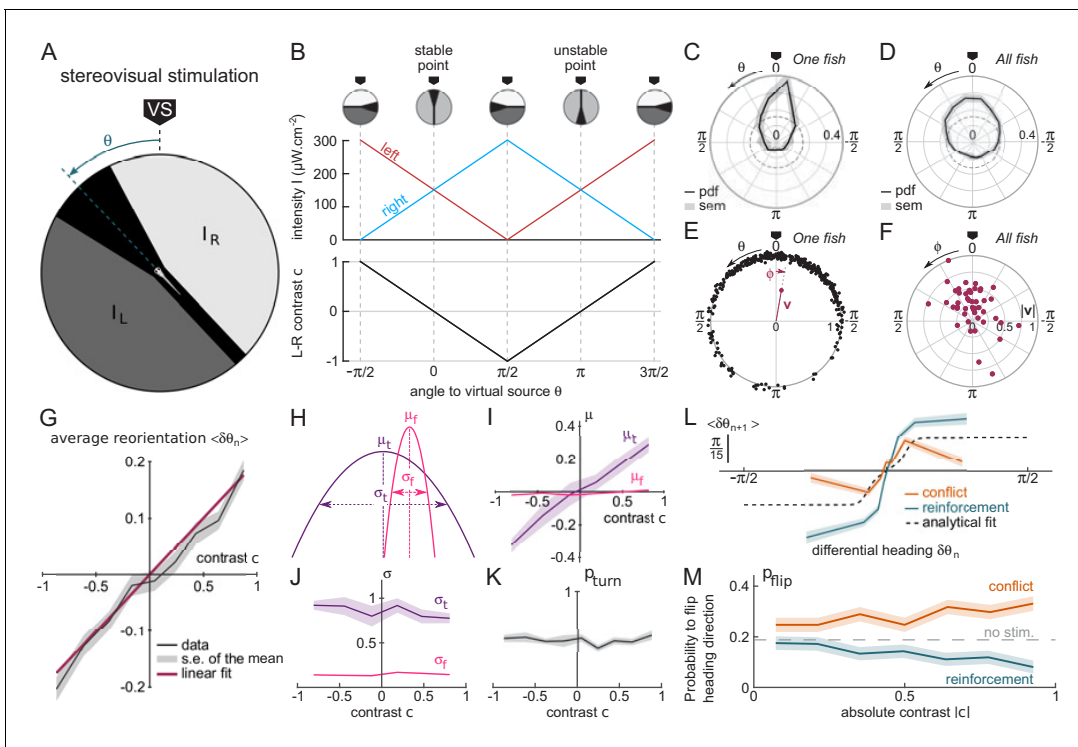


Figure 2. Contrast-driven phototaxis as a biased random walk. $N = 47$ fish, 18, 322 bouts, mean of 13 trajectories per fish. All statistical analyses are performed on the first 17 bouts, the first one excluded, for each assay. VS : virtual source. (A) Stimulus pattern delivered to the larva. The orientation relative to the virtual source is noted θ . (B) Left and right intensities (top panel) and contrast $c = \frac{I_L - I_R}{I_L + I_R}$ (bottom panel) as a function of θ . The virtual light source is defined by a null contrast ($c = 0$) and corresponds to a stable point ($\frac{dc}{d\theta} < 0$). (C) Probability density function (pdf) of orientations relative to the virtual light source for one fish during 20 trials, bouts 2 to 17 ($n = 320$ bouts). (D) Probability density function (pdf) of orientations for all tested fish ($N = 47$). Significantly biased toward the virtual source (V-test for non-uniformity with specified mean 0, $p_{val} < 10^{-11}$) (E) Definition of the mean resultant vector \mathbf{v} for one fish. The points represent the angular positions θ_n of the fish relative to the source. The vector \mathbf{v} is defined as $\mathbf{v} = \frac{1}{N} \sum \exp i\theta_n$. The mean angle to the source is $\phi = \arg(\mathbf{v})$ (F) Resultant vectors \mathbf{v} for individual fish. (G) Mean reorientation $\langle \delta\theta_n \rangle$ per bout as a function of contrast c for all fish. Error bars represent the standard error of the mean. Red line is the linear fit with slope 0.2 rad. (H) Illustration of the shift in turning distribution ($\mu_t < 0$) induced by a negative contrast. (I) Means, (J) standard deviations and (K) relative weight of the turning distribution as a function of the contrast. For each value of the contrast, these quantities were extracted by double-Gaussian fitting of the bout angles. The error bars represent the 99% confidence interval from the fit. (L) Average reorientation at bout $n + 1$ as a function of the reorientation at bout n in reinforcing (contrast and previous bout orientation are consistent) or conflicting (contrast and previous bout orientation are in conflict) situations. The dashed line is the analytical prediction in the absence of stimulation. (M) Probability of switching direction p_{flip} as a function of the contrast, in situations of conflict or reinforcement. The online version of this article includes the following figure supplement(s) for figure 2:

Figure supplement 1. Evolution of the mean resultant vector projected on the direction of the virtual light source with the bout index.

Figure supplement 2. Evolution of contrast-driven bias slope with the bout index.

biased towards $\theta = 0$, as shown in **Figure 2C–D**. This bias was quantified by computing the population resultant \mathbf{v} defined as the vectorial mean of all orientations (**Figure 2E**).

Trajectories that are strongly biased towards the source tend to exit the ROI earlier than unbiased trajectories, which are more tortuous and thus more spatially confined. This generates a progressive selection bias as the number of bouts considered is increased, as revealed by the slow decay of the resultant vector length (**Figure 2—figure supplement 1**). In order to mitigate this selection bias, all analyses of stationary distributions were restricted to bout indices lower than the median number of bouts per trial ($N \leq 17$), and excluding the first bout. Under this condition, we found that ~77% of zebrafish larvae display a significant phototactic behavior (**Figure 2D–F**, test of significance based on a combination of two circular statistic tests, see Materials and methods), a fraction consistent with values reported by **Burgess et al. (2010)** in actual phototactic assays .

From these recordings, we could characterize how the contrast experienced during the inter-bout interval impacts the statistics of the forthcoming bout. **Figure 2G** displays the mean reorientation

$\langle \delta\theta \rangle$ as a function of the instantaneous contrast c . This graph reveals a quasi-linear dependence of the mean reorientation with c , directed toward the brighter side. Notice that the associated slope shows a significant decrease in the few first bouts, before reaching a quasi-constant value (**Figure 2—figure supplement 2**). This effect likely reflects a short term habituation mechanism as the overall intensity drops by a factor of 2 at the initiation of the assay.

For a more thorough analysis of the bout selection mechanisms leading to the orientational bias, we examined, for all values of the contrast, the mean and variance of the two distributions associated with turning bouts and forward scoots, as well as the fraction of turning bouts p_{turn} (**Figure 2H–K**). We found that the orientational drift solely results from a probabilistic bias in the selection of the turning bouts (left vs right) orientation: the mean orientation of the turning bouts varies linearly with the imposed contrast (**Figure 2I**). Reversely, the ratio of turning bouts and the variance of the two distributions are insensitive to the contrast (**Figure 2J–K**). These results indicate that the stereo-visual contrast has no impact neither on bout type selection nor on bout amplitude.

As discussed in the preceding section, in the absence of visual cue, successive bouts tend to be oriented in the same direction. During phototaxis, the selection of the turning orientation is thus expected to reflect a competition between two distinct mechanisms: motor persistence, which favors the previous bout orientation, and stereo-visual bias, which favors the brighter side. To investigate how these two processes interfere, we sorted the bouts into two categories. In the first one, called ‘reinforcement’, the bright side is in the direction of the previous bout, such that both the motor and sensory cues act in concert. In the second one, called ‘conflicting’, the contrast tends to evoke a turning bout in a direction opposite to the previous one. For each category, we plotted the mean reorientation angle at bout n as a function of the reorientation angle at bout $n - 1$ (**Figure 2L**). We further estimated, for each condition and each value of the contrast, the probability of flipping orientation p_{flip} (**Figure 2M** and Appendix 2). These two graphs show that the stereo-visual contrast continuously modulates the innate motor program by increasing or decreasing the probability of flipping bout orientation from left to right and vice versa. Noticeably, in the conflicting situation at maximum contrast, the visual cue and motor persistence almost cancel each other out such that the mean orientation is close to ($p_{flip} \sim 0.4$).

Phototaxis under uniform stimulation is driven by a modulation of the orientational diffusivity

We now turn to the second paradigm, in which the stereo-visual contrast is null (both eyes receive the same illumination at any time), but the total perceived illumination is orientation-dependent (klinotaxis regime). We thus imposed a uniform illumination to the fish whose intensity I was locked onto the fish orientation θ relative to a virtual light source. We tested three different illumination profiles $I(\theta)$ as shown in **Figure 3A**: a sinusoidal and two exponential profiles with different maxima. Despite the absence of any direct orientational cue, a large majority of the larvae (78%) displayed positive phototactic behavior: their orientational distribution showed a significant bias towards the virtual light source, that is the direction of maximum intensity (**Figure 3B–E**).

Although the efficiency of the phototactic behavior is comparable to the tropotaxis case previously examined, here we did not observe any systematic bias of the reorientation bouts towards the brighter direction (**Figure 3F**). This indicates that the larvae do not use the change in intensity at a given bout to infer the orientation of the source in order to bias the orientation of the forthcoming turn. Instead, the phototactic process originates from a visually driven modulation of the orientational diffusivity, as measured by the variance of the bout angle distributions (**Figure 3G**). The use of different profiles allowed us to identify which particular feature of the visual stimulus drives this modulation. Although the bout amplitude variance was dependent on the intensity I and intensity change δI experienced before the bout, these relationships were found to be inconsistent across the different imposed intensity profiles. In contrast, when plotted as a function of $\delta I/I$, all curves collapse (**Figure 3—figure supplement 1**). This observation is in line with the Weber-Fechner law (**Fechner, 1860**), which states that the perceived change scales with the relative change in the physical stimulus. One noticeable feature of this process is that the modulation of the turning amplitude is limited to illumination *decrement* (i.e. negative values of $\delta I/I$). In the terminology of bacterial chemotaxis (**Oliveira et al., 2016**), the zebrafish larva can thus be considered as a ‘pessimistic’ phototactic animal: the orientational diffusivity increases in response to a decrease in illumination

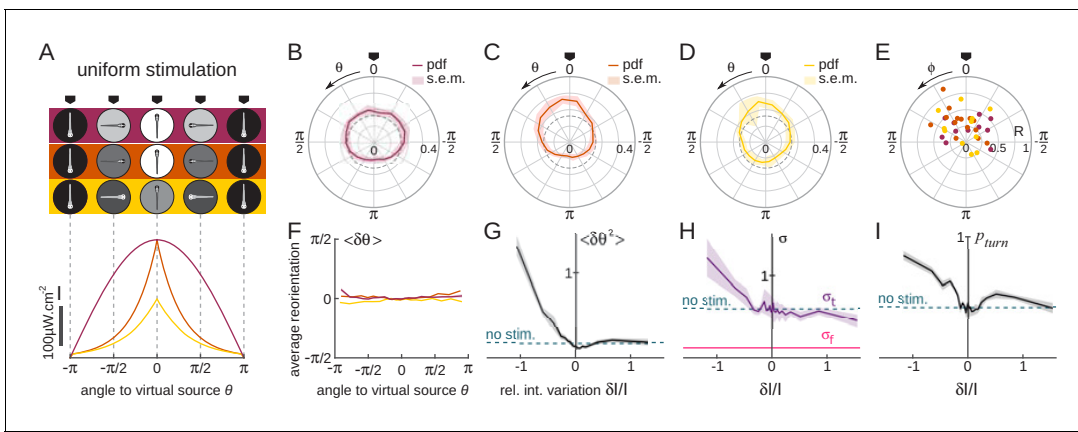


Figure 3. Orientational phototaxis driven by modulation of the global illumination. $N = 37$ fish, $n = 26,443$ bouts, mean of 23 trajectories per fish. (A) Top panel: Angle-dependent intensity profiles delivered to the larva. The virtual light source is located at $\theta = 0$, defined as the point of maximum intensity. The profiles are sinusoidal (uniform 1, purple) or exponentially shaped (uniform 2 and 3 orange and yellow, respectively). All statistics were computed using bout index two to the median number of bouts per sequence (resp. 27, 17 and 15 for the three profiles). (B–D) PDF of the fish orientations for the three profiles. All three distributions are significantly biased towards the virtual source (V-test for non-uniformity of circular data with specified mean, p_{vals} respectively 9.10^{-3} , 2.10^{-7} and 3.10^{-5}). (E) Resultant vector v for all individual fish. (F) Mean reorientation per bout $\langle \delta\theta \rangle$ of all fish as a function of θ for the three profiles. No significant bias towards the source ($\theta = 0$) is observed. (G) Variance of the reorientation angles $\langle \delta\theta^2 \rangle$ as a function of the relative change in intensity experienced at the previous bout $\delta I/I$. Error bars are standard error of the mean. (H) Standard deviation σ_{turn} of turning bouts as a function of $\delta I/I$. The standard deviation of forward scouts was set at σ_{fwd} , and σ_{turn} was then estimated using a double-Gaussian fitting of the bout angles. Error bars are the 99% confidence interval from fit. (I) Probability of triggering a turning bout as a function of $\delta I/I$. Error bars are the 99% confidence interval from the fit.

The online version of this article includes the following figure supplement(s) for figure 3:

Figure supplement 1. Variance of $\delta\theta$ as a function of three different illumination parameters.

Figure supplement 2. Control for retinal origin of klinotaxis.

(corresponding to a negative subjective value), whereas its exploratory kinematics remain unchanged upon an increase of illumination (positive subjective value).

Two kinematic parameters can possibly impact the orientational diffusivity: the fraction of turning bouts p_{turn} and their characteristic amplitude σ_{turn} . We thus extracted these two quantities and plotted them as a function of $\delta I/I$ (Figure 3H–I). They appear to equally contribute to the observed modulation.

To test whether this uniform phototactic process has a retinal origin, or whether it might be mediated by non-visual deep-brain photoreceptors (Fernandes et al., 2012), we ran similar assays on binucleated fish. In this condition, no orientational bias was observed, which indicates that the retinal pathway is involved in orientational klinotaxis (Figure 3—figure supplement 2, all p-values > 0.14, pairwise T-tests).

A biased random walk model for phototaxis provides a quantitative prediction of light-driven orientational bias

In the preceding sections, we quantified how visual stimuli stochastically modulate specific kinematic parameters of the subsequent bout. We used these relationships to build a biased random walk model of phototaxis. We then tested how such a model could reproduce the statistical orientational biases toward the directions of minimal contrast and maximal illumination. The phototactic model thus incorporates a visually-driven bias to the discrete Markov-chain model introduced to represent the spontaneous navigation (Figure 4A). In line with the observation of Figure 2M, the rate of flipping orientational state (left-to-right or right-to-left) was a linear function of the imposed contrast: $k_{R \rightarrow L} = k_{flip} + ac$ and $k_{L \rightarrow R} = k_{flip} - ac$. The value of a was set so as to capture the contrast-dependent orientational drift (Figure 2G) and was made dependent on bout index in order to account for the observed short-term habituation process (Figure 2—figure supplement 2).

The selection of bout type was in turn linearly modulated by the relative change in intensity after negative rectification, $[\delta I/I]^- = \min(\delta I/I, 0)$. Hence, the turn-to-forward and forward-to-turn transition

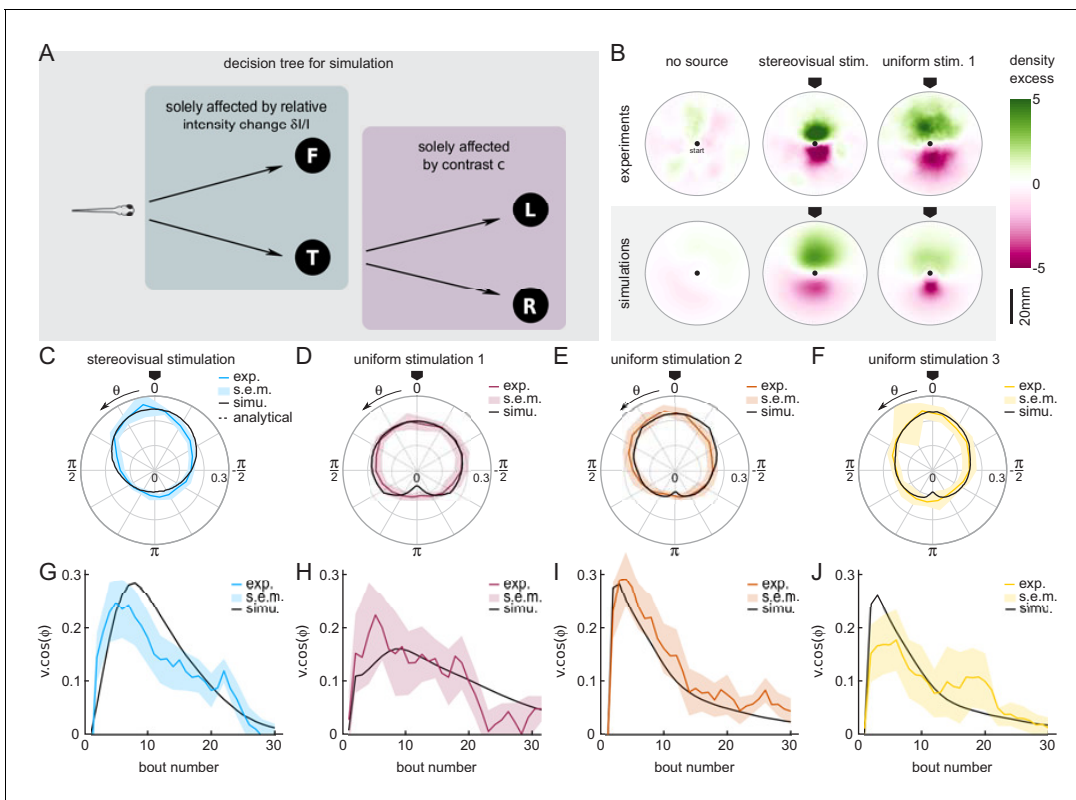


Figure 4. A Markov-chain model of phototaxis captures the observed orientational distribution. (A) Decision tree for simulation: selection of forward scoots vs turning bouts are governed by the relative intensity change at the previous bout. If a turning bout is triggered, the selection of left-right orientation is biased by the stereovisual contrast. (B) 2D density profiles computed from all experimental and simulated trajectories for the three different paradigms (no stimulation, lateralized illumination and uniform illumination). The color encodes the excess or deficit of density with respect to the radially-averaged density without any stimulation. (C–F) Experimental (color) and simulation (solid line) probability density distributions of orientations for the four phototactic configurations (stereo-visual stimulation, uniform stimulation with angular profiles 1 to 3). (G–J) Evolution of the projection of the resultant vector onto the direction of the light source as a function of the bout number for the experiment (color) and simulation (solid line). Error bar : standard error of the mean.

The online version of this article includes the following figure supplement(s) for figure 4:

Figure supplement 1. Inter-bout distance distribution.

rates read $k_{t \rightarrow f} = k_{turn} + \beta[\delta I/I]^-$ and $k_{f \rightarrow t} = k_{turn} - \beta[\delta I/I]^-$, respectively. We also imposed a linear modulation of the turn amplitude variance $\sigma_{turn} = \sigma_{turn}^{spont} - \gamma[\delta I/I]^-$. The values of β and γ were adjusted to reproduce the observed dependence of the turn-vs-forward ratio and bout amplitude with $\delta I/I$ (Figure 3H–I).

This stochastic model was tested under two conditions, tropo- and klino-phototaxis, similar to those probed in the experiments (Figure 4B). In order to account for the sampling bias associated with the finite size of the experimental ROI, the particles in the simulations also progressed in a 2D arena. At each time step, a forward displacement was drawn from a gamma distribution adjusted on the experimental data (Figure 5—figure supplement 1). Statistical analysis was restricted to bouts executed within a circular ROI as in the experimental assay.

The comparison of the data and numerical simulation is shown in Figure 4C for the tropotaxis protocol and in Figure 4D–F for the klinotaxis protocols. This minimal stochastic model quantitatively captures the distribution of orientations. It also reproduces the evolution of the orientational bias with the bout index as measured by the length of the resultant vector (Figure 4G–J).

A neuronal model of the ARTR captures spontaneous and contrast-driven navigation

The behavioral description proposed above indicates that larvae navigation can be correctly accounted for by two independent stochastic processes: one that organizes the sequence of successive bouts amplitude and in particular the selection of forward vs turning events, while a second one selects the left vs right orientation of the turning bouts. These two processes are independently modulated by two distinct features of the visual stimulus, namely the global intensity changes and the stereo-visual contrast, leading to the two phototactic strategies.

This in turn suggests that, at the neuronal level, two independent circuits may control these characteristics of the executed swim bouts. As mentioned in the introduction, the ARTR is a natural candidate for the neuronal selection of bouts orientation. This small bilaterally-distributed circuit located in the anterior hindbrain displays antiphasic activity oscillation with ~ 20 s period (Ahrens et al., 2013). The currently active region (left or right) constitutes a strong predictor of the orientation of turning bouts (Dunn et al., 2016). This circuit further integrates visual inputs as each ARTR subpopulation responds to the stimulation of the ipsilateral eye (Wolf et al., 2017).

Here, we adapted a minimal neuronal model of the ARTR, introduced in Wolf et al. (2017) to interpret the calcium recordings, and tested whether it could explain the observed statistics of exploration in both spontaneous and phototactic conditions. The architecture of the model is depicted in Figure 5A and the equations governing the network dynamics are provided in Appendix 2. The network consists of two modules selective for leftward and rightward turning, respectively. Recurrent excitation (w_E) drives self-sustained persistent activities over finite periods of time. Reciprocal inhibition (w_I) between the left and right modules endows the circuit with an antiphasic dynamics. Finally, each ARTR module receives an input current from the visual system proportional to the illumination of the ipsilateral eye. Such architecture gives rise to a stimulus-selective attractor as described in Freeman (1995) and Wang (2002).

The various model parameters were adjusted in order to match the behavioral data (see Appendix 2). First, the self-excitatory and cross-inhibitory couplings were chosen such that the circuit displayed spontaneous oscillatory dynamics in the absence of sensory input. Figure 5B shows example traces of the two units' activity in this particular regime. From these two traces, we extracted a binary 'orientational state' signal by assigning to each time point a left or right value (indicated in red and blue, respectively), based on the identity of the module with the largest activity.

In the present approach, tail bouts are assumed to be triggered independently of the ARTR activity. The latter thus acts as mere orientational hub by selecting the orientation of the turning events: incoming bouts are oriented in the direction associated with the currently active module. In the absence of information regarding the circuit that organizes the swim bouts emission, their timing and absolute amplitude were drawn from the behavioral recordings of freely swimming larvae. Combined with the ARTR dynamics, this yielded a discrete sequence of simulated bouts (leftward, rightward and forward, Figure 5B, inset). With adequate choice of parameters, this model captures the orientational persistence mechanism as quantified by the slow decay of the turning bout autocorrelation with the interbout interval (Figure 5C and Figure 5—figure supplement 1).

In the presence of a lateralized visual stimulus, the oscillatory dynamics become biased towards the brighter direction (Figure 5D–E). Hence, illuminating the right eye favors longer periods of activation of the rightward-selective ARTR unit. The mean reorientation displays a quasi-linear dependence with the imposed contrast (Figure 5D) consistent with the behavioral observations (Figure 2G). At intermediate contrast values, the orientation of bouts remains stochastic; the effect of the contrast is to lengthen streaks of turning bouts toward the light (Figure 5E). We also tested whether this model could capture the competition mechanism between stereovisual bias and motor persistence, in both conflicting and reinforcement conditions. We thus computed the dependence of the flipping probability p_{flip} as a function of the contrast in both conditions (Figure 5F). The resulting graph is in quantitative agreement with its experimental counterparts (Figure 2M).

We finally used this model to emulate a simulated phototactic task. In order to do so, a virtual fish was submitted to a contrast whose amplitude varied linearly with the animal orientation, as in the lateralized assay. When a turning bout was triggered, its orientation was set by the ARTR instantaneous activity while its amplitude was drawn from the experimental distributions. After a few bouts, a stationary distribution of orientation was reached that was biased toward the virtual light

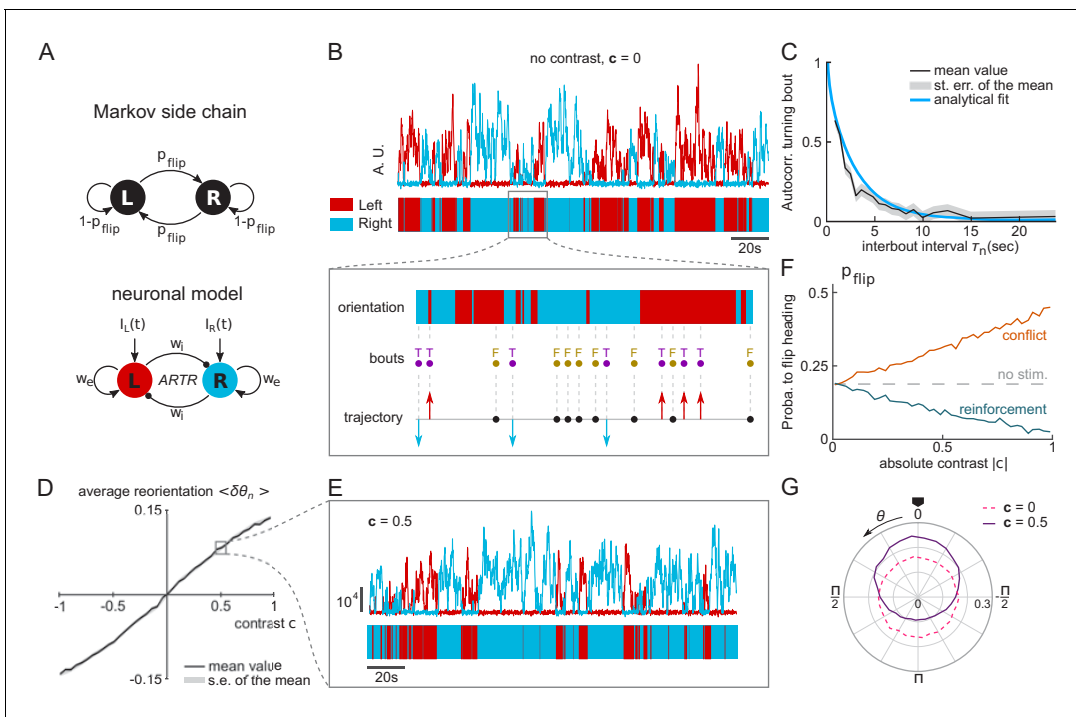


Figure 5. A neuronal model of turning bout selection captures spontaneous and contrast-driven navigation. (A) Scheme of the Markov-chain model of the orientation selection, and corresponding neuronal model of the ARTR. The latter consists of two units whose relative activation controls the orientation of bouts. Persistent and self-alternating dynamics result from the recurrent excitation (w_e) and reciprocal inhibition (w_i) between each unit. They further receive input currents proportional to the illumination of the ipsilateral eye. (B) Top: example traces of the simulated activity of the left (red) and right (blue) modules in the absence visual stimulation (AU : arbitrary units). These continuous dynamics control the alternation between right and left orientational states. Close-up: forward and turning bouts are triggered independently with a statistics drawn from the behavioral recordings. The orientational state governs the orientation of the turning bouts. (C) Orientation correlation of turning bouts (thresholded at 0.22 rad) as a function of the inter-bout interval τ_n . Result from the neuronal model is in blue, experimental data are in black. (D) Mean reorientation $\langle \delta\theta \rangle$ as a function of the contrast c . (E) Example traces of the simulated activity for a constant contrast $c = 0.5$. (F) Probability of flipping orientation as a function of the imposed contrast c in situations of conflict or reinforcement (neuronal model). (G) Probability distribution function of θ for 10 simulated phototactic trajectories with a linear dependence of average reorientation on contrast. Each trajectory lasted 50,000 s. The dotted line is the orientational distribution in the absence of visual stimulation.

The online version of this article includes the following figure supplement(s) for figure 5:

Figure supplement 1. Comparison of experimental and simulated trajectories.

Figure supplement 2. Simulated trajectories with different inter-bout intervals τ_n .

source (Figure 5G). Its profile was in quantitative agreement with its experimental counterpart (mean resultant vector length $\nu = 0.23$ in simulation for $\nu = 0.24$ in experimental data for bouts 2 to 17).

Discussion

Sensorimotor transformation can be viewed as an operation of massive dimensionality reduction, in which a continuous stream of sensory and motor-related signals is converted into a discrete series of stereotyped motor actions. The challenge in understanding this process is (i) to correctly categorize the motor events, that is to reveal the correct parametrization of the motor repertoire, and (ii) to unveil the statistical rules for action selection. Testing the validity of such description can be done by building a minimal model based on these rules. If the model is correct, the motor variability unaccounted for by the model should be entirely random, that is independent of the sensorimotor history.

Here, we implemented a minimal model approach in order to unveil the basic rules underlying phototaxis. We showed that zebrafish light-driven orientational navigation can be quantitatively

described by a stochastic model consisting of two independent Markov chains: one that selects forward scoots vs turning bouts and a second one that sets the orientation of the latter. We established that the stereo-visual contrast and global intensity modulation act separately on each of these selection processes. The contrast induces a directed bias of turning bouts toward the illuminated side, but does not impact the prevalence of turning bouts vs forward scoots. Reversely, a global decrement in illumination increases the ratio of turning bouts but does not favor any particular direction. For the contrast-driven configuration (tropotaxis), the minimal model corresponds to an Ornstein-Uhlenbeck process (**Uhlenbeck and Ornstein, 1930**), which describes the dynamics of a diffusive brownian particle in a quadratic trap. In the klinotaxis configuration (in the absence of stereo-visual contrast), the orientational bias solely results from a light-dependent modulation of the diffusivity, a mechanism reminiscent of bacterial chemotaxis.

This stochastic minimal model is built on a simple decision tree (**Figure 4A**) with a set of binary choices. However, to fully capture the orientational dynamics, we had to incorporate the continuous increase in turning bout amplitude with the light decrement in an ad-hoc way. It is currently unclear whether all turn bouts in our experiments can be assigned to a single class of swim maneuvers that are modulated in amplitude, or whether these encompass distinct motor programs executed with varying frequencies. In the latter case, it might be possible to represent this amplitude modulation through an extension of the decision tree that would select between distinct turn bout categories.

Compared to previous studies on phototaxis, for example (**Burgess et al., 2010**), our approach allowed us to clearly disentangle the contributions of spatial (stereovisual contrast) and time-dependent (motion-induced change in global illumination) visual cues. Hence, the contrast-driven assays were performed under constant overall illumination intensity (the sum of left and right intensities). This allowed us to establish that, rather surprisingly, the probability of triggering a turn (vs a forward swim) is insensitive to the imposed contrast. This possibility constitutes an important asset with respect to standard experimental configurations, such as the one examined by **Burgess et al. (2010)**, in which the animal is submitted to an actual light source. Although these configurations provide a more realistic context, the visual stimulus effectively perceived by each eye can not be quantitatively assessed, which precludes the design of predictive models. Conversely, once adjusted on well-controlled virtual assays, our model could be numerically implemented in realistic environments, and the trajectories could then be directly confronted with behavioral data. This would require to first infer how the intensity impinging on each eye depends on the source distance and orientation relative to the animal body axis.

Another critical and distinct aspect of the present work is its focus on the steady-state dynamics. Our aim was to mimic the continuous exploration of an environment in which the brightness level displayed slowly varying angular modulations. The luminosity profiles were thus chosen to ensure that individual bouts elicited relatively mild changes in illumination. By doing so, we tried to mitigate visual startle responses that are known to be elicited upon sudden darkening (**Easter and Nicola, 1996**). Although we could not avoid the initial large drop in illumination at the onset of each trial, the associated short-term response (i.e. the first bout) was excluded from the analysis. In this respect, our experiment differs from the study of **Chen and Engert (2014)** in which a similar closed-loop setup was used to demonstrate the ability of larvae to confine their navigation within bright regions. This behavior was entirely controlled by the animal's response to light-on or light-off stimuli as it crossed the virtual border between a bright central disk and the dark outer area. These sharp transitions resulted in clear-cut behavioral changes that lasted for a few bouts. In comparison, our experiment addresses a different regime in which subtle light-driven biases in the spontaneous exploration cumulatively drive the animal toward brightest regions.

As we aimed to obtain a simple and tractable kinematic description, we ignored some other aspects of the navigation characteristics. First, we focused on the orientation of the animal and thus did not systematically investigate how the forward components of the swim bouts were impacted by visual stimuli. However, in the context of angle-dependent intensity profiles, this effect should not impact the observed orientational dynamics. More importantly, we ran most of our analysis using the bout number as a time-scale, and thus ignored possible light-driven modulations of the inter-bout intervals (τ_n). We showed, however, that the orientational correlation is controlled by an actual time-scale. This result may have significant consequence on the fish exploration. In particular, we expect that changes in bout frequency, reflecting various levels of motor activity, may significantly affect the geometry of the trajectories (and not only the speed at which they are explored). We illustrated this

process by running numerical experiments at similar flipping rate k_{flip} but increasing bout frequencies. The trajectories, shown in **Figure 5—figure supplement 2**, exhibit increasing complexity as measured by the fractal dimension. This mechanism may explain the changes in trajectories' geometry observed by *Horstick et al. (2017)* in response to sudden light dimming.

An important outcome of this study is to show that light-seeking navigation uses visual cues over relatively short time scales. The bouts statistics could be captured with a first-order autoregressive process, indicating that the stimulus perceived over one τ_n is sufficient to predict the forthcoming bout. However, one should be aware that such observation is only valid provided that the sensory context remains relatively stable. Hence for instance, a prolonged uniform drop in luminosity is known to enhance the overall motor activity (generally estimated by the average displacement over a period of time) for up to several tens of minutes (*Prober et al., 2006; Emran et al., 2007; Emran et al., 2010; Liu et al., 2015*). This long-term behavioral change, so-called photokinesis, might be regulated by deep brain photoreceptors (*Fernandes et al., 2012; Horstick et al., 2017*) and thus constitutes a distinct mechanism. One particularly exciting prospect will be to understand how such behavioral plasticity may not only modulate the spontaneous activity (*Johnson et al., 2019*) but also affects the phototactic dynamics.

One of the motivations of minimal behavioral models is to facilitate the functional identification and modeling of neural circuits that implement the identified sensorimotor operations in the brain. Here, we used the behavioral results to propose a neuronal model of the ARTR that quantitatively reproduces non-trivial aspects of the bout selection process. This recurrent neural circuit is a simplified version of working memory models developed by *Brunel and Wang (2001); Wang (2001); Wang (2002); Wang (2008)* and adapted in *Wang (2002)* for a decision task executed in the parietal cortex (*Shadlen and Newsome, 1996; Shadlen and Newsome, 2001*). In this class of models, the binary decision process reflects the competition between two cross-inhibitory neural populations. The circuit is endowed with two major functional capacities: (1) it can maintain mnemonic persistent activity over long periods of time, thanks to recurrent excitatory inputs; (2) it can integrate sensory signals in a graded fashion to continuously bias the statistics of the decision. This model thus naturally recapitulates the major functional features of the sensory-biased Markov side-chain - motor persistence and contrast-driven continuous bias - that organizes the orientation selection.

It is tempting to generalize about this behavior-to-circuit approach, at least in small animals such as Zebrafish or *Drosophila*, by representing any behavior as a coordinated sequence of competing elemental actions biased by sensory feedback and organized within a hierarchical decision tree. The identification of such decision trees through quantitative behavioral analysis may provide a blueprint of the brain functional organization and significantly ease the development of circuit models of brain-scale sensorimotor computation.

Materials and methods

Zebrafish maintenance and behavioral setup

All experiments were performed on wild-type Zebrafish (*Danio Rerio*) larvae aged 5 to 8 days post-fertilization. Larvae were reared in Petri dishes in E3 solution on a 14/10 hr light/dark cycle at 28°C, and were fed powdered nursery food every day from 6 dpf.

Experiments were conducted during daytime hours (10 am to 6 pm). The arena consisted of a 14 cm in diameter Petri dish containing E3 medium. It was placed on a screen illuminated from below by a projector (ASUS S1). Infrared illumination was provided by LEDs to enable video-monitoring and subsequent tracking of the fish. We used an IR-sensitive Flea3 USB3 camera (FL3-U3-13Y13M-C, Point Grey Research, Richmond, BC, Canada) with an adjustable macro lens (Zoom 7000, Navitar, USA) equipped with an IR filter. The experimental setup was enclosed in a light-tight rig, which was maintained at 26°C using 'The Cube' (Life Imaging Services).

For the stereovisual paradigm $N = 47$ larvae were tested, and $N = 37$ for the temporal paradigm [(uniform 1) : 12, (uniform 2) : 11, (uniform 3) : 14]. All fish ($N=75$) that navigated in the ROI for a significant period of time during the habituation period were also used to assess spontaneous navigation statistics.

Behavioral assay

Closed-loop tracking and visual stimulation were performed at a mean frequency of 35 Hz, with a custom-written software (Karpenko, 2019b; copy archived at https://github.com/elifesciences-publications/Analysis_Behavioral_Phototaxis) in Matlab (The MathWorks), using the PsychToolBox (PTB) version 3.0.14 add-on. Positions and orientations (heading direction) of the fish, as well as bouts characteristics, were extracted online and the illumination pattern was updated accordingly, with a maximum latency of 34 ms. Heading direction was extracted with an accuracy of ± 0.05 rad ($\sim 3^\circ$). Behavioral monitoring was restricted to a circular central region of interest (ROI) of 8.2 cm diameter. When outside the ROI, the fish was actively brought back into the ROI through the opto-motor reflex (OMR), using a concentrically moving circular pattern. One second after the fish re-entered the ROI, a new recording sequence was started.

Prior to the phototactic assay, all tested fish were subjected to a period of at least 8 min of habituation under whole-field illumination at an intensity of $I_{max} = 450 \mu W.cm^{-2}$. For both phototactic paradigms, the absolute orientation of the virtual source was randomly selected when initiating a new experimental sequence (each time the animal would re-enter the ROI). The orientation of the fish relative to the light source θ_n was calculated online using the absolute orientation of the fish α_n and the orientation of the virtual light source α_{source} : $\theta_n = \alpha_n - \alpha_{source}$.

Lateralized paradigm. A circle of 6 cm in diameter was projected under and centered on the fish. The circle was divided into two parts, covering the left and right side of the fish. The separation between the two parts corresponded to the animal's midline. A separation band (2 mm thick) and an angular sector (30°) in front of the animal were darkened to avoid interception of light coming from the right side of the fish by its left eye and vice-versa. The left and right intensities (I_L and I_R) were varied linearly as a function of θ , such that $I_L + I_R = I_{max}$. Since during the habituation period, the whole arena was lit at maximum intensity I_{max} , the total intensity received by the fish drops by a factor of ≈ 2 with the establishment of the circle, at the onset of the assay.

Although our imposed contrast profile displays two angles for which the contrast is null, namely $\theta = 0$ and π , only does the first one correspond to a stable equilibrium point. When θ is close to zero, any excursion away from this particular direction results in a contrast that drives the animal back to the null angle. Conversely, when $\theta \approx \pi$, the contrast drives the animal away from π (unstable equilibrium).

Temporal paradigm. The whole arena was illuminated with an intensity locked onto the fish orientation θ relative to a virtual light source. The initial orientation was randomly chosen at the beginning of a recording sequence. Three different intensity angular profiles were implemented: (uniform 1) a sinusoidal profile, with a maximum intensity of 60% of I_{max} , (uniform 2) an exponential profile, with a maximum intensity of 60% of I_{max} and finally (uniform 3) an exponential profile with a maximum intensity of 30% of I_{max} .

Data analysis

Data analysis was performed using a custom-written code in Matlab. All analysis programs and data are available at Karpenko (2019a).

When representing the mean of one variable against another, bin edges were chosen such that each bin would encompass the same number of data points. Circular statistics analyses (mean, variance, uniformity) and circular statistics tests, namely the circular V-test of non-uniformity of data and the one-sample test for the mean angle of a circular distribution (tested on the orientation of the light virtual light source) were performed using CircStat toolbox for Matlab (Berens, 2009).

Individual fish often exhibit a small yet consistent bias toward one direction (either leftward or rightward). This bias was subtracted before performing the different analyses, in order to guarantee that $\langle \alpha \rangle = 0$ in the absence of a stimulus. The distribution of reorientation angles $\delta\theta_n$ during spontaneous swimming periods was fitted with a constrained double-Gaussian function. We imposed that both the mean absolute angle and variance of the fitting function be consistent with the experimental measurements. This yields an expression with only one independent fitting parameter p_{turn} in the form:

$$f(x) = \frac{1}{\sqrt{2\pi}} \left(\frac{p_{turn}}{\sigma_{turn}} e^{-\frac{1}{2} \left(\frac{x}{\sigma_{turn}} \right)^2} + \frac{1-p_{turn}}{\sigma_f} e^{-\frac{1}{2} \left(\frac{x}{\sigma_{fwd}} \right)^2} \right) \quad (1)$$

using

$$\sigma_{turn} = \frac{\mu_{abs} p_{turn} + \sqrt{\mu_{abs}^2 p_{turn}^2 - [\mu_{abs}^2 - V(1-p_{turn})] [p_{turn}^2 + p_{turn}(1-p_{turn})]}}{p_{turn}^2 + p_{turn}(1-p_{turn})}$$

and

$$\sigma_{fwd} = \frac{\mu_{abs} \sqrt{\pi/2} - p_{turn} \sigma_{turn}}{1-p_{turn}}$$

with

$$\mu_{abs} = \langle |\delta\theta| \rangle, V = \langle \delta\theta^2 \rangle$$

To evaluate the mean and variance of the forward and turn bouts under various visual contexts, the distributions in different bins were also fitted with a constrained double-Gaussian model as in (1). The stereovisual data distributions were fitted with two additional mean terms μ_{turn} and μ_{fwd} ; and for the klinotaxis assay, with a constraint on σ_{fwd} and μ_{fwd} . The bins were constructed either on the contrast c experienced just before bout n or on the relative difference of intensity experienced at bout $n-1$: $\delta I/I = 2 \frac{I_{n-1} - I_{n-2}}{I_{n-1} + I_{n-2}}$.

All distributions of θ_n and analyses of bias were computed using trajectories from bout index two to the median number of bouts per sequence in each type of experiment. The median number of bouts in each experiment was $med_{stereo} = 17$ for the tropotaxis experiment, and 27, 15, 17 for the klinotaxis assays for the 3 profiles 1–3, respectively.

Numerical simulations

The Markov-chain model simulations were performed using a custom-written code in MATLAB (Karpenko, 2019b). Initial orientations and positions within the ROI were randomly sampled from, respectively, a uniform distribution and a normal distribution centered on a circle of radius 20 mm from the center of the ROI with a standard deviation of 1.3 mm (mimicking the starting points of experimental data).

At each step, an angular step-size is drawn from the data: either from the turning distribution with a probability p_{turn} or from the forward distribution with a probability $1-p_{turn}$. Respective means are μ_{turn} and μ_{fwd} and standard deviation σ_{turn} and σ_{fwd} . The left-vs-right orientations of the turns is set by the probability of flipping sides p_{flip} . For the spatially constrained simulations, the walker also draws a distance step-size (between two successive positions) from two different gamma distributions: one for the turning bouts, a second one for the scoots. Under neutral conditions (uniform illumination), all parameters are constant.

For the simulation under stereovisual phototactic conditions, p_{flip} was varied linearly with the contrast (based on the data represented in Figure 2M). When simulating temporal phototaxis, the parameters σ_{turn} and p_{turn} were modulated by the relative illumination change $\delta I/I$ experienced at the previous steps (as represented in Figure 3H–I).

Acknowledgements

We thank the IBPS fish facility staff, and in particular Alex Bois and Stéphane Tronche, for their help with the fish maintenance. We are grateful to Raphaël Voituriez for fruitful discussions on the theoretical aspects. This work was funded by the CNRS and Sorbonne University, and supported in part by the National Science Foundation under Grant No. NSF PHY-1748958.

Additional information

Funding

Funder	Grant reference number	Author
Human Frontier Science Program	RGP0060/2017	Georges Debrégeas
H2020 European Research Council	71598	Volker Bormuth
Agence Nationale de la Recherche	ANR-16-CE16-0017	Raphaël Candelier Georges Debrégeas
Fondation pour la Recherche Médicale	FDT201904008219	Sophia Karpenko
ATIP-Avenir program		Volker Bormuth
Fondation pour la Recherche Médicale	SPF201809007064	Sebastien Wolf

The funders had no role in study design, data collection and interpretation, or the decision to submit the work for publication.

Author contributions

Sophia Karpenko, Conceptualization, Data curation, Formal analysis, Investigation; Sebastien Wolf, Formal analysis, Investigation; Julie Lafaye, Data curation, Investigation; Guillaume Le Goc, Data curation, Methodology; Thomas Panier, Investigation, Methodology; Volker Bormuth, Conceptualization, Supervision, Methodology; Raphaël Candelier, Conceptualization, Data curation, Supervision, Visualization, Methodology; Georges Debrégeas, Conceptualization, Formal analysis, Supervision

Author ORCIDs

Raphaël Candelier  <http://orcid.org/0000-0002-1523-6249>

Georges Debrégeas  <https://orcid.org/0000-0003-3698-4497>

Ethics

Animal experimentation: All experiments were approved by Le Comité d'Éthique pour l'Expérimentation Animale Charles Darwin C2EA-05 (02601.01).

Decision letter and Author response

Decision letter <https://doi.org/10.7554/eLife.52882.sa1>

Author response <https://doi.org/10.7554/eLife.52882.sa2>

Additional files

Supplementary files

- Transparent reporting form

Data availability

Data and analysis codes are available at Dryad Digital Repository, DOI: <https://doi.org/10.5061/dryad.v9s4mw6qx>.

The following dataset was generated:

Author(s)	Year	Dataset title	Dataset URL	Database and Identifier
Debrégeas G, Karpenko S, Wolf S, Lafaye J, Le Goc G, Panier T, Candelier R, Bormuth V	2019	From behavior to circuit modeling of light-seeking navigation in Zebrafish larvae	http://dx.doi.org/10.5061/dryad.v9s4mw6qx	Dryad Digital Repository, 10.5061/dryad.v9s4mw6qx

References

- Adler J, Tso WW. 1974. "Decision"-making in bacteria: chemotactic response of *Escherichia coli* to conflicting stimuli. *Science* **184**:1292–1294. DOI: <https://doi.org/10.1126/science.184.4143.1292>, PMID: 4598187
- Ahrens MB, Orger MB, Robson DN, Li JM, Keller PJ. 2013. Whole-brain functional imaging at cellular resolution using light-sheet microscopy. *Nature Methods* **10**:413–420. DOI: <https://doi.org/10.1038/nmeth.2434>, PMID: 23524393
- Berens P. 2009. CircStat: a MATLAB toolbox for circular statistics. *Journal of Statistical Software* **1**:128–129. DOI: <https://doi.org/10.1002/wics.10>
- Berg HC, Brown DA. 1972. Chemotaxis in *E. coli* analysed by 3D tracking. *Nature* **239**:500–504. DOI: <https://doi.org/10.1038/239500a0>
- Bianco IH, Kampff AR, Engert F. 2011. Prey capture behavior evoked by simple visual stimuli in larval zebrafish. *Frontiers in Systems Neuroscience* **5**:2011. DOI: <https://doi.org/10.3389/fnsys.2011.00101>
- Bianco IH, Engert F. 2015. Visuomotor transformations underlying hunting behavior in zebrafish. *Current Biology* **25**:831–846. DOI: <https://doi.org/10.1016/j.cub.2015.01.042>, PMID: 25754638
- Brunel N, Wang XJ. 2001. Effects of neuromodulation in a cortical network model of object working memory dominated by recurrent inhibition. *Journal of Computational Neuroscience* **11**:63–85. DOI: <https://doi.org/10.1023/a:1011204814320>, PMID: 11524578
- Budick SA, O'Malley DM. 2000. Locomotor repertoire of the larval zebrafish: swimming, turning and prey capture. *The Journal of Experimental Biology* **203**:2565–2579. DOI: <https://doi.org/10.1242/jeb.01529>
- Burgess HA, Schoch H, Granato M. 2010. Distinct retinal pathways drive spatial orientation behaviors in zebrafish navigation. *Current Biology* **20**:381–386. DOI: <https://doi.org/10.1016/j.cub.2010.01.022>, PMID: 20153194
- Burgess HA, Granato M. 2007. Modulation of locomotor activity in larval zebrafish during light adaptation. *Journal of Experimental Biology* **210**:2526–2539. DOI: <https://doi.org/10.1242/jeb.003939>, PMID: 17601957
- Celani A, Vergassola M. 2010. Bacterial strategies for chemotaxis response. *PNAS* **107**:1391–1396. DOI: <https://doi.org/10.1073/pnas.0909673107>, PMID: 20080704
- Chen X, Engert F. 2014. Navigational strategies underlying phototaxis in larval zebrafish. *Frontiers in Systems Neuroscience* **8**:1–13. DOI: <https://doi.org/10.3389/fnsys.2014.00039>, PMID: 24723859
- Dunn TW, Mu Y, Narayan S, Randlett O, Naumann EA, Yang C-T, Schier AF, Freeman J, Engert F, Ahrens MB. 2016. Brain-wide mapping of neural activity controlling zebrafish exploratory locomotion. *eLife* **5**:e12741. DOI: <https://doi.org/10.7554/eLife.12741>
- Easter SS, Nicola GN. 1996. The development of vision in the zebrafish (*Danio rerio*). *Developmental Biology* **180**:646–663. DOI: <https://doi.org/10.1006/dbio.1996.0335>, PMID: 8954734
- Emran F, Rihel J, Adolph AR, Wong KY, Kraves S, Dowling JE. 2007. OFF ganglion cells cannot drive the optokinetic reflex in zebrafish. *PNAS* **104**:19126–19131. DOI: <https://doi.org/10.1073/pnas.0709337104>, PMID: 18025459
- Emran F, Rihel J, Adolph AR, Dowling JE. 2010. Zebrafish larvae lose vision at night. *PNAS* **107**:6034–6039. DOI: <https://doi.org/10.1073/pnas.0914718107>
- Fechner GT. 1860. *Elemente Der Psychophysik*. Nabu Press.
- Fernandes AM, Fero K, Arrenberg AB, Bergeron SA, Driever W, Burgess HA. 2012. Deep brain photoreceptors control light-seeking behavior in zebrafish larvae. *Current Biology* **22**:2042–2047. DOI: <https://doi.org/10.1016/j.cub.2012.08.016>, PMID: 23000151
- Fiser J, Chiu C, Weliky M. 2004. Small modulation of ongoing cortical dynamics by sensory input during natural vision. *Nature* **431**:573–578. DOI: <https://doi.org/10.1038/nature02907>, PMID: 15457262
- Fraenkel GS, Gunn DL. 1961. *The Orientation of Animals, Kinesis, Taxes and Compass Reactions*. Dover Publications, Inc.
- Freeman WJ. 1995. The hebbian paradigm reintegrated: local reverberations as internal representations. *Behavioral and Brain Sciences* **18**:631. DOI: <https://doi.org/10.1017/S0140525X0004022X>
- Girdhar K, Gruebele M, Chemla YR. 2015. The behavioral space of zebrafish locomotion and its neural network analog. *PLOS ONE* **10**:e0128668. DOI: <https://doi.org/10.1371/journal.pone.0128668>, PMID: 26132396
- Gomez-Marin A, Stephens GJ, Louis M. 2011. Active sampling and decision making in *Drosophila* chemotaxis. *Nature Communications* **2**:410–441. DOI: <https://doi.org/10.1038/ncomms1455>, PMID: 21863008
- Gomez-Marin A, Louis M. 2012. Active sensation during orientation behavior in the *Drosophila* larva: more sense than luck. *Current Opinion in Neurobiology* **22**:208–215. DOI: <https://doi.org/10.1016/j.conb.2011.11.008>, PMID: 22169055
- Horstick EJ, Bayleyen Y, Sinclair JL, Burgess HA. 2017. Search strategy is regulated by somatostatin signaling and deep brain photoreceptors in zebrafish. *BMC Biology* **15**:1–16. DOI: <https://doi.org/10.1186/s12915-016-0346-2>, PMID: 28122559
- Humbert TH, Bruegger P, Afonso B, Zlatić M, Truman JW, Gershow M, Samuel A, Sprecher SG. 2018. Dedicated photoreceptor pathways in *Drosophila* larvae mediate navigation by processing either spatial or temporal cues. *Nature Communications* **9**:1–16. DOI: <https://doi.org/10.1038/s41467-018-03520-5>, PMID: 29593252
- Johnson RE, Linderman S, Panier T, Wee CL, Song E, Herrera KJ, Miller A, Engert F. 2019. Probabilistic models of larval zebrafish behavior: structure on many scales. *bioRxiv*. DOI: <https://doi.org/10.1101/672246>
- Kane EA, Gershow M, Afonso B, Larderet I, Klein M, Carter AR, de Bivort BL, Sprecher SG, Samuel AD. 2013. Sensorimotor structure of *Drosophila* larva phototaxis. *PNAS* **110**:E3868–E3877. DOI: <https://doi.org/10.1073/pnas.1215295110>, PMID: 24043822

- Karpenko S.** 2019a. Programs closed-loop phototaxis. *GitLab*. 6666d5039e. https://gitlab.com/Phiasso/programs_closed-loop_phototaxis.git
- Karpenko S.** 2019b. Analysis behavioral phototaxis. *GitLab*. 999a0c66. <https://gitlab.com/Phiasso/analysis.git>
- Liu Y, Carmer R, Zhang G, Venkatraman P, Brown SA, Pang CP, Zhang M, Ma P, Leung YF.** 2015. Statistical analysis of zebrafish locomotor response. *PLOS ONE* **10**:e0139521. DOI: <https://doi.org/10.1371/journal.pone.0139521>, PMID: 26437184
- Lovely PS, Dahlquist FW.** 1975. Statistical measures of bacterial motility. *Journal of Theoretical Biology* **50**:477–496. DOI: [https://doi.org/10.1016/0022-5193\(75\)90094-6](https://doi.org/10.1016/0022-5193(75)90094-6)
- Macnab RM, Koshland DE.** 1972. The gradient-sensing mechanism in bacterial chemotaxis. *PNAS* **69**:2509–2512. DOI: <https://doi.org/10.1073/pnas.69.9.2509>, PMID: 4560688
- Marée AFM, Panfilov AV, Hogeweg P.** 1999. Phototaxis during the slug stage of *Dictyostelium discoideum*: a model study. *Proceedings of the Royal Society of London* **266**:1351–1360. DOI: <https://doi.org/10.1098/rspb.1999.0787>
- Marques JC, Lackner S, Félix R, Orger MB.** 2018. Structure of the zebrafish locomotor repertoire revealed with unsupervised behavioral clustering. *Current Biology* **28**:181–195. DOI: <https://doi.org/10.1016/j.cub.2017.12.002>, PMID: 29307558
- Matsuo Y, Uozumi N, Matsuo R.** 2014. Photo-tropotaxis based on projection through the cerebral commissure in the terrestrial slug *Limax*. *Journal of Comparative Physiology A* **200**:1023–1032. DOI: <https://doi.org/10.1007/s00359-014-0954-7>
- Maximino C, Brito TM, Moraes FD, Oliveira FVC, Taccolini IB, Pereira PM, Colmanetti R, Lozano R, Gazolla RA, Rodrigues STK, Pontes AAA, Romão CF, Prado VM, Gouveia A.** 2007. A comparative analysis of the preference for dark environments in five teleosts. *International Journal of Comparative Psychology* **20**:351–367.
- McClenahan P, Troup M, Scott EK.** 2012. Fin-tail coordination during escape and predatory behavior in larval zebrafish. *PLOS ONE* **7**:e32295. DOI: <https://doi.org/10.1371/journal.pone.0032295>, PMID: 22359680
- Mello BA, Tu Y.** 2007. Effects of adaptation in maintaining high sensitivity over a wide range of backgrounds for *Escherichia coli* chemotaxis. *Biophysical Journal* **92**:2329–2337. DOI: <https://doi.org/10.1529/biophysj.106.097808>, PMID: 17208965
- Miller AC, Thiele TR, Faumont S, Moravec ML, Lockery SR.** 2005. Step-response analysis of chemotaxis in *Caenorhabditis elegans*. *Journal of Neuroscience* **25**:3369–3378. DOI: <https://doi.org/10.1523/JNEUROSCI.5133-04.2005>, PMID: 15800192
- Oliveira NM, Foster KR, Durham WM.** 2016. Single-cell twitching chemotaxis in developing biofilms. *PNAS* **113**:6532–6537. DOI: <https://doi.org/10.1073/pnas.1600760113>, PMID: 27222583
- Orger MB, Baier H.** 2005. Channeling of red and green cone inputs to the zebrafish optomotor response. *Visual Neuroscience* **22**:275–281. DOI: <https://doi.org/10.1017/S0952523805223039>, PMID: 16079003
- Panier T, Romano SA, Olive R, Pietri T, Sumbre G, Candelier R, Debrégeas G.** 2013. Fast functional imaging of multiple brain regions in intact zebrafish larvae using selective plane illumination microscopy. *Frontiers in Neural Circuits* **7**:1–11. DOI: <https://doi.org/10.3389/fncir.2013.00065>, PMID: 23576959
- Prober DA, Rihel J, Onah AA, Sung R-J, Schier AF.** 2006. Hypocretin/Orexin overexpression induces an Insomnia-Like phenotype in zebrafish. *Journal of Neuroscience* **26**:13400–13410. DOI: <https://doi.org/10.1523/JNEUROSCI.4332-06.2006>
- Sawin EP, Harris LR, Campos AR, Sokolowski MB.** 1994. Sensorimotor transformation from light reception to phototactic behavior in *Drosophila* larvae (Diptera: Drosophilidae). *Journal of Insect Behavior* **7**:553–567. DOI: <https://doi.org/10.1007/BF02025449>
- Serra EL, Medalha CC, Mattioli R.** 1999. Natural preference of zebrafish (*Danio rerio*) for a dark environment. *Brazilian Journal of Medical and Biological Research* **32**:1551–1553. DOI: <https://doi.org/10.1590/S0100-879X1999001200016>
- Shadlen MN, Newsome WT.** 1996. Motion perception: seeing and deciding. *PNAS* **93**:628–633. DOI: <https://doi.org/10.1073/pnas.93.2.628>, PMID: 8570606
- Shadlen MN, Newsome WT.** 2001. Neural basis of a perceptual decision in the parietal cortex (area LIP) of the rhesus monkey. *Journal of Neurophysiology* **86**:1916–1936. DOI: <https://doi.org/10.1152/jn.2001.86.4.1916>, PMID: 11600651
- Stephens GJ, Johnson-Kerner B, Bialek W, Ryu WS.** 2008. Dimensionality and dynamics in the behavior of *C. elegans*. *PLOS Computational Biology* **4**:e1000028. DOI: <https://doi.org/10.1371/journal.pcbi.1000028>, PMID: 18389066
- Tastekin I, Khandelwal A, Tadres D, Fessner ND, Truman JW, Zlatic M, Cardona A, Louis M.** 2018. Sensorimotor pathway controlling stopping behavior during chemotaxis in the *Drosophila Melanogaster* larva. *eLife* **7**:e38740. DOI: <https://doi.org/10.7554/eLife.38740>, PMID: 30465650
- Tsodyks M, Kenet T, Grinvald A, Arieli A.** 1999. Linking spontaneous activity of single cortical neurons and the underlying functional architecture. *Science* **286**:1943–1946. DOI: <https://doi.org/10.1126/science.286.5446.1943>, PMID: 10583955
- Uhlenbeck GE, Ornstein LS.** 1930. On the theory of the brownian motion. *Physical Review* **36**:823–841. DOI: <https://doi.org/10.1103/PhysRev.36.823>
- Wang XJ.** 2001. Synaptic reverberation underlying mnemonic persistent activity. *Trends in Neurosciences* **24**:455–463. DOI: [https://doi.org/10.1016/S0166-2236\(00\)01868-3](https://doi.org/10.1016/S0166-2236(00)01868-3), PMID: 11476885
- Wang XJ.** 2002. Probabilistic decision making by slow reverberation in cortical circuits. *Neuron* **36**:955–968. DOI: [https://doi.org/10.1016/S0896-6273\(02\)01092-9](https://doi.org/10.1016/S0896-6273(02)01092-9), PMID: 12467598

- Wang XJ.** 2008. Decision making in recurrent neuronal circuits. *Neuron* **60**:215–234. DOI: <https://doi.org/10.1016/j.neuron.2008.09.034>, PMID: 18957215
- Ward S.** 1973. Chemotaxis by the nematode *Caenorhabditis elegans*: identification of attractants and analysis of the response by use of mutants. *PNAS* **70**:817–821. DOI: <https://doi.org/10.1073/pnas.70.3.817>, PMID: 4351805
- Ward A, Liu J, Feng Z, Xu XZ.** 2008. Light-sensitive neurons and channels mediate phototaxis in *C. elegans*. *Nature Neuroscience* **11**:916–922. DOI: <https://doi.org/10.1038/nn.2155>, PMID: 18604203
- Wolf S, Dubreuil AM, Bertoni T, Böhm UL, Bormuth V, Candelier R, Karpenko S, Hildebrand DGC, Bianco IH, Monasson R, Debrégeas G.** 2017. Sensorimotor computation underlying phototaxis in zebrafish. *Nature Communications* **8**:1–12. DOI: <https://doi.org/10.1038/s41467-017-00310-3>
- Yuan J, Fahrner KA, Turner L, Berg HC.** 2010. Asymmetry in the clockwise and counterclockwise rotation of the bacterial flagellar motor. *PNAS* **107**:12846–12849. DOI: <https://doi.org/10.1073/pnas.1007333107>, PMID: 20615986

Appendix 1

Modelling spontaneous navigation of zebrafish larvae

We model the discrete trajectories (sequences of bouts) as a stochastic process using two independent Markov chains, depicted in **Figure 1E**. The *bout type* chain (top) controls the alternation between forward and turning bouts, with possible states F_n and T_n at time n , while the *side* chain (bottom) controls the left/right orientations of turning bouts, with possible states L_n and R_n . All possible states are combinations of the states of the two chains, namely $\{FL\}_n$, $\{FR\}_n$, $\{TL\}_n$, and $\{TR\}_n$. The transition rates of the bout type chain are $k_{F \rightarrow T}$ and $k_{T \rightarrow F}$, where $k_{F \rightarrow T}/k_{T \rightarrow F} = p_{turn}$ is the overall fraction of turning bouts. For the side chain, under constant uniform illumination, the right and left states are equiprobable, and the two transition probabilities are thus equal: $k_{R \rightarrow L} = k_{L \rightarrow R} = p_{flip}$.

The two chains operate synchronously: at every time step transitions on both chains are triggered simultaneously, and a reorientation value $\delta\alpha_n$ is drawn based on the resulting state. When the fish is in a turning state, $\{TL\}_n$ or $\{TR\}_n$, the reorientation angle is sampled from the positive and negative side of a centered normal distribution with standard deviation σ_{turn} for left and right turns, respectively. When the fish is in a forward state, $\{FL\}_n$ or $\{FR\}_n$, the reorientation angle is drawn from a normal distribution with standard deviation σ_{fwd} . Therefore, for forward bouts the resulting $\delta\alpha_n$ can be positive or negative, irrespective of the left/right state of the side chain. Altogether, the general statistical distribution of turning amplitudes $\delta\alpha_n$ used in **Figure 1F** reads

$$P(\delta\alpha_n) = \phi_l(\delta\alpha_n) + \phi_f(\delta\alpha_n) \quad (A1)$$

with

$$\phi_l = p_{turn}\mathcal{N}(0, \sigma_{turn}^2) \quad \text{and} \quad \phi_f = (1 - p_{turn})\mathcal{N}(0, \sigma_{fwd}^2) \quad (A2)$$

Mean amplitude at $n + 1$

Within this framework, one can analytically compute the mean square angle at time $n + 1$, as detailed below:

$$\langle \delta\alpha_{n+1}^2 \rangle = \mathbb{P}(F_{n+1})\sigma_{fwd}^2 + \mathbb{P}(T_{n+1})\sigma_{turn}^2 \quad (A3)$$

The two probabilities read:

$$\mathbb{P}(F_{n+1}) = \mathbb{P}(F_n)(1 - k_{F \rightarrow T}) + \mathbb{P}(T_n)k_{T \rightarrow F}$$

$$\mathbb{P}(T_{n+1}) = \mathbb{P}(T_n)(1 - k_{T \rightarrow F}) + \mathbb{P}(F_n)k_{F \rightarrow T}$$

such that

$$\langle \delta\alpha_{n+1}^2 \rangle = \mathbb{P}(F_n) \left[\sigma_{fwd}^2 + k_{F \rightarrow T}(\sigma_{turn}^2 - \sigma_{fwd}^2) \right] + \mathbb{P}(T_n) \left[\sigma_{turn}^2 + k_{T \rightarrow F}(\sigma_{fwd}^2 - \sigma_{turn}^2) \right]$$

Using the functions defined in **Equation A2** we introduce the function $f(\delta\alpha_n)$:

$$f(\delta\alpha_n) = \mathbb{P}(T_n | \delta\alpha_n) = \frac{\phi_l(\delta\alpha_n)}{\phi_l(\delta\alpha_n) + \phi_f(\delta\alpha_n)} \quad (A4)$$

The mean square amplitude at time $n + 1$ can thus be written, as a function of $\delta\alpha_n$ as:

$$\langle \delta\alpha_{n+1}^2 \rangle = \sigma_{fwd}^2 + k_{F \rightarrow T}(\sigma_{turn}^2 - \sigma_{fwd}^2) + f(|\delta\alpha_n|)(\sigma_{turn}^2 - \sigma_{fwd}^2)(1 - k_{T \rightarrow F} - k_{F \rightarrow T}) \quad (A5)$$

This expression is used to fit the data in **Figure 1F** and estimate the two transition rates. These are found to be close to the ratio of turning and forward bouts, that is $k_{F \rightarrow T}/p_{turn} = k_{T \rightarrow F}/(1 - p_{turn}) \approx 0.8$. In the following, we set $k_{F \rightarrow T} = p_{turn}$ and

$k_{T \rightarrow F} = 1 - p_{turn}$, thus ignoring the weak memory component in the selection of turning vs forward bouts.

Mean reorientation at $n + 1$

Similarly, one can compute the theoretical expression of the mean reorientation angle at time $n + 1$:

$$\langle \delta\alpha_{n+1} \rangle = \mathbb{P}(\{FL\}_{n+1})\mu_f + \mathbb{P}(\{FR\}_{n+1})\mu_f + \mathbb{P}(\{TL\}_{n+1})\mu_L + \mathbb{P}(\{TR\}_{n+1})\mu_R \quad (A6)$$

with

$$\mu_f = 0 \quad \text{and} \quad \mu_L = -\mu_R = \sqrt{\frac{2}{\pi}}\sigma_{turn} \quad (A7)$$

Then:

$$\mathbb{P}(\{TL\}_{n+1}) = \mathbb{P}(T_{n+1})\mathbb{P}(L_{n+1}) = p_{turn} [p_{flip}\mathbb{P}(R_n) + (1 - p_{flip})\mathbb{P}(L_n)]$$

$$\mathbb{P}(\{TR\}_{n+1}) = \mathbb{P}(T_{n+1})\mathbb{P}(R_{n+1}) = p_{turn} [p_{flip}\mathbb{P}(L_n) + (1 - p_{flip})\mathbb{P}(R_n)]$$

and

$$\langle \delta\alpha_{n+1} \rangle = p_{turn}(1 - 2p_{flip})\sqrt{\frac{2}{\pi}}\sigma_{turn}[\mathbb{P}(L_n) - \mathbb{P}(R_n)] \quad (A8)$$

Without further assumption, this simply confirms $\langle \delta\alpha_{n+1} \rangle = 0$. Given the reorientation at time n , this expression now writes:

$$\langle \delta\alpha_{n+1} \rangle_{\delta\alpha_n} = p_{turn}(1 - 2p_{flip})\sqrt{\frac{2}{\pi}}\sigma_{turn}[\mathbb{P}(L_n|\delta\alpha_n) - \mathbb{P}(R_n|\delta\alpha_n)] \quad (A9)$$

Since

$$\mathbb{P}(L_n|\delta\alpha_n) = \mathbb{P}(L_n|T_n, \delta\alpha_n)\mathbb{P}(T_n|\delta\alpha_n) + \mathbb{P}(L_n|F_n, \delta\alpha_n)\mathbb{P}(F_n|\delta\alpha_n)$$

$$\mathbb{P}(R_n|\delta\alpha_n) = \mathbb{P}(R_n|T_n, \delta\alpha_n)\mathbb{P}(T_n|\delta\alpha_n) + \mathbb{P}(R_n|F_n, \delta\alpha_n)\mathbb{P}(F_n|\delta\alpha_n)$$

and

$$\mathbb{P}(L_n|F_n, \delta\alpha_n) = \mathbb{P}(R_n|F_n, \delta\alpha_n) = 1/2$$

we obtain

$$\langle \delta\alpha_{n+1} \rangle_{\delta\alpha_n} = [\mathbb{P}(L_n|T_n, \delta\alpha_n) - \mathbb{P}(R_n|T_n, \delta\alpha_n)]p_{turn}(1 - 2p_{flip})\sqrt{\frac{2}{\pi}}\sigma_{turn}f(\delta\alpha_n) \quad (A10)$$

Then, noting that

$$\begin{cases} \mathbb{P}(L_n|T_n, \delta\alpha_n > 0) = 1 \\ \mathbb{P}(R_n|T_n, \delta\alpha_n > 0) = 0 \end{cases} \quad \text{and} \quad \begin{cases} \mathbb{P}(L_n|T_n, \delta\alpha_n < 0) = 0 \\ \mathbb{P}(R_n|T_n, \delta\alpha_n < 0) = 1 \end{cases}$$

we finally obtain the formula used to fit the data in **Figure 1G**:

$$\langle \delta\alpha_{n+1} \rangle_{\delta\alpha_n} = \text{sign}(\delta\alpha_n)\sqrt{\frac{2}{\pi}}p_{turn}(1 - 2p_{flip})\sigma_{turn}f(\delta\alpha_n) \quad (A11)$$

Autocorrelation of the reorientations

One can then compute the correlation of reorientation amplitudes, defined for $q \in \mathbb{N}^*$ as:

$$C_q = \frac{\langle \delta\alpha_n \delta\alpha_{n+q} \rangle - \langle \delta\alpha_n \rangle \langle \delta\alpha_{n+q} \rangle}{\sqrt{\langle \delta\alpha_n^2 \rangle} \sqrt{\langle \delta\alpha_{n+q}^2 \rangle}} = \frac{\langle \delta\alpha_n \delta\alpha_{n+q} \rangle}{\langle \delta\alpha_n^2 \rangle} \tag{A12}$$

with the normalization coefficient equal to the variance of reorientations

$$\langle \delta\alpha_n^2 \rangle = p_{turn} \sigma_{turn}^2 + (1 - p_{turn}) \sigma_{fwd}^2 \tag{A13}$$

The term $\langle \delta\alpha_n \delta\alpha_{n+q} \rangle$ can be computed in a similar manner as for **Equation A6**, but with more terms corresponding to the 16 possible combinations of states:

$$\begin{matrix} \{FL\}_n, \{FL\}_{n+q} & \{FL\}_n, \{FR\}_{n+q} & \{FL\}_n, \{TL\}_{n+q} & \{FL\}_n, \{TR\}_{n+q} \\ \{FR\}_n, \{FL\}_{n+q} & \{FR\}_n, \{FR\}_{n+q} & \{FR\}_n, \{TL\}_{n+q} & \{FR\}_n, \{TR\}_{n+q} \\ \{TL\}_n, \{FL\}_{n+q} & \{TL\}_n, \{FR\}_{n+q} & \{TL\}_n, \{TL\}_{n+q} & \{TL\}_n, \{TR\}_{n+q} \\ \{TR\}_n, \{FL\}_{n+q} & \{TR\}_n, \{FR\}_{n+q} & \{TR\}_n, \{TL\}_{n+q} & \{TR\}_n, \{TR\}_{n+q} \end{matrix}$$

Only the four states in the bottom-right corner have a finite contribution, since all the others terms are multiplied by $\mu_f = 0$. Thus:

$$\langle \delta\alpha_n \delta\alpha_{n+q} \rangle = \mathbb{P}(\{TL\}_n, \{TL\}_{n+q}) \mu_L^2 + \mathbb{P}(\{TL\}_n, \{TR\}_{n+q}) \mu_L \mu_R + \mathbb{P}(\{TR\}_n, \{TL\}_{n+q}) \mu_R \mu_L + \mathbb{P}(\{TR\}_n, \{TR\}_{n+q}) \mu_R^2$$

and, using **Equation A7** and

$$\begin{aligned} \mathbb{P}(\{TL\}_n, \{TL\}_{n+q}) &= \mathbb{P}(T_n) \mathbb{P}(T_{n+q}) \mathbb{P}(L_n) \mathbb{P}(L_{n+q} | L_n) = \frac{p_{turn}^2}{2} \mathbb{P}(L_{n+q} | L_n) \\ \mathbb{P}(\{TL\}_n, \{TR\}_{n+q}) &= \mathbb{P}(T_n) \mathbb{P}(T_{n+q}) \mathbb{P}(L_n) \mathbb{P}(R_{n+q} | L_n) = \frac{p_{turn}^2}{2} \mathbb{P}(R_{n+q} | L_n) \\ \mathbb{P}(\{TR\}_n, \{TL\}_{n+q}) &= \mathbb{P}(T_n) \mathbb{P}(T_{n+q}) \mathbb{P}(R_n) \mathbb{P}(L_{n+q} | R_n) = \frac{p_{turn}^2}{2} \mathbb{P}(L_{n+q} | R_n) \\ \mathbb{P}(\{TR\}_n, \{TR\}_{n+q}) &= \mathbb{P}(T_n) \mathbb{P}(T_{n+q}) \mathbb{P}(R_n) \mathbb{P}(R_{n+q} | R_n) = \frac{p_{turn}^2}{2} \mathbb{P}(R_{n+q} | R_n) \end{aligned}$$

and noting that

$$\begin{aligned} \mathbb{P}(L_{n+q} | L_n) = \mathbb{P}(R_{n+q} | R_n) &= \sum_{\substack{i=1 \\ i \sim \text{odd}}}^{q+1} \binom{q}{i} p_{flip}^{i-1} (1 - p_{flip})^{q-i+1} \\ \mathbb{P}(L_{n+q} | R_n) = \mathbb{P}(R_{n+q} | L_n) &= \sum_{\substack{i=1 \\ i \sim \text{even}}}^{q+1} \binom{q}{i} p_{flip}^{i-1} (1 - p_{flip})^{q-i+1} \end{aligned}$$

one obtains

$$\langle \delta\alpha_n \delta\alpha_{n+q} \rangle = p_{turn}^2 \left[\sum_{i=1}^{q+1} (-1)^{q+1-i} q i p_{flip}^{i-1} (1 - p_{flip})^{q-i+1} \right] \mu_L^2 = \frac{2}{\pi} (1 - 2p_{flip})^q p_{turn}^2 \sigma_{turn}^2$$

and finally:

$$C_q = \frac{2}{\pi} \frac{p_{turn}^2 \sigma_{turn}^2}{p_{turn} \sigma_{turn}^2 + (1 - p_{turn}) \sigma_{fwd}^2} (1 - 2p_{flip})^q \tag{A14}$$

This is the equation used to fit the data in **Figure 1H**.

An estimate of p_{flip} was calculated as follows. If only turns are considered :

$$\begin{aligned} \langle \delta\alpha_n \delta\alpha_{n+1} \rangle &= p_{turn}(1 - p_{flip}) \langle |\delta\alpha_n| |\delta\alpha_{n+1}| \rangle - p_{turn} p_{flip} \langle |\delta\alpha_n| |\delta\alpha_{n+1}| \rangle \\ &= p_{turn}^2 [(1 - 2p_{flip}) \langle |\delta\alpha_n| |\delta\alpha_{n+1}| \rangle] \end{aligned}$$

thus :

$$\frac{\langle \delta\alpha_n \delta\alpha_{n+1} \rangle}{\langle |\delta\alpha_n| |\delta\alpha_{n+1}| \rangle} = p_{turn}^2 (1 - 2p_{flip}) = C_1$$

And finally

$$p_{flip} = \frac{1}{2} \left(1 - \frac{C_1}{p_{turn}^2} \right) \tag{A15}$$

Mean square reorientation (MSR)

The mean square reorientation for a lag $q \in \mathbb{N}^*$ is defined by:

$$M_q = \left\langle (\alpha_{n+q} - \alpha_n)^2 \right\rangle \tag{A16}$$

and can be expressed as a sum of correlations as follows:

$$\begin{aligned} M_q &= \left\langle \left(\sum_{i=1}^q \delta\alpha_{n+i-1} \right)^2 \right\rangle \\ &= \left\langle \sum_{i=1}^q \sum_{j=1}^q \delta\alpha_{n+i-1} \delta\alpha_{n+j-1} \right\rangle \\ &= \sum_{i=1}^q \sum_{j=1}^q \langle \delta\alpha_{n+i-1} \delta\alpha_{n+j-1} \rangle \\ &= q \langle \delta\alpha_n^2 \rangle + \sum_{i=1}^q \sum_{\substack{j=1 \\ j \neq i}}^q \langle \delta\alpha_{n+i-1} \delta\alpha_{n+j-1} \rangle \\ &= q \langle \delta\alpha_n^2 \rangle + 2 \sum_{i=1}^{q-1} (q-i) \langle \delta\alpha_n \delta\alpha_{n+i} \rangle \\ &= \left[q + 2 \sum_{i=1}^{q-1} (q-i) C_i \right] \langle \delta\alpha_n^2 \rangle \end{aligned}$$

and using **Equation A13** we finally obtain the expression used in **Figure 11**:

$$M_q = \left[q + 2 \sum_{i=1}^{q-1} (q-i) C_i \right] \left(p_{turn} \sigma_{turn}^2 + (1 - p_{turn}) \sigma_{fwd}^2 \right) \tag{A17}$$

Appendix 2

Neuronal model of the ARTR

The architecture of the ARTR neuronal model is shown in **Figure 5A**. The circuit consists of two modules selective to lefward or rightward turning. Each module receives recurrent excitatory, cross-inhibitory and sensory inputs. The firing rates of the left/right ARTR modules, noted $r_{L,R}$, are governed by two differential equations:

$$\begin{cases} \tau \dot{r}_L = -r_L + \phi(w_E r_L - w_I r_R + I_0 + I_L(t)) + \epsilon(t) \\ \tau \dot{r}_R = -r_R + \phi(w_E r_R - w_I r_L + I_0 + I_R(t)) + \epsilon(t) \end{cases} \quad (\text{A18})$$

where $w_E r_{L,R}$ is the recurrent excitatory current and $w_I r_{L,R}$ is the cross-inhibitory current originating from the contralateral side of the network. I_0 is a constant input current and $\epsilon(t)$ is a white noise. The function ϕ is a non-negative spiking constraint such that $\phi(x > 0) = x$ and $\phi(x < 0) = 0$. We fixed $\tau = 100 \text{ms}$, a typical slow synaptic time constant, as in **Wang (2002)**. The constant input current is set to $I_0 = 20 \text{s}^{-1}$ and the standard deviation of the noise current ϵ is set at 500s^{-1} as in **Wolf et al. (2017)**. I_R and I_L are the visual input currents, proportional to the intensity impinging the right and left eyes, respectively.

In this dynamical system, w_I controls the anticorrelation between left and right module activities. We fixed $w_I = 7$ such that the anticorrelation of the left and right signals (in the absence of visual inputs) was comparable to the value -0.4 measured through calcium imaging of the ARTR as reported in **Wolf et al. (2017)**. The parameter w_E controls the ability for each side of the network to exhibit stable activity across time periods longer than τ . The network exhibits three different dynamic regimes depending on w_E . One is characterized by an absence of stable activity (low w_E). For $w_E \sim 1$, one module is constantly active while the other remains silent. At intermediate values of w_E , the network displays stochastic slow alternations between both states. The fixation time, that is the characteristic decay time of the autocorrelation of $r_{L,R}$, is governed by w_E . We chose $w_E = 0.925$ such that the auto-correlation in orientation of turning bouts is similar to its experimental counterpart (**Figure 5C** and **Figure 1J**).

To examine the effect of a stereovisual contrast c on the network dynamics, the sensory input currents were set such that:

$$\begin{cases} I_L(t) = I_{light}(1 - c)/2 \\ I_R(t) = I_{light}(1 + c)/2 \end{cases} \quad (\text{A19})$$

The value of the maximum current I_{light} was set at $I_{light} = 1000 \text{s}^{-1}$ in order to reproduce the contrast-dependent orientational bias (**Figure 5D** and **Figure 2G**).

Chapter 4

Interlude: Head-fixed virtual orientation of zebrafish larva to a light source

Having reached a thorough understanding of the two complementary strategies at play during larval zebrafish light-seeking behavior, we now seek to understand the neuronal processes that subserve this behavior. An intermediate step is then to either build a moving microscope which is able to follow the larva as it navigates (Kim et al., 2017), or a less but still sufficiently challenging approach is to elicit a similar behavior under a fixed microscope, thus in tethered and virtual-reality conditions.

In this Chapter I will describe a setup that enables the emulation of a setting in which a partially restrained zebrafish larva can reorient with respect to a virtual light source. The larva is fixed by the abdomen, while eyes and tail, whose orientation and position, are monitored are free to move. In the first part of the chapter, I will describe the attempted swim kinematics under constant illumination. In a second part, I will show how a virtual orientation of the animal was computed and used to update the visual stimulus such as to mimick a distant virtual light source.

4.1 Spontaneous dynamics

4.1.1 Methods: monitoring of head-fixed dynamics

Setup. Zebrafish larvae were restrained in a drop of gelified agarose (2% low melting point, UltraPure LMP Agarose, Invitrogen) on a petri dish filled with E3 medium. The agarose was removed from regions around the eyes and tail, allowing for optical tracking of the ocular saccades and tail bouts. The larvae were then positioned at the center of a 5cm in diameter frosted glass disk lit from below with an infra-red LED and

positioned inside a dark chamber at 28°C. Eye and/or tail movements were recorded using an infrared sensitive Flea3 USB3 Camera (FL3-U3-13Y3M-C, Point Grey Research, Richmond, BC, Canada) with an adjustable macro lens (Zoom 7000, Navitar, USA). Controlled stereo-visual stimulation was obtained using two LEDs (LED465E -Thorlabs) separated by a partition and projected onto the frosted screen, so that each LED delivered a uniform illumination to one side of the animal’s visual field of view. The assays were performed using stimuli in the blue domain, as phototaxis is mainly triggered by this spectrum. Analog outputs of a DAQ device (USB6000 -National Instrument) were used to control the intensity of the visual stimulation in the range $0 < I < I_{max}$, with $I_{max} = 60 \mu W/cm^2$. Matlab (MathWorks) was used for image analysis and on-line control of the visual stimuli.

Movement recordings. To evaluate swim bout orientation, the image of the tail region (from the caudal border of the swim bladder to the tip of the tail) was binarized and we computed at each time the moment of area with respect to the animal rostral-caudal axis, *i.e.* the mean distance to this axis computed over the tail pixels. To allow for across-samples comparison, this quantity was normalized by the tail length yielding an adimensional parameter $m(t)$ characterizing the instantaneous lateral excursion of the tail (figure 4.1, a).

The time derivative of the moment $m(t)$ signal was used to identify and separate discrete tail bouts. For each event the onset t_{on} and offset t_{off} times were extracted, as well as a turning score defined as $M = \int_{t_{on}}^{t_{off}} m(t) dt$. Large positive (negative) M values corresponded to ample leftward (rightward) attempted turns.

We assume a linear relationship between M and the resulting reorientation angle. Thus, the reorientation angle in virtual space $\delta\alpha$ of the larva was computed as the turning score M multiplied by a gain a : $\delta\alpha(t) = a * M$. The gain a was empirically set such that the mean M of a reorienting bout would correspond to the mean reorientation angle $\delta\alpha$ in free swimming conditions, would roughly correspond to $a = \frac{\pi}{6}$.

The orientation of each eye was extracted by computing the angle between the equivalent-ellipse minor axis (*i.e.* the eye optical axis) and the medial-lateral axis of the fish (left: β_l , right: β_r), from which the gaze angle was defined as $g = (\beta_l - \beta_r)/2$ (figure 4.1, a).

The normalized gaze angle associated with a given tail-bout was defined as its value evaluated in the middle of the bout, $g(t_{on} + t_{off})/2$. The onset of each saccade was extracted using the time-derivative of the gaze signal (figure 4.1, b).

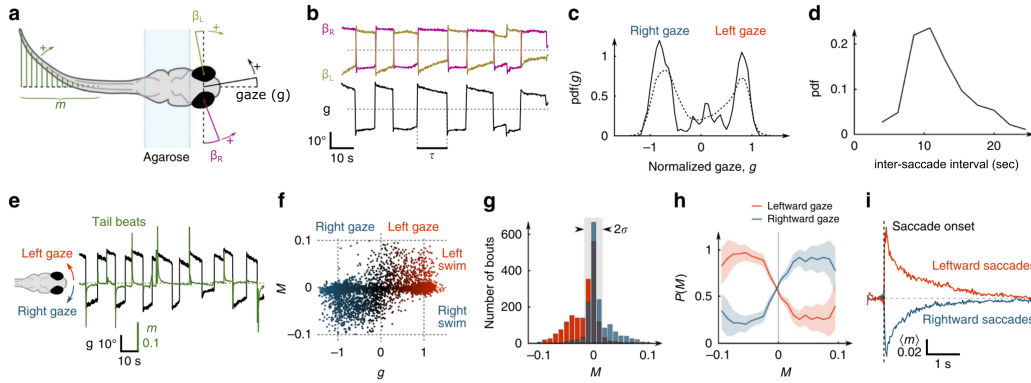


Figure 4.1: Coordination between gaze and tail movements. Definition of the eye and tail kinematic parameters. The gaze angle is defined as the mean orientation of both eyes. The parameter m characterizes the instantaneous tail deflection. (b–d) Gaze dynamics. (b) Example time-traces of the eye and gaze angles. (c) Probability distribution function (PDF) of the normalized gaze angle, for one fish (solid line) and for $N=29$ fish (dashed line). (d) PDF of the delay between successive reorienting saccades for one fish. (e–i) Saccade & tail-beat coordination. (e) Gaze angle and tail deflection signals. (f) Individual tail-beats turning score M , defined as the integral of $m(t)$ over the swim-bout, vs. the normalized gaze angle g ($N=11$ fish). (g) Histograms of M for leftward (red) and rightward (blue) gaze orientation. The central part of the distribution corresponds to forward bouts. (h) Conditional probability of the gaze to be orientated to the left (red) or right (blue) given the tail-beat turning score M ($N=11$ fish). The shaded region corresponds to the s.e.m. (i) Mean peri-saccadic tail deflection signal averaged over leftward (blue) and rightward (red) saccades. Adapted from Wolf et al. (2017)

4.1.2 Results

4.1.2.1 Eye and tail direction coordination

This setup is very similar to the one used in Wolf et al. (2017) to monitor saccade and tail movement dynamics. In these partially-tethered conditions, the zebrafish larva is fixed by the head/abdomen (figure 4.1 a), both eye positions (gaze) and tail position (moment) were monitored (figure 4.1 e). Instantaneous tail movements are quantified using the tail deflection parameter m , and the direction of an attempted bout is extracted using the turning score M , being the integral of m over the time of the bout event (see methods for details). Gaze g is defined as the mean angle of left and right eyes. Saccadic eye movements are displayed intermittently, with fixation times of the order of 12s (figure 4.1 c, d). A coordination between saccade direction and tail movement is observed, even if both events are not necessarily concomitant, on average every 1 in 4 saccades happen in less than 0.5 sec before or after a tail-bout (figure 4.1 f-i).

4.1.2.2 Tail bout kinematics

While in Wolf et al. (2017) we mostly examined eye saccade dynamics, for the closed-loop phototaxis experiments, I focused on the spontaneous tail movement dynamics, to evaluate to what extent the virtual navigation compared with the free swimming kinematics.

The spontaneous dynamics of freely swimming zebrafish locomotion are unfortunately not exactly reproduced in partially tethered conditions, even with tail and eyes free to move. The main discrepancy is the tail-bout frequency : from a mean of 1Hz in freely moving conditions, it drops to 0.03 Hz when the larva is restrained (figure 4.2 A).

Nevertheless, the bimodality of the bout type distribution is conserved: the distribution of the turning score M can be fitted with the sum of two gaussians, in line with the distribution of reorientation angles $\delta\alpha$ observed in freely swimming assays. M can be considered a reasonable proxy of the bout amplitude, and the value of M can be directly converted into a reorientation : $\delta\alpha = 1.2 * M$ (figure 4.2 B). In tethered conditions, the fraction of turning bouts seems to be slightly increased: $p_T = 0.49$ vs 0.41 in free swimming conditions.

As the inter-bout interval is multiplied by 30 on average, and the correlation of successive reorientation bouts is time-dependent, we might expect almost no correlation in successive M values. Still, if we compute the correlation between bouts as a function of the time interval between them, we can still observe a significant correlation C_τ (figure 4.2 C). On average, though, the correlation of successive bouts C_q drops to 0 after the first bout (figure 4.2 D). If we select only the bouts that are separated by a maximum of 10 seconds in time, the correlation is still visible at moderate bout amplitudes when computing M_{n+1} as a function of M_n (figure 4.2 E). For high values

of M , correlation seems to vanish, which may be interpreted as resulting from struggle movements, which bear no correlation in their orientation.

All in all, the difference between attempted-swim and real-swim dynamics might be encapsulated in a lower event sampling frequency, which masks the orientational motor persistence observed in freely moving animals.

Nevertheless, some aspects of the navigational kinematics being conserved, we may have a look at how these are biased by a luminous stimulus.

4.2 Virtual orientation towards light

4.2.1 Gaze orientation bias

Before looking at the dynamics in the closed-loop virtual phototaxis experiment, I will briefly summarize the results of experiments to which I contributed in Wolf et al. (2017), which give interesting insights as for the eye movements involved in light-seeking behavior. As a coordination exists between tail-bout and gaze directions, we assumed the gaze to be a proxy for the direction of potential tail movements.

In these experiments, larvae were partially embedded with their eyes free and submitted to two illumination sequences. In a first one (see figure 4.3 A), they were exposed to periods of leftward or rightward illumination (contrast) in an open-loop fashion. This induced a bias of the gaze toward the illuminated region, with an increase of fixation times.

The second illumination pattern was temporal: its intensity was locked on the larva's gaze (see figure 4.3 B). If the larva would look to the left, the intensity would rise and vice versa. Here again the gaze was biased towards the side the larva would find the highest illumination.

In both conditions, the light gradient induced a statistical bias of the spontaneous saccadic dynamics whose net result was to increase the relative duration of gaze fixations towards the brightest region, which would suggest that eye movements also participate in the light-seeking behavior.

Our next question was to understand the tail movement dynamics in a closed-loop setup for partially embedded larva. This setup has thus been adapted to a closed-loop setup to retroact by updating the illumination not only on eye movements, but also on tail movements. In the next section I will detail the methods related to this adapted setup.

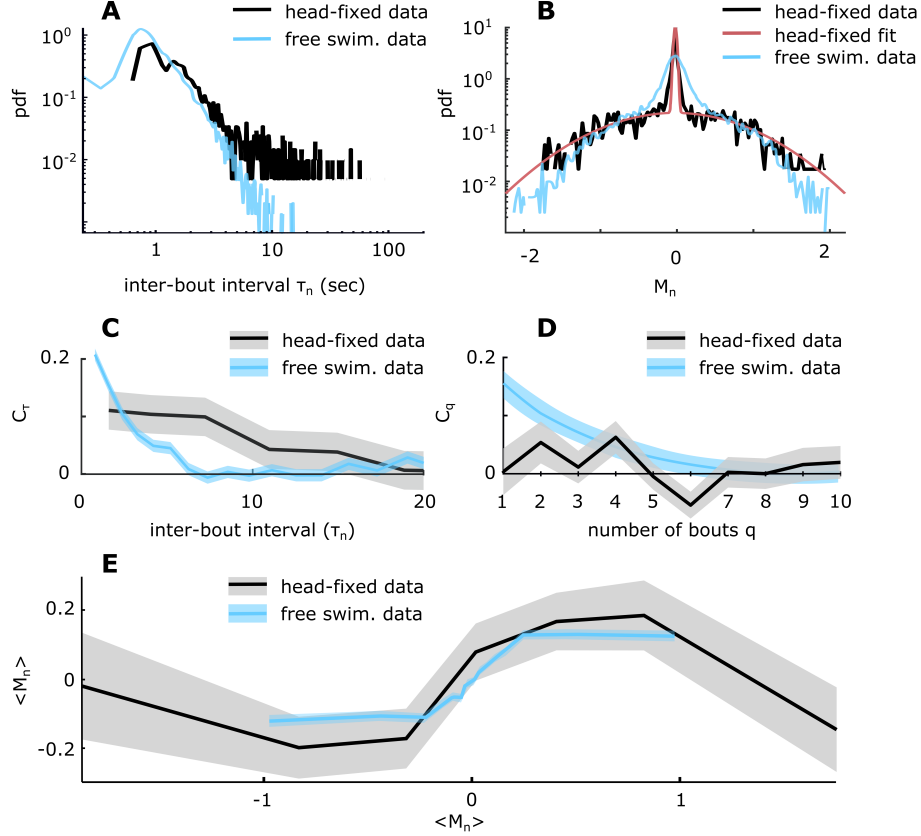


Figure 4.2: Spontaneous dynamics of partially tethered larvae. Data: 24 fish. Distribution of inter-bout intervals τ in partially tethered larvae (black) and free swimming (blue). Median values resp. 0.9 and 1.8 s. Mean values resp. 1.3 and 13 s. (B) Distribution of M , data (black) and custom fit (red), free swimming reorientation distribution (blue) scaled to show similarity. (C) Correlation in all reorientation angles (turns and forward swims taken together) C_q as a function of the interval between bouts τ_n , head-fixed (black) compared to free swimming data (blue). (D) Correlation in reorientation angles C_q as a function of the number of bouts q , head-fixed (black) compared to free swimming data (blue). (E) Mean reorientation value at bout $n+1$ as a function of mean reorientation at preceding bout n , head-fixed (black) compared to free swimming data scaled (blue). Only successive bouts with an inter-bout interval smaller than 10 seconds were taken into account.

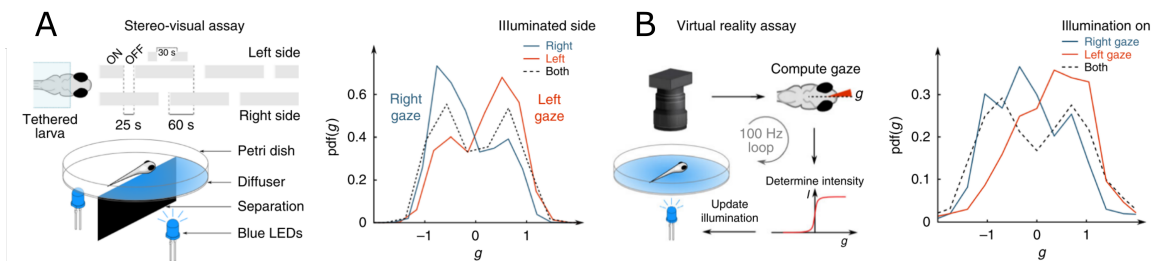


Figure 4.3: (left) Scheme of the experimental assay and the imposed illumination pattern. (right) PDF of the normalized gaze during periods of unilateral stimulation for animals displaying positive phototaxis ($N=18$ fish). Red and blue curves correspond to illumination on the left and right eye, respectively. Dashed curve indicates bilaterally symmetric illumination. (B) Spatio-temporal gaze phototaxis. (left) Scheme of the virtual-reality assay. The fish is submitted to a uniform illumination whose intensity is driven in real-time by the animal's gaze angle. (right) PDF of the normalised gaze angle for virtual leftward (red) and rightward (blue) illumination ($N=13$ fish). The dashed curve corresponds to the neutral runs (constant illumination). From Wolf et al. (2017)

4.2.2 Methods: closed-loop with feedback on tail-bouts

Building on the setup described in the previous section, here tail and eye movement are used to control the orientation of a virtual light source the larva can navigate toward. The animal is submitted to a controlled visual stimulation using LEDs placed below a diffusive screen under the larva, on each side of its body (figure 4.4 A). The intensity targeting each side is updated in realtime (every 5 ms, 200Hz) based on the animal's gaze orientation and attempted swim turn. The light intensity emitted by each LED is calculated based on the angle between the larva's rostro-caudal axis and the light source as well as its eyes orientation. At the start of an experiment, a light source angle relative to the body axis is randomly chosen, and updated each time the larva executes a tail bout.

The illumination profile imposed on the zebrafish larva was chosen to mimic a distant light source. Both contrast ($c = I_L - I_R$) and whole-field intensity ($I = I_L + I_R$) are set to vary with its virtual angle relative to the source $\theta = \alpha - \theta_s$ and with its gaze direction g (figure 4.4 B, C). When the light source is straight in front of the larva, $\theta = 0$, and the gaze points towards it, $g = 0$, the intensities received on left and right eye are equal, but not maximal.

4.2.3 Results

Virtual orientation towards light. The illumination profile used here combines both variation of global intensity and of left/right intensity (contrast), to mimic a

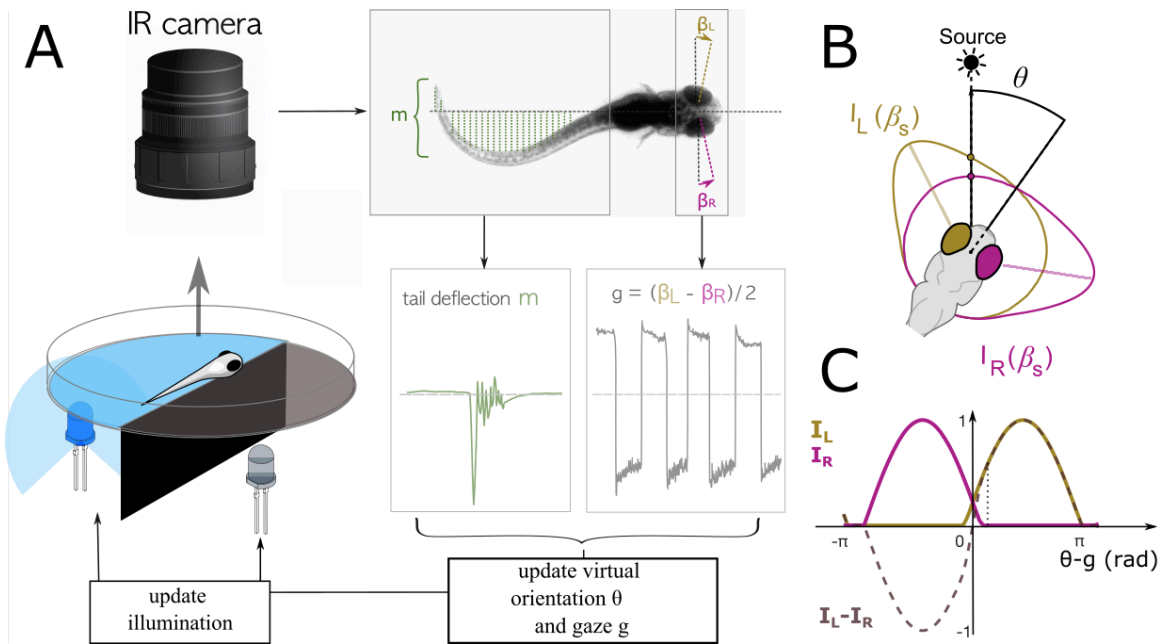


Figure 4.4: Closed-loop partially tethered phototaxis setup. The zebrafish larva is fixed in a drop of agarose in the centre of a petri dish. Its eyes and tail are freed from the gel, allowing saccades and tail movements to occur. It is monitored from above, and illuminated from below by two blue LEDs controlled in closed-loop. Eye and tail movements are recorded through the values of tail deflection m and gaze g . Using these values, a virtual orientation θ relative to a light source is calculated, and the illumination below the animal updated accordingly. (B) Scheme of the intensity received by each eye from a distant light source. Both the animal's body axis angle to the light source θ_s and its gaze direction determined by the angle of each of its eyes β_R and β_L determine the intensity I_R and I_L . (C) Illumination profile of each eye as a function of the larva's body orientation and gaze $\theta - g$. When the source is at the azimuth, $\theta = 0$.

distant light source the zebrafish larva can orient towards (figure 4.5 A), which is located at $\theta = 0$.

As in free swimming conditions, partially tethered larvae robustly reorient themselves to find a steady-state where on average they are facing the virtual light source (figure 4.5 B). This steady state is reached after only a few bouts: the “aggregation” around $\theta = 0$, described as $v \cos < \theta >$, where v is the mean resultant vector of the orientations at each bout, is maximal after about 6-8 bouts following a novel light-source orientation, as seen on the orientational trajectory with bout number (figure 4.5 C).

To investigate more precisely how this reorientation is enabled, we first analyzed how the reorientation score M at each bout may be driven by the contrast. Here, the contrast is again defined as $c = I_L - I_R = f(\theta_s)$ (note that in this case $I_L + I_R$ is also variable). As in the free swimming conditions, there is a linear relationship between the experienced contrast and triggered tail movement direction at low values of absolute contrast ($|c| < 0.4$, figure 4.5 D). At high values of contrast ($|c| > 0.4$), which correspond to high varying values of intensity on only one eye, while the second eye is in the dark, there is a saturation of the mean turning score $< M >$. The bias induced by a stereo-visual contrast thus has a maximum, above which increasing the intensity will have no effect or may even induce negative phototaxis. Stereo-visual phototaxis is thus clearly displayed in head-fixed conditions.

As global intensity also varies with θ in our assay, we looked into how a relative change in intensity $\delta I/I$ might affect the amplitudes of subsequent tail movements. When the animal experiences a decrease in relative intensity $\delta I/I$, during a given bout, the amplitude of the forthcoming bout (as measured by M^2) is increased. A drop in $\delta I/I$ also seems to trigger a faster response: the mean inter-bout interval τ is decreased by a factor of two for $\delta I/I = -2$ compared to a positive $\delta I/I$ (figure 4.5 E).

These results demonstrate that the main features of light-seeking behaviors observed in freely-swimming conditions, are conserved in the head-restrained configuration, allowing the animal to perform efficient orientational phototaxis.

Virtual diffusion towards light. While the contrast paradigm was known to trigger direct reorientation also in tethered conditions, what was interesting here was to observe a consistent response to a decrease in illumination. To check whether this temporal response alone was sufficient for phototaxis in the head-fixed setup, a small subset of experiments done on 6 different fish was performed using a kino-phototaxis paradigm. The whole-field illumination was here varied with θ_s following a normal (gaussian) profile, with $I = I_L = I_R$, such that no direct spatial information on the gradient was available to the animal (figure 4.6 A).

In this case the larvae also tend to aggregate around $\theta_s = 0$, seeking the maximum intensity (figure 4.6 B, the distribution skewness is due to the small sample size). The reorientation happens quickly here again: after only about 4 bouts following the presentation of a new light source orientation, the aggregation is maximal (figure 4.6

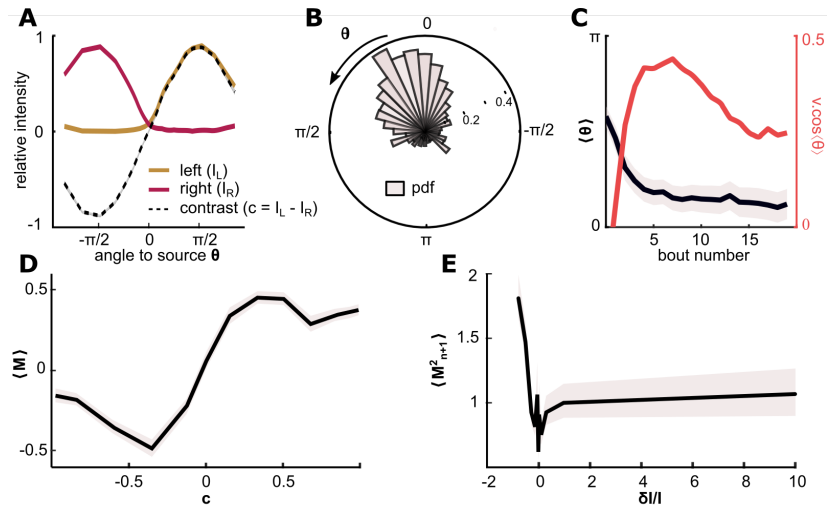


Figure 4.5: Intensity profile used to simulate a distant light source. The value $\theta = 0$ is a stable point. (B) Probability density function (pdf) of θ biased towards 0. (C) Evolution of the absolute mean orientation $|\langle \theta \rangle_q|$ with bout number q (black) and of the projection of the resultant vector onto the direction of the light source $v \cdot \cos \langle \theta \rangle$ with bout number, showing a non-uniform distribution biased toward $\theta = 0$ after ~ 5 bouts. (D) Mean turning score $\langle M \rangle$ as a function of the contrast. For low absolute values of contrast the bias is linear. For higher values, a saturation is visible. (E) Variance of the turning score as a function of relative intensity variation experienced at previous bout. $N=24$ fish.

D). Again, this process is mediated by a simple increase in the tail-bout amplitude evoked by a light intensity decrease (figure 4.6 C).

Thus, in spite of the largely reduced bout frequency, temporal light-seeking strategy can be observed in partially immobilized zebrafish larva.

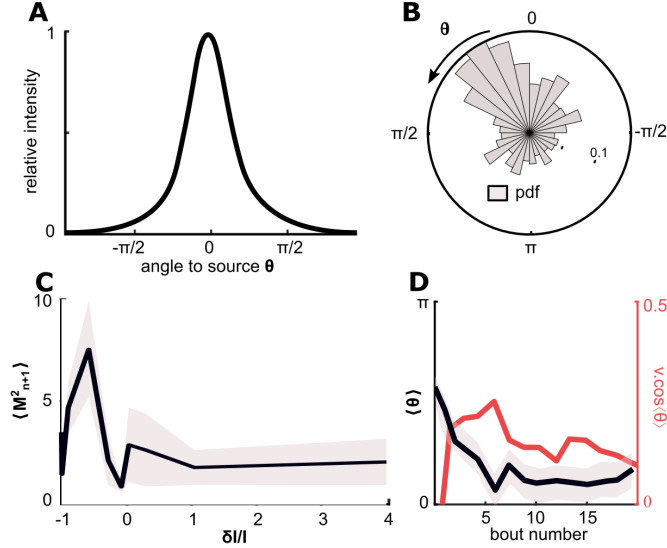


Figure 4.6: Intensity profile varying with θ . (B) Probability density function (pdf) of θ , biased toward 0. (C) Variance of the turning score as a function of relative intensity variation experienced at previous bout. (D) Evolution of the absolute mean orientation $|\langle \theta \rangle_q|$ with bout number q (black) and of the projection of the resultant vector onto the direction of the light source $v \cdot \cos \langle \theta \rangle$ with bout number, showing a non-uniform distribution biased toward $\theta = 0$ after ~ 3 -5 bouts. $N=6$ fish

4.3 Discussion

We were able to successfully build and use a closed-loop behavioral assay system for partially tethered larvae to elicit virtual light-seeking behavior. The free-swimming dynamics in the absence of a stimulus were obviously not reproduced, the main difference being the bout frequency which drastically drops in tethered conditions. Nevertheless, the key parameters for reorientation towards a light spot are conserved: a direct bias of attempted reorientations in the presence of a contrast, and an increase of reorientation amplitude after a drop in relative illumination. Thus the light-seeking behavior described in the previous part can be replicated in head-fixed conditions.

What enabled us to circumvent the problem of bout frequencies in comparing this behavior in both freely swimming and fixed conditions, was “getting rid” of time by discretizing time sequences into sequences of swim bouts. This enables to focus on

specific moments of a sensorimotor sequence and know what motor action followed what stimulus.

Here again we limited our analysis to orientation only. But in such a setup, it is very feasible to add a second dimension and allow the fish navigate in two dimensions, thus generating virtual trajectories in the horizontal plane.

The low frequency of tail movements points towards the fact that a phototactic stimulus is not engaging enough to completely mimic a sensorimotor loop in head-fixed virtual conditions. A recent study investigated the capacity of larval zebrafish to evaluate the “utility” or “futility” of a motor action (an attempted swim): in the absence of a visual feedback (motion perception) following an action, the attempted swim events are eventually considered as futile. Thus, the larva gives up and stops triggering movements that yield no outcome (Mu et al., 2019). In this setup the larva might indeed lack a visual flow, which makes it fall into a passive state rather than an active one. One possibility to circumvent this problem would be to add an engaging stimulus to the phototactic one, as for example whole-field motion, in closed-loop, to trigger the optomotor response. I tried to implement this option in our setup, but did not succeed in triggering significantly more tail movements: after a few minutes of closed-loop OKR the larvae seemed to give up anyway. But this might have been simply an issue of the gain setting. Still, if implementing such a closed-loop with combined visual cues, the process would be - if not multisensory, as it would still rely solely on vision - but multitasking: maintaining a steady image of the surroundings while performing light-seeking behavior. Such that one might interfere with the other: if for example not being swept away by the current is more important than finding a luminous spot, the optomotor reflex would get the upper hand.

Chapter 5

Neural circuit underlying orientational phototaxis

As we now have a closed-loop setup for the larva to perform head-fixed virtual phototaxis, we can combine it with a functional imaging setup to gain insight into the neural computations during a sensorimotor loop. This will be the aim of this final chapter.

I will first introduce the single-plane illumination (or light-sheet) microscope setup after a quick prior on fluorescence imaging techniques. I will then present the known neural correlates of zebrafish larva light-seeking behavior as well as some results from functional light-sheet imaging in a closed-loop with phototactic stimuli.

5.1 Light-sheet imaging with visual stimulation

5.1.1 Fluorescence Calcium imaging

5.1.1.1 Fluorescence microscopy

The first recorded observation of fluorescence was made by Sir Frederik William Herschel in 1845: “although itself colorless and transparent, (it) exhibits a “vivid and beautiful celestial blue color” when illuminated and observed under certain incidences of sunlight”, referring to a quinine solution. It was later explained that the UV spectrum of sunlight excites quinine which then emits blue light.

Fluorescence was discovered when microscopy was already well-established, in the early XXth century. Ellinger and Hirt generated the first fluorescent samples by treatment of living organisms with fluorescent substances. They were illuminated by incident light (generally UV) and the fluorescent signal observed thanks to a set of illumination/observation filters, akin to contemporary fluorescence microscopy (Renz, 2013). Since then, the ways of fluorescence labelling evolved tremendously: from fluorescent

antibody labelling in the 40s to cloning of the Green Fluorescent Protein (GFP) and its spectral variants (YFP, RFP) in the 90s, after it was extracted from the jellyfish *Aequorea victoria* in 1962.

The latter eventually enabled the engineering of genetic encoding of fluorescence: combined with a Calcium sensor molecule, leading to the so-called GECIs (Genetically Encoded Calcium Indicators) to probe intracellular calcium levels. Along with synthetic calcium reporters, directly injected into the studied cell, GECIs are today widely used in various fields of biology to study calcium dynamics either for itself or as a proxy.

In neuroscience, the most widely used GECI is GCaMP, developed by Nakai et al. (2001) and continuously improved and adapted since. GCaMP is composed of the calcium sensor calmodulin (calcium-modulated protein) and a fluorescent reporter, a modified version (circularly permuted & enhanced) of GFP. Upon calcium binding to the calmodulin region, a conformational change is triggered resulting in an increase in fluorescence.

Transgenic zebrafish lines expressing GECIs have quickly spread, after the first one established by Higashijima et al. (2003) (not GCaMP but Cameleon) who monitored calcium transients in motoneurons and spinal interneurons in behaving fish (Muto et al., 2011).

5.1.1.2 Calcium imaging

Calcium sensing in neurons is of interest as it is involved in the transmission of depolarizing signals and in synaptic activity (Brini et al., 2014) - it is incidentally a universal signalling molecule in all eukaryotic cells. The electrical activity of a neuron is accompanied with transient changes of calcium concentration in the cytosol. At rest, calcium levels are of the order of 50–100 nM in the cytosol (very low compared to the other ions involved in the transducing of an electrical signal: K^+ 140 mM & Na^+ 12 mM), but a depolarizing signal, and in particular an action potential, triggers a Ca^{2+} influx from extracellular and intracellular compartments through voltage-gated calcium channels, increasing calcium levels 10- or 100-fold (Grienberger & Konnerth, 2012). Thus, in organisms expressing GCaMP in neurons, neural activity manifests itself as transient fluorescence increase which can be optically recorded. Absolute values of fluorescence are highly dependent on many factors (calcium reporter type, expression level, excitation power, detection efficiency, etc), thus the quantity of interest to estimate the activation of a neuron is the relative variation in its fluorescence intensity

$$DFF = \Delta F / F = \frac{F_{response} - F_{baseline}}{F_{baseline} - F_{background}}.$$

Other indicators of neural activity, not targetting calcium dynamics also exist: vesicular release indicators, voltage sensors (Yang & St-Pierre, 2016), neurotransmitter indicators (Deo & Lavis, 2018; Lin & Schnitzer, 2016), but their implementation is less “mature” than that of calcium indicators. Focusing on calcium dynamics allows

the functional study of neural ensembles, but also of dendritic processing, or synaptic function, sometimes in long-term time-lapse imaging settings. Still the DFF is a very indirect measure of neural activity: calcium dynamics may vary across neuron types, and calcium indicators have also their specific kinetics which have to be taken into account. The 2 main GCaMP lines used in our lab are GCaMP6s, GCaMP6f:

Dynamics <i>in vitro</i>	GCaMP6f	GCaMP6s
Kd (nM)	380	140
Rise time (ms)	50–75	100–150
Half-decay time in tissue <i>in vitro</i> (ms)	140	550

In vivo values for rise and decay times following a single spike are comparable to *in vitro* values cited in the table above (Chen et al., 2013).

GCaMP6 has an excitation spectrum peaking at 488nm (blue) and an emission spectrum peaking around 510nm (green) (Wright et al., 2017)

Kd corresponds to the calcium concentration at which half of the indicator molecules are bound to calcium, inverse of the affinity. GCaMP6s produces larger responses to single APs, but at the cost of decays that are 93–190% longer than that of GCaMP6f (Hires et al., 2008).

Nuclear calcium indicators have also been developed. In the one used in the lab, the GCaMP molecule is bound to a histone protein H2B, a protein involved in chromosome coiling. The fluorescence signal of such indicators is - additionally to the previously discussed parameters - modulated by their localization: nuclear Ca²⁺ elevations are dependent on diffusion from a cytoplasmic source and lag behind cytoplasmic levels by approximately 60 ms (Nakazawa & Murphy, 1999).

It is thus important to keep in mind, that calcium imaging is only a proxy for neural activity. Its main limitation is that kinetics are slow compared to an AP (which lasts 3–5 ms), thus individual spikes in rapid spike trains cannot be distinguished and spike rate changes might also be difficult to evaluate. Less crucial limitations are that there is no reporting of neurotransmitter receptor activation, of membrane hyperpolarizations nor of sub-threshold voltage changes.

5.1.1.3 Inference of neural activity

It is possible - though challenging - to infer action potentials, or spiking activity through deconvolution or unsupervised learning algorithms. This may be useful for denoising data and inferring precise spiking times, as imaging techniques have much lower temporal resolution compared to electrophysiological techniques. The challenge resides in the non-linearities of the spike–calcium reporter fluorescence relationship, low temporal resolution of the calcium signal compared to the time scale of an action potential as

well as noise. Two main methods of spike inference from calcium imaging have been developed:

- one based on non-negative deconvolution (NND) of calcium signal (assuming fluorescence traces represent an approximate convolution of the underlying spike train with the cell’s calcium response and based on the hypotheses that spikes are sparse and non-negative) (Vogelstein et al., 2010 *Fast nonnegative deconvolution for spike train inference from population calcium imaging*)
- a second one based on supervised learning techniques using convolutional neural networks (Theis et al., 2016).

Each new spike inference method from calcium imaging data published these past 10 years claimed to outperform its predecessors. So a community-based benchmarking, the spikefinder challenge, has been performed to select the better performing algorithms (Berens et al., 2018 *Community-based benchmarking improves spike inference from two-photon calcium imaging data*). The conclusion of the benchmark postulated that algorithms based on supervised learning outperformed unsupervised non-negative deconvolution methods.

Both methods have their qualities and drawbacks:

- supervised methods might best perform on a particular set of data but are poorly generalizable to “out-of-sample” data, on which they haven’t been trained
- spike deconvolution methods might be more generalizable, they are often good enough (Chen et al., 2013), but may fail in more complex situations (some of which have been addressed by Deneux et al. (2016) *Accurate spike estimation from noisy calcium signals for ultrafast three-dimensional imaging of large neuronal populations in vivo*). Also they strongly rely on a sparsity of spikes as well as rise and decay time parameters.

As the technique evolves quickly, efforts still go into the development or improvement of generalizable unsupervised deconvolution algorithms. Among them:

- Pachitariu et al. (2018) using NND, with simple parameter settings, which performs better than supervised algorithms when evaluated on out-of-sample data, and adapted to the performance metric of the spikefinder challenge. In addition, we find that NND is highly robust to assumptions on the assumed shape of the calcium kernel response to single spikes.
- Blind Sparse Deconvolution algorithm (Tubiana et al., 2017), addressing the strong dependence on sparsity and time constants parameters, and estimating false positive rates.

5.1.2 2P Light-sheet imaging

5.1.2.1 Point scanning microscopy

Fluorescence microscopy applied to 3D tissue requires optical sectioning, *i.e* the ability to produce an image “of a single layer” of cells for example, and to eliminate signals coming from the out-of-focus surrounding tissue. This is not enabled in bright-field microscopy for example, where the sample is illuminated by transmitted light.

In point scanning techniques, pixels are imaged one by one (the sample needs to move relatively to the illumination/observation branches), eventually forming the complete image. Thus there is a trade-off between the size of the imaged region, composed of N pixels, and the acquisition frequency $f = \frac{1}{t_{exp} \cdot N}$, where t_{exp} is the exposure time.

In confocal microscopy, optical sectioning is achieved with a pinhole, which selects fluorescent photons originating from the sole focal point.

Two-photon microscopy

Two-photon excitation microscopy is an alternative to confocal microscopy that provides advantages for three-dimensional and deep tissue imaging. Optical sectioning is enabled through the 2-photon effect (Benninger & Piston, 2013).

This effect was theoretically predicted by (Göppert-Mayer, 1931), and experimentally demonstrated with the invention of lasers thirty years later (Kaiser & Garrett, 1961). In one-photon excitation, a fluorophore in its ground state can absorb a single photon that excites it to a higher energy state and then relaxes back to its ground state while emitting a photon. For best efficiency, the exciting photon should have a wavelength λ_1 that corresponds to an energy which matches the energy transition ΔE between the ground state and the excited state of the fluorophore $\Delta E = hc/\lambda_1$ (h Plank constant ; c speed of light).

In two-photon excitation the fluorophore absorbs two photons of half the energy of the corresponding 1-photon excitation, in a very short time-window. The first photon transits the fluorophore to a virtual state, the second one to the excited state. Thus the time-window of this almost simultaneous excitation must be shorter than the virtual state lifetime, of the order of 0.5fs. To heighten the probability that 2-photon excitation occurs, the use of a femtosecond pulsed laser is required (generating femtosecond-long pulses of light at high frequency typically 80 MHz).

As the energy of a photon is inversely proportional to its wavelength, in two-photon excitation, the photons should have a wavelength λ_2 of approximately twice that of the photons required to achieve an equivalent transition under one-photon excitation. $\Delta E \simeq 2hc/\lambda_2$.

For the excitation of GCaMP6, $\lambda_1 = 488nm$ and $\lambda_2 = 920 - 930nm$.

5.1.2.2 Light-sheet imaging

Light-sheet imaging, or selective-plane illumination microscopy, achieves optical sectioning by illumination of a whole plane (instead of a point) of the sample perpendicularly to the observation. Here, acquisition frame-rate and dimensions of the imaged region are independent: $f = \frac{1}{t_{exp}}$, and only the imaged plane is illuminated thus reducing photo-bleaching or phototoxicity effects (Hires et al., 2008).

The plane illumination may be done by several methods (digital scanning (Panier et al., 2013; Wolf et al., 2015), cylindrical-lens (Huisken et al., 2004), lattice light-sheet (B. C. Chen et al., 2014)), we use the technique of scanning a laser beam in the horizontal plane at a frequency of at least $1/t_{exp}$, but usually faster ($\sim 200\text{Hz}$). Some research has focused on the improvement of these cited methods, for artifact reduction (reduction of striping Huisken & Stainier (2007), adaptive optics Liu et al. (2018), increasing image quality and penetration depth with bessel beams Fahrbach & Rohrbach (2010) and Planchon et al. (2011))

First uses of light-sheet technique in life sciences were to image myocytes expressing GFP of a Medaka larva, and to observe the development of drosophila embryo during several hours (Huisken et al., 2004). The in-plane resolution was $6\ \mu\text{m}$, for a field of view of $1.5 \times 0.9\ \text{mm}$. A few years later, Keller et al. (2008) observe the development of genetically modified zebrafish larva expressing GFP. The resolution of $1\ \mu\text{m}$ of images of size $700\ \mu\text{m} \times 700\ \mu\text{m}$, enabled the imaging of the whole embryo at single-cell resolution during more than 24h.

Zebrafish larva with its small size and transparency thus appeared to be an excellent candidate for light-sheet imaging, and this technique quickly was adapted for calcium imaging of larval zebrafish neurons (Ahrens, Orger, et al., 2013b; Chen et al., 2018; Jiao et al., 2018; Panier et al., 2013; Privat et al., 2019).

5.1.3 2P Light-sheet imaging in zebrafish

As the developed light-sheet setups illuminate larval zebrafish from the side to obtain a horizontal/transverse section of the brain, its eyes are partly irradiated. The blue light of the laser may thus interfere with the experiment when one studies zebrafish's responses to light. Especially when the laser wavelength $\lambda_1 = 488$ lies within the most sensitive region of the fish visible spectrum (Risner et al., 2006) and is responsible for the fish's phototactic behavior.

To circumvent this problem, the lab developed a 2-photon light-sheet microscope. It enables to illuminate the sample with an infrared laser beam and create the 2-photon effect only in the focal region of the beam (Wolf et al., 2015).

5.1.3.1 Methods

Here I will describe the adaptation of the 2-photon light-sheet microscope developed in the lab (Wolf et al., 2015).

It is an almost identical twin of a 1-photon light-sheet microscope, except that the illumination wavelength is shifted from 488nm - in the blue spectrum, which could interfere with behaviors mediated by the blue cones, such as phototaxis - to 930nm, in the infrared domain, invisible to the larva's eye.

The pulsed illumination is provided by a titanium:sapphire laser (pulses of <100fs and 80MHz repetition rate, figure 5.1 A). The emitted beam passes through two telescopes (pairs of conjugated lenses 1 & 2, 3 & 4), which magnifies the laser beam by a factor of 6. These two telescopes also enable to transform a rotational movement of two scanning mirrors into a translational movement at the focal point of the illumination objective, where the sample is located: a first 3D scanning mirror (figure 5.1 B) displaces the beam vertically, thus defining the plane of illumination in the sample; and a second scanning mirror (figure 5.1 C) oscillates horizontally at ~200Hz to create a sheet of light (a plane of illumination).

The observation arm consists of a water-immersible objective mounted on a piezo which is locked onto the first 3D scanning mirror to match the focal point of observation with the plane of illumination. A green detection band-pass filter keeps out all light but the sample fluorescence, which is collected by a sCMOS camera (figure 5.1 D) after going through a tube lens.

The stimulation part simply consists of a projector casting onto a thin white opaque plastic screen fixed on the observation objective, enabling its illumination over 180° from the front. The larva is placed in a drop of 2% low melting point agarose on a holder which enables eyes and/or tail to be freed. Behavior is monitored from below: a mirror is placed under the tank, reflecting the image of the fish into an infra-red sensitive Flea3 USB3 Camera (FL3-U3-13Y3M-C, Point Grey Research, Richmond, BC, Canada) with an adjustable lens (Navitar, USA).

To avoid the laser beam damaging the larva's eye, a small mask was put on the trajectory of the laser beam, after the fourth lens, in the image plane of the illumination objective. Its width was chosen to correspond, in the object plane of the illumination objective, to the width of the larval zebrafish eye. (not represented on the figure)

The recordings were done on larval zebrafish 6-8 dpf. The acquisition rate of the microscope was set at 1 stack per second (10 to 20 brain sections, 8 μ m inter-slice separation), and typical recordings lasted for ~30 min. Closed-loop tracking and visual stimulation were performed at a mean frequency of 60 Hz, corresponding to the refreshing rate of the projector, with a custom-written software in Matlab (Mathworks) available on my gitlab page: <https://gitlab.com/Phiasso/trackingandstimulation>.

Image pre-processing and calcium transient extraction were performed offline using

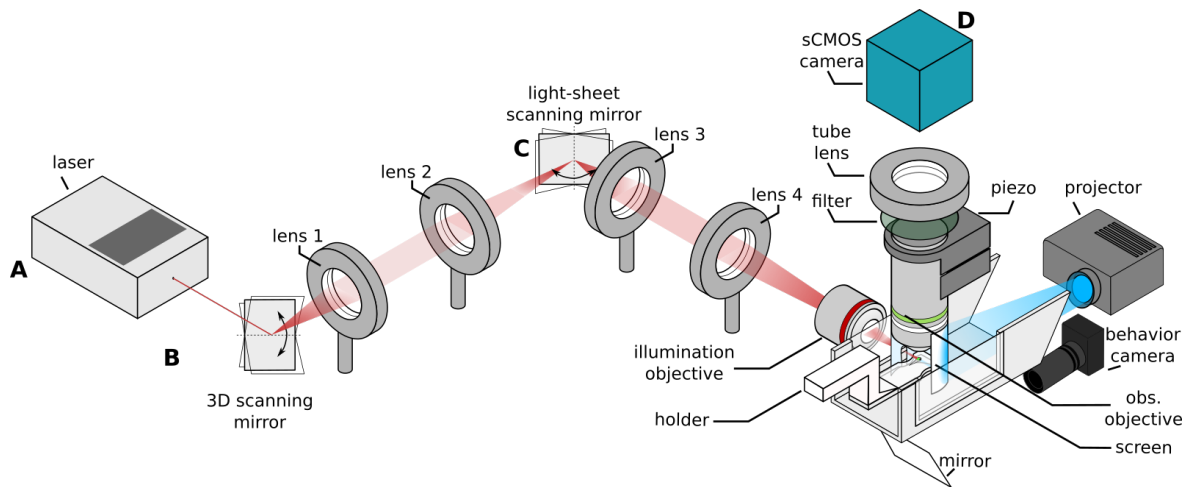


Figure 5.1: Scheme of the 2-photon light-sheet setup with closed-loop stimulation.

MATLAB, according to the workflow previously reported (Panier et al., 2013; Wolf et al., 2015). Further analysis was made with custom-written software in Matlab.

5.2 Neuronal correlates of zebrafish larva phototaxis

The idea one can have in mind when looking for a neuronal circuit responsible for light-seeking behavior, is a circuit that can control navigation (triggering bout movements and/or selecting their direction), and whose dynamics may be biased by specific luminous stimuli. Here I will review what is known of a good candidate for such a circuit, correlated with eye and tail movements, but also modulated by light.

In this part some references will be made to anatomical regions of the zebrafish brain, most of them being represented in figure 5.2.

5.2.1 The saccadic circuit

The saccadic pathway originates in the eye: ganglion cells transmit an information (for example motion) to the optic tectum (OT), which in turn (among other areas) activates the excitatory burst neurons (EBN or saccade generating burst neurons). The burst neurons provide a direct input to the abducens nucleus (ABD) and oculomotor nucleus III, which innervates the extraocular muscles; and the velocity-position neural integrator (VPNI or NI), which provides positional information to the abducens nucleus (Ma et al., 2020; Schoonheim et al., 2010).

In Wolf et al. (2017), neuronal populations potentially involved in the saccadic circuit were mapped using regression analysis of functional recordings on a saccadic event.

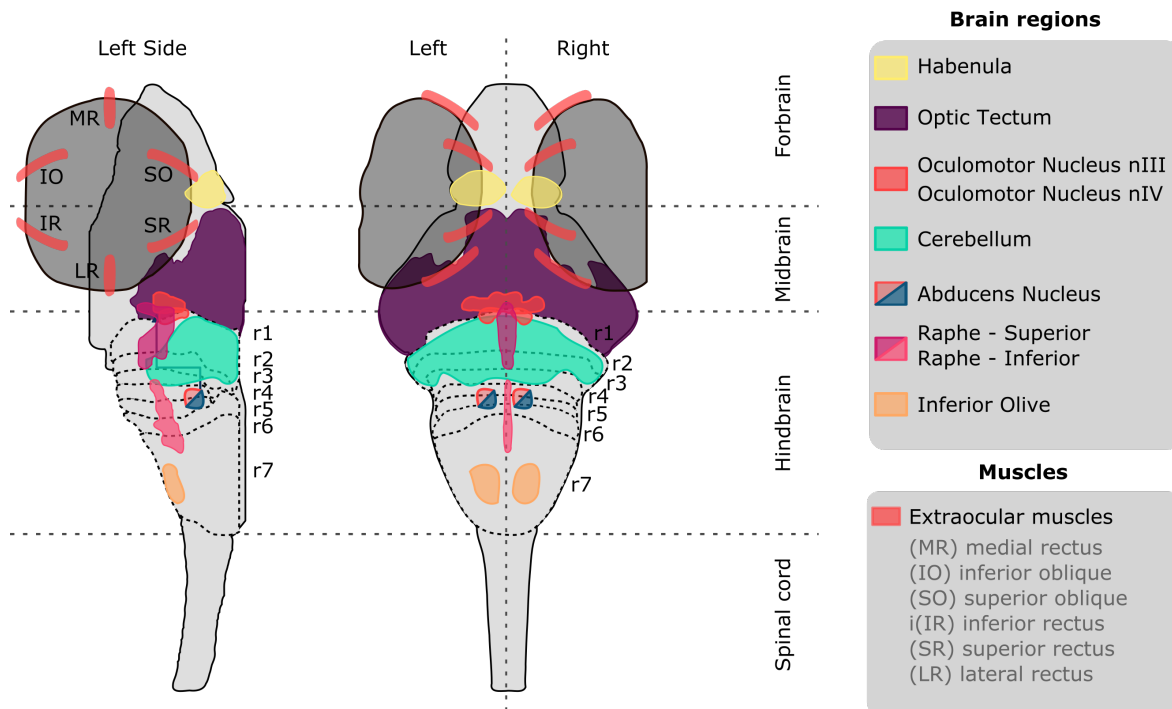


Figure 5.2: Anatomical drawing of some known anatomical structures that are involved or supposed to be involved in zebrafish exploratory or light-seeking navigation. Habenula is located in the Diencephalon, the optic tectum in the Mesencephalon, the most caudal part being the rhombencephalon, or hindbrain. The hindbrain is composed of 7 rhombomeres. Region contours from ZBrain Atlas (Randlett et al., 2015).

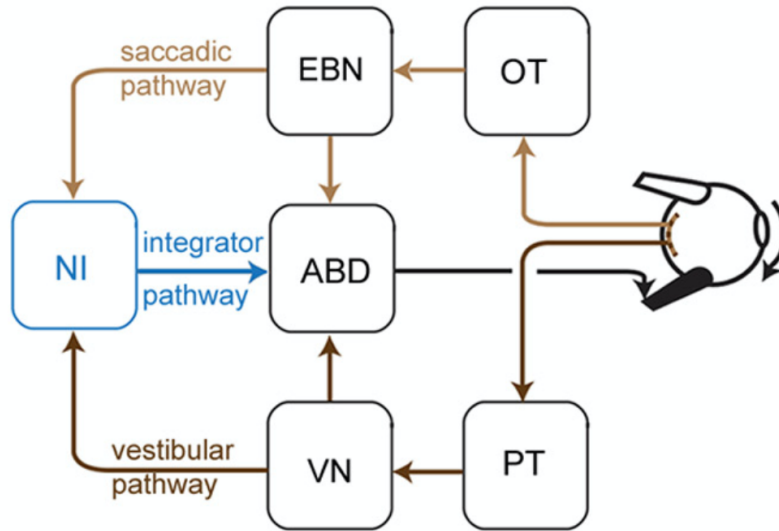


Figure 5.3: Diagram of the oculomotor circuit for horizontal eye movement from Ma et al. (2020). The saccadic, vestibular, and integrator pathways are labeled light brown, dark brown, and blue, respectively. (OT) optic tectum; (PT) pre-tectum; (VN) vestibular nucleus; (EBN) excitatory burst neurons; (ABD) abducens nucleus; (NI) innervate the velocity-position neural integrator

This analysis identified the previously described velocity-tuned saccade generator burst neurons (Schoonheim et al., 2010), the position-tuned velocity-position neural integrator (Miri et al., 2011), and also enabled the discovery of contraversive position-tuned clusters at the rostral border of the hindbrain (rhombomere 1) ventral to the cerebellum and of ipsiversive position-tuned clusters forming bilateral stripes in the rostral hindbrain (rhombomeres 2-3) (figure 5.4, regions numbered 1, 2, 4 and 3 respectively).

It is this latter population that caught the attention of our group, since these clusters displayed sustained antiphasic dynamics, each side activated alternatively, even in the absence of saccades. It was termed the hindbrain oscillator (HBO). The period distribution of this observed oscillation peaked at ~ 20 s, which is close to the saccadic period. Furthermore, an optogenetic actuation of the left or right part of this region was found to trigger ipsiversive saccades quite robustly.

5.2.2 Global responses to stereovisual contrast

5.2.2.1 Stimulus-responses to phototactic stimuli

A global stimulus response map

Chen et al. (2018) recently constructed a phototactic stimulus-response map. The stimulus being a high-contrast onset (light extinction on one eye) after a period of

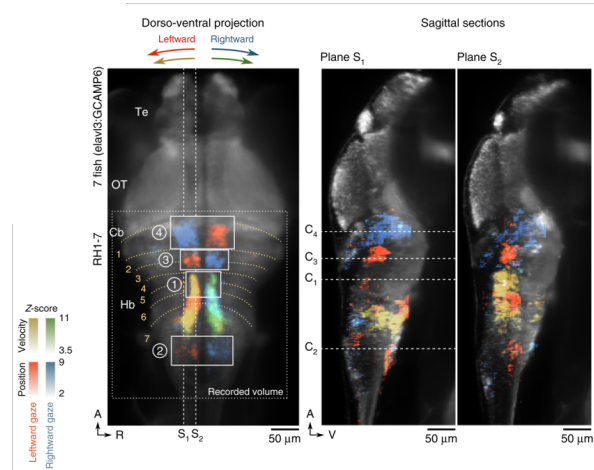


Figure 5.4: Dorso-ventral projection view and sagittal sections along two planes of the 3D functional map showing neuronal populations whose activity is tuned to the gaze orientation (blue and red) and to the gaze angular velocity (green and yellow). The voxel colour encodes the Z-score values obtained through multilinear regression. Te, telencephalon; OT, optic tectum; Cb, cerebellum; Hb, hindbrain; RH, rhombomere. The grey dotted rectangle indicates the effective recorded volume. From Wolf et al. (2017)

illumination for both eyes (see figure 5.5 A). The stimulus regressors were constructed by convolving the stimulus signal with a GCaMP6 response kernel, resulting in the selection of the shown $\langle DFF \rangle$ on the basis of a high correlation coefficient with the regressor trace.

The selected neurons, with color corresponding to their regressor are represented in figure 5.5 B. A lateralized light extinction (which triggers a tropophototactic response (Burgess et al., 2010) mediated by the OFF-ganglion cell pathway) triggers a contralateral response, illustrating the exclusively contralateral projections of ganglion cells.

A finer map was made, based on clustering of neuron's responses (color traces in figure 5.5 C) and anatomy, revealing the ramping activity of the superior raphe nucleus and in the posterior hindbrain (violet clusters, third & fourth arrows), sustained activity in the midbrain (blue), and sparse activity all over the optic tectum corresponding to OFF-responses of the contralateral eye.

5.2.2.2 Motor output involved in phototactic reorientation

Chen et al. applied the same regression-based method to construct a map of phototactic-related motor responses. Fictive swims (swim attempts) were recorded using electrodes attached to the animal's tail, close to motoneuron axons (Ahrens et al., 2012; Dunn et al., 2016). This functional map highlighted the known downstream of the processing,

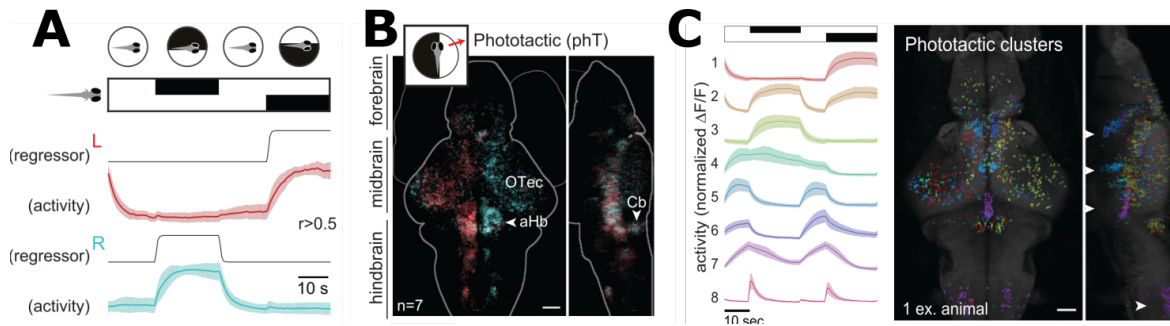


Figure 5.5: Regression analysis of phototactic stimulus. (A) Used regressors (onset of darkness for each eye). (B) Stimulus-response “phototactic” map, sparse mean activity ipsilateral optic tectum (OTec), a cluster in the cerebellum (Cb) and two distinct clusters in the anterior hindbrain (aHb). (C) Phototactic clusters: the cells with the most highly periodic activity for the stimulus were selected and sorted into clusters. From Chen et al. (2018)

at the motor output level: a population of spinal projection neurons (RoV3, MiV1, and MiV2) controlling turning behaviors. Their activity increased with the turn amplitude to the ipsilateral side, and weakly active during forward swims. It seems these neurons act as modulators of an independently generated symmetric motor output produced by a close-by population, to generate a turn. (Huang et al., 2013; Orger et al., 2008)

As motor output and sensory input might be correlated, Chen et al. (2018) decomposed motor outputs into trial average and residual, which revealed an identical motor pattern posterior to rhombomere 2, regardless of the imposed stimulus (OMR/looming/phototaxis). They also decomposed the motor output into turning and forward swims, revealing one bilateral and a second lateralized maps (see fig. 5.6). The two clusters identified by red arrows, near motoneurons MiD2 (right panel), could potentially be responsible for generating a generic oscillatory waveform of a swim, which then is biased by the ARTR (left panel), the anterior rhombencephalic turning region, also known as **the previously described HBO**.

Indeed, ARTR seemed like a denomination more representative of its anatomy and function. As briefly mentioned before, this region was shown to be tightly tuned with turning movements, and to subserve the persistent exploratory turning dynamics observable in free swimming zebrafish larvae, *i.e* the chaining of similarly orientated turn bouts. The ARTR is necessary for turns to occur and predictive of their direction (Dunn et al., 2016).

In their study, Chen et al. (2018) noticed that the ARTR is more prominently clustered in spontaneous conditions rather than under stimulus-driven conditions, interpreting that the ARTR would be “an internal generator of turning biases for future swims”, and would be most influential in the absence of stimuli. They hypothesize, that a sensory convergence population they observed in the anterior hindbrain (aHb, rhom-

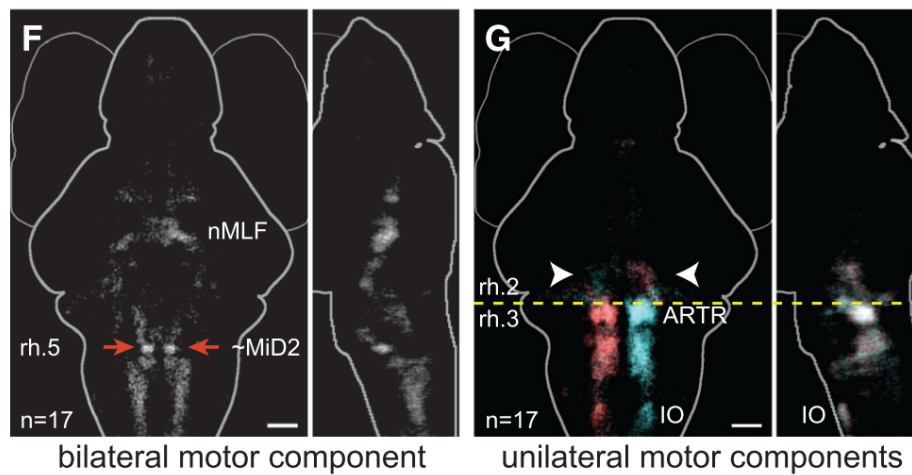


Figure 5.6: Forward swimming (bilateral) regression only (calculated using all stimulus blocks together). Red arrows point onto MiD2 reticulospinal neurons (according to ZBrain), highlighting the dense white cluster located nearby. (G) Turning (unilateral) regressions only. Dotted yellow lines: boundary between rhombomeres 2 and 3. Scale bars: 50 mm. pTec: pretectum. nMLF: nucleus of the medial longitudinal fasciculus. aHB: anterior hindbrain. pHB: posterior hindbrain. vSPN: ventral spinal projection neurons. rh: rhombomere. aHB(1-2): anterior hindbrain rhombomeres 1,2. ARTR: anterior rhombencephalic turning region. IO: inferior olive. From Chen et al. (2018)

bomeres 1-2) specifically processes multiple sensory signals (phototactic, but also OMR, looming, etc.) to generate turn biases, overriding the ARTR in the presence of stimuli. Not excluding the hypothesis that the sensory convergence cells and ARTR could be interconnected, based on proximity and (anti-)correlation.

5.2.3 Responses of the ARTR to illumination changes

We ought to take a step back and look at what had been shown regarding specifically the ARTR's response to contrast and whole-field illumination changes. This was done in a study by our lab in Wolf et al. (2017).¹

5.2.3.1 Reinforcement and phase-locking

Stereo-visual contrast. In stereo-visual contrast conditions, upon stimulation of the right (left) eye, the activity in the right (left) ARTR, which is associated with a rightward (leftward) reorienting bias, increased - consistent with a stereo-visual positive phototaxis mechanism (figure 5.7 A-C). Also, light-ON and light-OFF (as in Chen et al. (2018)) stimuli induced a sharp increase in activity of the ipsilateral and contralateral sub-populations, respectively, which indicates that the ON and OFF pathways both contribute to driving the ARTR (figure 5.7 D-F).

Bilaterally uniform illumination. The responses of the ARTR were also sampled upon delivering series of short (100 ms) flashes simultaneously to both eyes, interspaced by 10 s (figure 5.7 D-F). This revealed a phase-dependent response type: each subpopulation is responsive to the visual stimulus only within a particular phase range in its cycle, a flash selectively reinforces the cluster that is already active or about to become active. The oscillation period of the HBO was also found to be entrainable by stimulation periods close to the intrinsic oscillation period (in the range of 10 to 30s). (Wolf et al., 2017)

All in all, the ARTR's self-sustained oscillations drive a quasi-periodic sequence of gaze shifts that allow the animal to actively explore the light angular gradient. Asymmetric visual stimuli enhance the activity of the ARTR clusters ipsilateral to the eye that receives the larger illumination, which in turn biases the fish reorientation towards the light source.

5.2.3.2 Models of the ARTR

A first rate model. To help the interpretation of these experimental findings, a stochastic neuronal model of phototaxis was built: it aimed at capturing the oscillatory dynamics of the ARTR and its visually-evoked responses (Wolf et al., 2017). It

¹At that time convinced by its oscillatory properties, we still defiantly called it HBO (hindbrain oscillator).

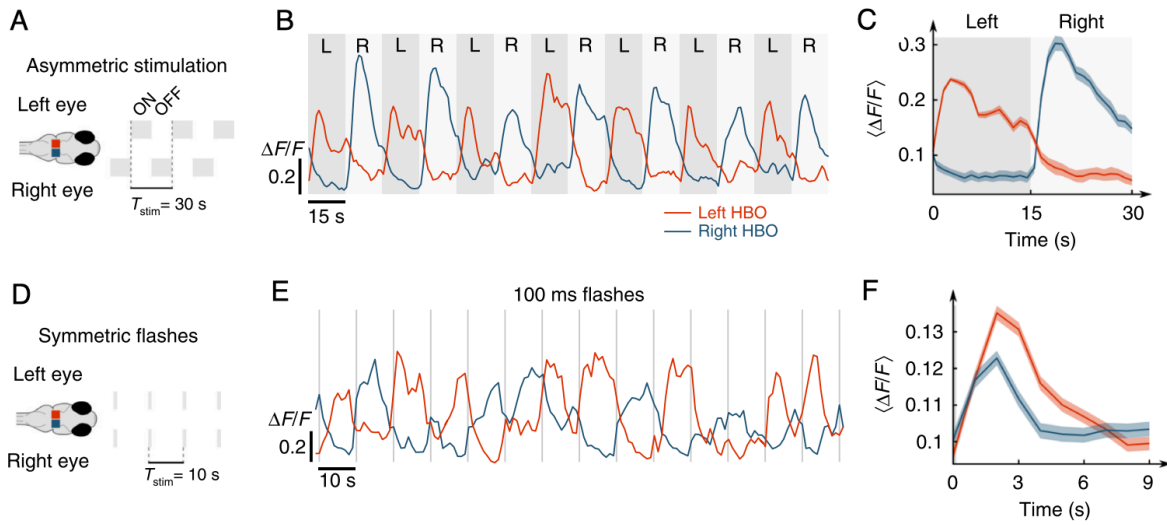


Figure 5.7: Response of the HBO to asymmetric and symmetric visual stimuli. Alternated unilateral visual stimulation. (B) Example traces of left and right HBO. (C) Trial-averaged response of the HBO over 20 stimulation periods. Shaded regions correspond to left (dark grey) and right (pale grey) illumination. (D) Bilaterally symmetric 100 ms-long flashes. (E) Example traces of the right and left HBO. The grey lines indicate the flashes. (F) Trial-averaged flash-induced responses of each subpopulation. From Wolf et al. (2017).

was implemented using a rate-model on two symmetric modules endowed with recurrent excitation, reciprocal inhibition and adaptation currents, each receiving intensity currents from the left/right eye (figure 5.8 a). A step increase in the illumination of the right eye was associated with a burst of current in the right circuit, followed by a plateau, whereas a step decrease in the illumination induced a transient current in the left circuit to account for the OFF pathway contribution (figure 5.8, b).

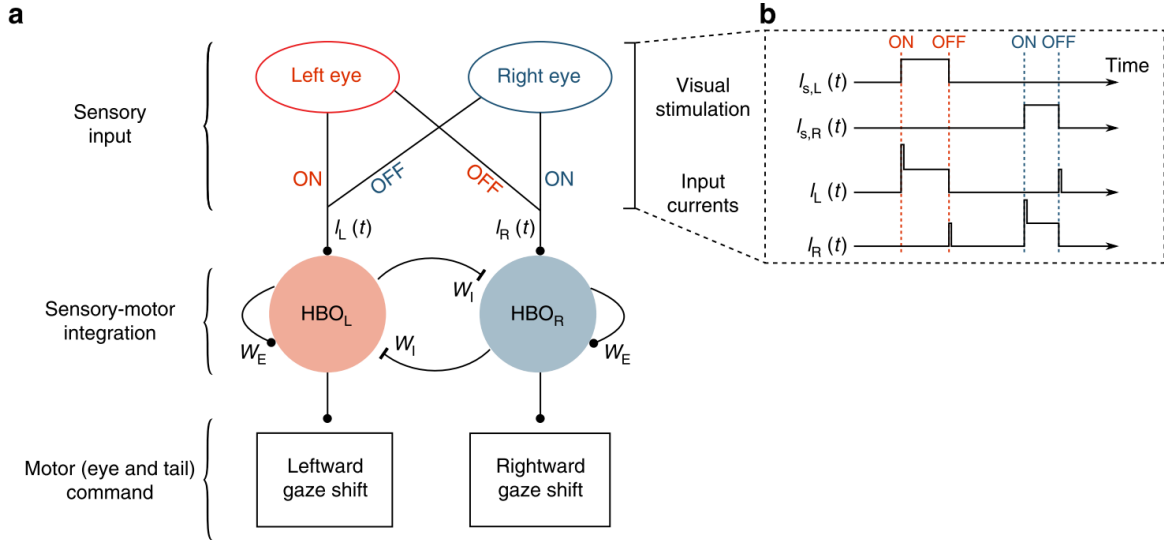


Figure 5.8: A rate model of the ARTR’s visually entrained dynamics leading to phototaxis. (a-b) Schematic of ARTR network connectivity. Visual stimuli are relayed to the HBO via the ON and OFF pathways, as detailed in (b). The ARTR activity controls gaze shifts via ocular saccades and turning bouts. Self-oscillatory dynamics result from the recurrent excitation (W_E), reciprocal inhibition (W_I) and adaptation currents. From Wolf et al. (2017).

The numeric ARTR oscillations were statistically biased towards the subnetwork ipsilateral to the light source, in presence of a contrast. Both the mean activity as well as the fraction of time during which a subnetwork is more active than the other are biased.

Adaptation of the rate model to free swimming behavior. We further adapted this rate model in Karpenko et al. (2020), to our recent behavioral findings. The afore stated description of the ARTR’s dynamics being in close agreement with the spontaneous or contrast-driven dynamics of freely swimming larvae, we used it to explain the observed statistics of exploration in both spontaneous and phototactic conditions.

We used the behavioral results to propose a neuronal model of the ARTR that quantitatively reproduces non-trivial aspects of the bout orientation selection process. Tail bouts are assumed to be triggered independently of the ARTR activity: they can be

forward or turning, and if turning, they are biased by the ARTR’s activity. This last binary decision process (left or right) reflects the competition between two cross-inhibitory neural populations (figure 5.9 A).

In the presence of a lateralized visual stimulus, the oscillatory dynamics become biased towards the brighter direction (figure 5.9 B, bottom). Hence, illuminating the right eye favors longer periods of activation of the rightward-selective ARTR unit. The mean reorientation displays a quasi-linear dependence with the imposed contrast, consistent with the behavioral observations. At intermediate contrast values, the orientation of bouts remains stochastic; the effect of the contrast is to lengthen streaks of turning bouts toward the light.

We also tested whether this model could capture the competition mechanism between stereovisual bias and motor persistence, in both conflicting and reinforcement conditions. The computed dependence of the flipping probability p_{flip} as a function of the contrast in both conditions shows quantitative agreement with its experimental counterpart (figure 5.9 C).

It was also successful in emulating a phototactic task, where a virtual fish was submitted to a linearly varying contrast locked on the animal’s orientation, as in the lateralized assay. When a turning bout was triggered, its orientation was set by the ARTR instantaneous activity while its amplitude was drawn from the experimental distributions. After a few bouts, a stationary distribution of orientation was reached that was biased toward the virtual light source (figure 5.9 D).

This circuit has thus two main functions: maintaining mnemonic persistent activity over long periods of time, thanks to recurrent excitatory inputs, and integrating sensory signals in a graded fashion to continuously bias the statistics of the decision. This is not in contradiction with the idea of a sensory-convergence cluster upstream of the ARTR, as proposed by Chen et al. (2018), a cluster that could be a relay to bias the dynamics of the ARTR for the animal to navigate towards “brighter” environments.

5.3 Virtual phototaxis under a microscope

Results of open-loop experiments might not accurately reflect the functional dynamics of the nervous system when it performs a sensorimotor task. It is thus useful to try to disrupt the sensorimotor loop as little as possible, and at the same time be able to control the parameters of the sensorimotor task.

Here I transposed the behavioral closed-loop setup for immobilized zebrafish larvae described in the previous chapter under the two-photon light sheet microscope to study the neural correlates of the light-seeking behavior. I will focus mainly on the dynamics of the ARTR during this sensorimotor task.

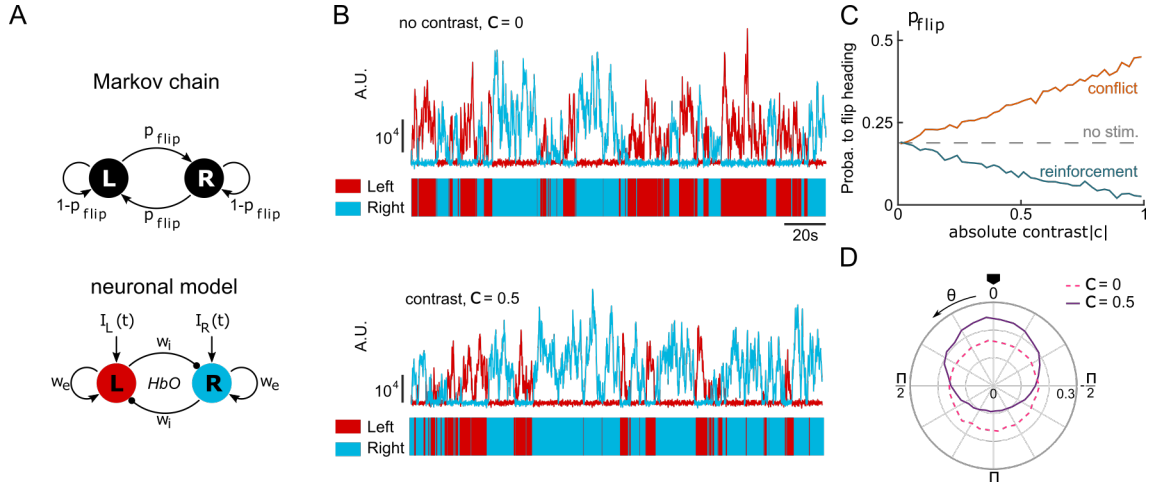


Figure 5.9: A neuronal model of turning bout selection captures spontaneous and contrast-driven navigation. Scheme of the Markov-chain model of the orientation selection, and corresponding neuronal model of the ARTR. The latter consists of two units whose relative activation controls the orientation of bouts. Persistent and self-alternating dynamics result from the recurrent excitation (w_E) and reciprocal inhibition (w_I) between each unit. They further receive input currents proportional to the illumination of the ipsilateral eye. (B) Top: example traces of the simulated activity of the left (red) and right (blue) modules in the absence visual stimulation (AU: arbitrary units). These continuous dynamics control the alternation between right and left orientational states. Bottom: Example traces of the simulated activity for a constant contrast $c = 0.5$. (C) Probability of flipping orientation as a function of the imposed contrast c in situations of conflict or reinforcement (neuronal model). (G) Probability distribution function of θ for 10 simulated phototactic trajectories with a linear dependence of average reorientation on contrast. Each trajectory lasted 50,000 s. The dotted line is the orientational distribution in the absence of visual stimulation. (adapted from Karpenko et al. (2020)).

5.3.1 Methods

The setup used for these experiments is described in [Chapter 3](#).

Protocol. For a robust identification of the ARTR, I used an OKR stimulus, composed of vertical red and black horizontally moving bars, projected on the screen in front of the fish. The pattern movement was sinusoidal of a period of 12 seconds (figure [5.10 B](#)). This pattern was projected for about 3 minutes at the start of an experiments.

After this initialization period, the fish was exposed to a ~30 min period during which the stereovisual contrast was changed whenever the larva performed a tail movement. The projected contrast could correspond to 3 different patterns: (1) $I_L = 0.5, I_R = 0.5$; (2) $I_L = 1, I_R = 0$; (3) $I_L = 0, I_R = 1$. A direct transition between state (2) and (3) is not possible, otherwise any other transition is equiprobable, regardless of the direction of the tail movement (figure [5.10 C](#)).

Image analysis. The general routine used for functional image analysis is described in Wolf et al. ([2017](#)). Custom functions were written in Matlab available on this gitlab page: gitlab.com/Phiasso/lightsheetanalysis.

For identification of the ARTR stripes, a Fourier transform was computed from the DFF signal of each pixel as well as from the OKR stimulus (Migault et al., [2018](#); Portugues et al., [2014](#)). Subtracting the two transforms yields the phase-shift of the activity of each pixel relative to the stimulus phase. This enables to compute a phase-map, in which the color encodes the phase-shift and the intensity the amplitude of the response ([5.10 A](#)). The region encompassing the ARTR was selected manually, and the ARTR pixels automatically extracted based on the phase and amplitude of their response.

The response of the ARTR was computed as follows: for a tail movement to one side, the DFF of the contralateral side was subtracted from the DFF of the ipsilateral side: $DFF_{ARTR} = DFF_{ipsi} - DFF_{contra}$ (see example for a left turn in figure [5.10 D](#)).

Turns were distinguished from forward swim attempts based on their turning score M , as described in the [previous chapter](#).

5.3.2 Results

The ARTR's asymmetrical activity is known to be predictive of the direction of a following turn (Dunn et al., [2016](#)). It is also sensitive to contrast changes (Wolf et al., [2017](#)). Thus we sought to (i) characterize the activity of the ARTR at the onset of a tail-bout, hypothesizing its activity would be asymmetrical in the case of turns and (ii) see whether there is a modulation of the ARTR response by different contrast transitions following a turn.

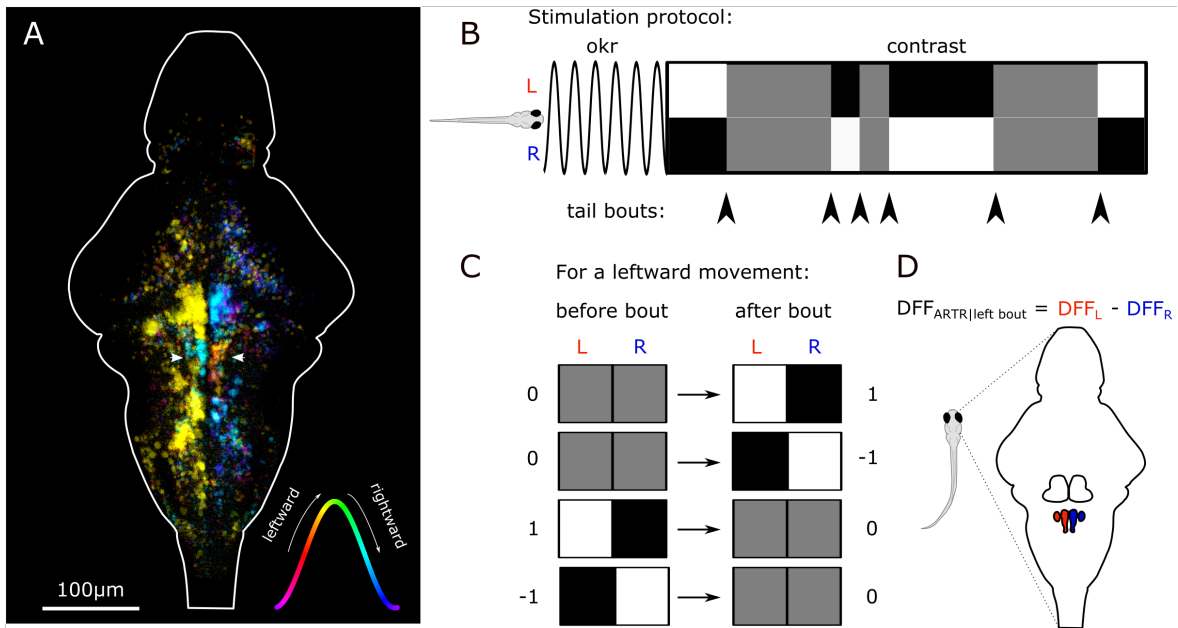


Figure 5.10: Phase map obtained from the difference of the Fourier transforms of single pixels and the OKR stimulus. The stimulus is a sinusoidal leftward or rightward movement of horizontal bars in front on the larva. For leftward movement, the left (ipsilateral) side mostly responds and vice-versa. For a notable exception of the ARTR (white arrows), which responds contralaterally, enabling its identification. (B) Stimulation protocol: OKR (~3min) then contrast modulation which occurs only upon a tail movement. (C) Possible contrast transition combinations following a left bout, with their corresponding values. The same contrast transitions are possible for a right turn, then the sign of the contrast value is inverted. (D) ARTR response definition: if a leftward turn occurs, the response of the ARTR is defined as the DFF of the left side minus the DFF of the right side, and vice-versa.

5.3.2.1 Asymmetrical ARTR activity translates turning movements

Following their findings, Dunn et al. (2016) speculated, that when a fish performs a turn in the direction where the ARTR is active, a motor efferent copy reactivates the ipsilateral ARTR and inhibits the contralateral side, thus generating the observed motor persistence in turning events.

First we characterized the response of the ARTR to turning or forward swimming movements, regardless of the imposed contrast. Swimming events were categorized into three groups: forward movements, left turns and right turns, based on their turning score M (figure 5.11).

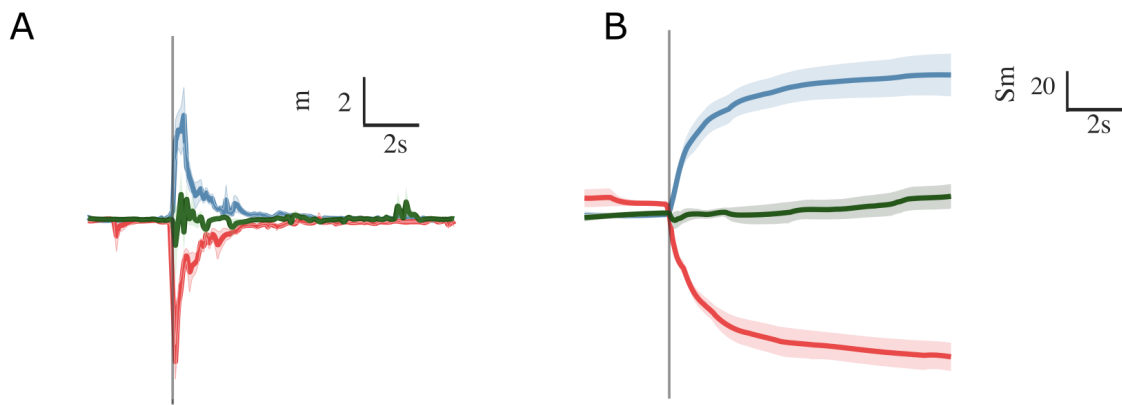


Figure 5.11: Turn or forward bouts selection and ARTR response for $N=12$ fish. Mean m traces of leftward bouts (blue, $n=155$), rightward bouts (red, $n=161$), forward bouts (green, $n=99$). Vertical grey bar: bout onset. (B) $\int m$ mean cumulative sums of m , equivalent to turning score M , from bout onset from leftward (blue), rightward (red) and forward (green) bouts. Vertical grey bar: bout onset.

The activity of the two ARTR subpopulations - ipsilateral and contralateral to a turn bout - was then extracted. The post-bout activity of the ipsilateral ARTR to the direction of the turn was consistently higher than the activity of the contralateral side (figure 5.12 A, individual traces in E). To quantify this effect, we compare the difference in activity post-bout (1-3s after the bout) and pre-bout (-3 to -1s) (figure 5.12 B). Note that the response of the contralateral side is lower than that of the ipsilateral side, but is still significantly higher than zero.

In the case of a forward tail-bout, the “ipsilateral” (“contralateral”) side of the ARTR was considered to be the side with highest (lowest) response to the tail movement. Both sides appear to respond to a forward movement equally (figure 5.12 C), though with a higher variability (figure 5.12 F). The mean responses are undistinguishable from one another (figure 5.12 C, D), are lower in amplitude than the response of the ipsilateral

side to a turn, but similar to the response of the contralateral side to a turn.

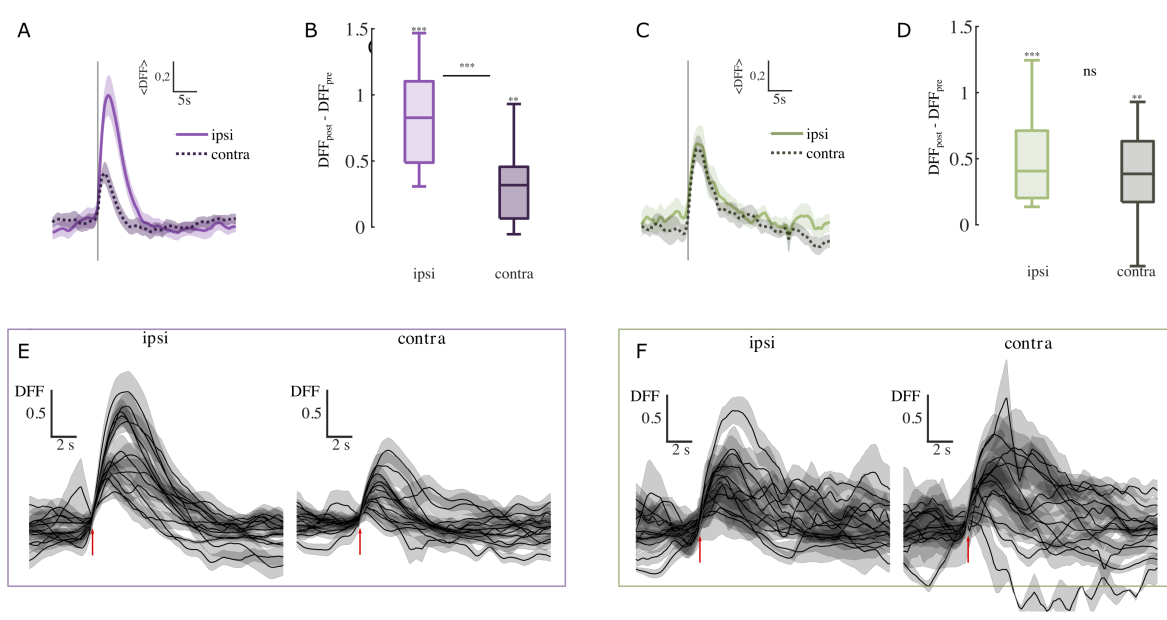


Figure 5.12: Mean ARTR DFF traces during (A) turns and (C) forward swims: ipsilateral ARTR side to the turn (solid line) and contralateral ARTR side (dashed line). In the case of forward swims, the ipsilateral side was taken to be the one with the highest response. (B, D) Response of ARTR per fish ($\langle DFF \rangle_{post} - \langle DFF \rangle_{pre}$ where pre is the time-window -3 to -1 seconds before a bout and $post$ the time window from 1 to 3 seconds after a bout) for the ipsilateral and contralateral sides following a swim bout. The response of ipsilateral and contralateral sides were found to be significantly different from 0 (one-sided t-test), the responses of each side are significantly different from one another (two-sided t-test). (B) Turn movement only. (D) Forward swims only. (E-F) Average traces of ipsilateral (ipsi) and contralateral (contra) ARTR region for 12 different fish for (E) turning bouts and (F) forward bouts. The red arrows indicate the bout onset.

These results corroborate the hypothesis formulated by Dunn et al. (2016): the ARTR's asymmetrical activity encodes the direction of an ongoing tail-bout if it is a turning one. It may well be that this response is an efferent copy of the motor event, which reinforces the activity on the ipsilateral ARTR side, and thus participates in the motor persistence effect in the direction of successive turns. In the case of forward bouts, the ARTR also responds, but this time in a symmetrical manner. It looks as if both ARTR sides would always receive an input following a bout, be it a forward or a turn. But in the case of a turn, this basal input is intensified on the ipsilateral side, reinforcing a “memory” of the previous turn.

5.3.2.2 Response of the ARTR to contrast change

We then assessed the response of the ARTR region to contrast changes. In this section I will refer to the ipsilateral side of the ARTR as the side of the fish on which the illumination shift is positive ($dc/dt > 0$), and vice-versa for the contralateral side.

Preliminarily, as expected from our previous behavioral experiments, the fish tends to perform tail movements towards the illuminated side. When the contrast just before the bout is 1 (-1), *i.e.* brighter side on the left (right), the mean direction of reorientation will be to the left (right) (black traces in figure 5.13 A). An interesting effect is the passage from a null contrast 0 to a contrast of 1. On average, for a null contrast, the turning score M (here approximated with the cumulative sum of m , figure 5.13 A) should be 0. This is true on a short timescale of a single bout < 0.5 seconds. What seems to happen is a correction of the tail-bout direction towards the most illuminated side of subsequent bouts. And the resulting turning score from the time of contrast change is effectively higher than in the case where the contrast tips over to the neutral state.

At the level of the ARTR, very subtle effects are visible: upon a contrast shift towards one side, the ipsilateral side of the ARTR seems to display slower decay dynamics than the contralateral side (~ 1 seconds shift, figure 5.13 B). This results in the ipsilateral side “winning over”, which might participate in the reinforcement of the ipsilateral side turning direction (figure 5.13 D). On the other hand, when the contrast shifts from 1 to 0, the contralateral side displays a slightly slower decay time (figure 5.13 C), thus the contralateral side wins over the activity (figure 5.13 E). In this case, as the final contrast is evened out, this last effect can be interpreted as a subtle damping of the turning persistence.

On average, at the onset of a bout, the response of the ARTR to contrast is very subtle. The described effects might play a role in slightly biasing the temporal dynamics towards the side opposite of the one with highest loss of illumination. But as the stimulus is locked on the animal’s movements, the seen response cannot be completely separated from a motor response.

5.3.2.3 Response to conflicting or reinforcing contrast stimuli

To disentangle the contributions of turning direction and contrast shift direction in the response of the ARTR following a turn movement, we systematically characterized the response of ipsilateral and contralateral sides of ARTR, by separating all different scenarios of possible contrast change.

A turn in one direction may trigger the following contrast transitions (fig 5.10 C) :

- $0 \rightarrow 1$: from null contrast to positive contrast toward the **ipsilateral** side. Following a turn in one direction, the same side gets lit up. In this case one should

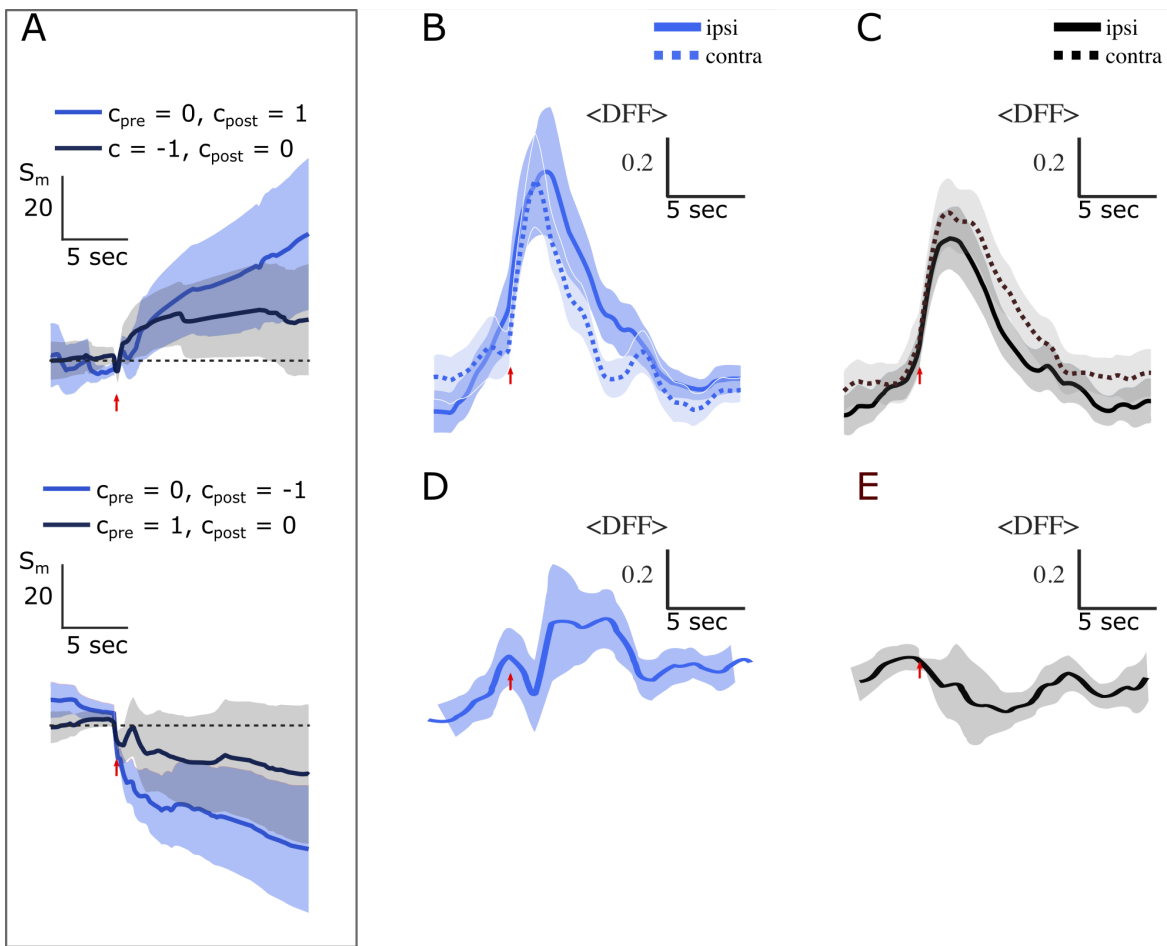


Figure 5.13: Cumulative sum of the moment signal S_m following a contrast transition (red arrow). Top: positive contrast transitions ($dc > 0$). An initial equal illumination from left and right ($c_{pre} = 0$) shifts to a contrast with light from the left ($c_{post} = 1$, blue curve). An initial contrast with light from the right shifts to a null contrast (black curve). Bottom: negative contrast transitions ($dc < 0$). The two situations are symmetrical and thus combined together in the following panels. (B-C) ARTR responses following a contrast shift triggered by a tail movement. The ipsilateral side (ipsi) corresponds to the side on which illumination **increases**. And vice-versa for the contralateral side. (B) Response when shifting from a null contrast (both eyes equally illuminated) to an asymmetrical illumination. (C) Response when shifting from an asymmetrical contrast to an equal illumination of both eyes. (D-E) Responses of the ARTR represented as $ARTR_{ipsi} - ARTR_{contra}$, correspondence to panels B and C respectively.

expect a positive reinforcement, since the contrast would drive the animal again in the same direction as the previous bout.

- $0 \rightarrow -1$: from null contrast to positive contrast toward the **contralateral** side. Following a turn in one direction, the opposite side gets lit up. In this case one should expect a negative reinforcement, since the direction of the light gradient is opposite to the direction of the previous bout.
- $1 \rightarrow 0$: from positive contrast on the **ipsilateral** side to null contrast. In this case, following a contrast to one side, a turn in the direction of this same side triggers evens out the intensity received by each eye. Behavioral results show that this is the situation sought after in stereovisual phototaxis, making this a coherent stimulus.
- $-1 \rightarrow 0$: from positive contrast on the **contralateral** side to null contrast. Following a contrast to one side, the animal performs a turn in the opposite direction, rebalancing the intensity each eye receives. The contrast change occurs in the opposite direction of the movement, making this an incoherent stimulus.

The behavioral response is slightly modulated in the four different situations (figure 5.14 A). In the cases where the contrast is evened out (to 0), the mean cumulative moment $\int m$ is slightly lower than in the cases of a shift to an asymmetrical contrast (to 1 or -1). In the case of a transition from 0 to 1, the cumulative moment rises faster than in the other cases: there seems indeed to be a slight reinforcement of the turning direction to the ipsilateral side. In a situation of negative reinforcement contrast shift, Sm rises slower than in the positive reinforcement case, but faster than in the situations where the contrast is evened out. This indicates that the negative reinforcement does not happen at this time scale.

The response of the ipsilateral ARTR in a situation where the initial contrast is non-zero shows a slight tendency to be higher than when the contrast is null (figure 5.14 B, C). When the contrast shifts from 0 to 1, there seems to be a “rebound” in the activity of the ipsilateral ARTR 10 to 20 seconds after the onset of the new contrast (figure 5.14, B violet curve), which is also visible in the behavioral traces (figure 5.14). This is coherent with the idea of a reinforcing stimulus: from a situation with no stereovisual information, a movement to one side triggers a new contrast biased toward this same side, thus driving the animal again to the same direction as the previous turn.

A shift of the contrast from 0 to -1, *i.e.* the contralateral side of the turn gets illuminated, seems to increase very slightly the response of the contralateral ARTR side (figure D). If this effect were significant, it would indicate a reinforcement of the contralateral side by the contrast change, and thus a negative reinforcement of the turning direction.

Transitions to a null contrast are quantitatively identical, no matter whether the previously experienced contrast was negative or positive, the ARTR does not show a modulation in response amplitude.

The ARTR robustly encodes the direction of a turn. Additionally to be predictive

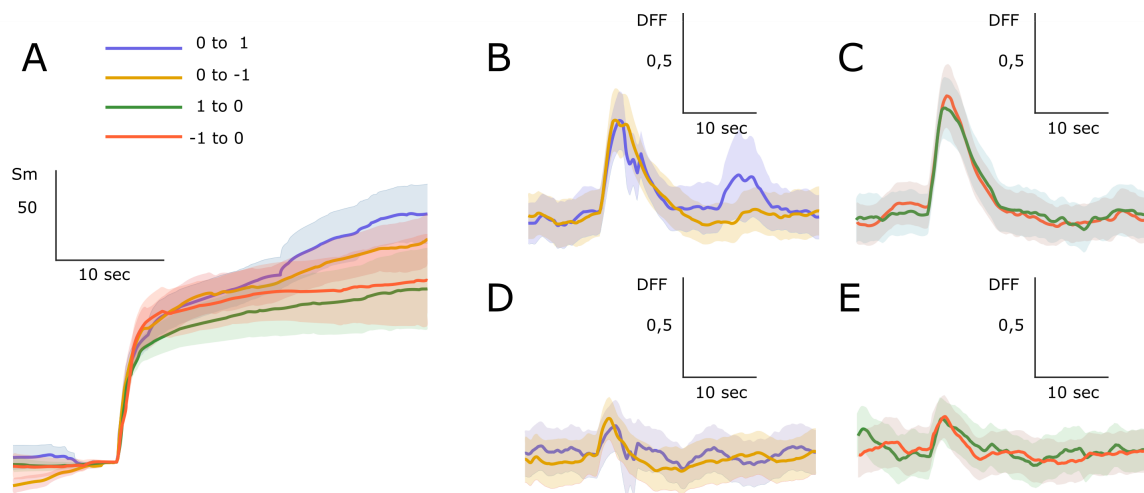


Figure 5.14: $N = 11$ fish, 316 turn events. (A) Cumulative sum of absolute moments S_m (left and right combined) for different scenarios of contrast transitions. (B-C) Responses of the side of the ARTR ipsilateral to a turn to the different contrast transitions. (D-E) Responses of the ARTR (contralateral side subtracted from ipsilateral side) to the different contrast transitions.

of an upcoming turn direction, as demonstrated by Dunn et al. (2016), the ARTR seems to receive an efferent copy of the ongoing movement. In the case of a forward movement, the rise of activity in the two sides of the ARTR is symmetrical. In the case of a turning movement, the activity is significantly heightened on the ipsilateral side of the turn.

A change in contrast has a much milder effect on its activity. The observed effects of slight reinforcement of the turning direction - positive in the case of a contrast changing in the direction of the turn, negative in the opposite situation - might be the effect of the contrast, but could also be due to motor activity only. Even when trying to differentiate all possible scenarios of bout direction and contrast change, the effect of contrast change appears very mildly.

The response of the ARTR to a contrast is much higher when it occurs independently from the animal's movements (Wolf et al., 2017). When locked on the animal's movement, the response to contrast is sub-linear, the motor event dominating the ARTR's activity. We can hypothesize this as being a sensory suppression effect, where the sensory entries are transiently inhibited when the animal performs a voluntary movement (Crevecoeur & Kording, 2017; Foo & Mason, 2005; Wolpert et al., 1995). This could be tested using a "play-back experiment": after a period of closed-loop stimulation like the experiments presented here, the second half of the experiment would consist of playing back the sequence of contrast transitions, but independently of a motor event. This way it could be possible to directly compare the response of the ARTR to a con-

trast change during or in between bouts, and see to what extent this masking effect is important.

Also it would seem that the dynamics of the ARTR, rather than getting direct information from a contrast transition, are more significantly biased on a longer-term, by a prolonged contrast. At a short time-scale, the predominant effect comes from the motor copy. As it has been hypothesized by Chen et al. (2018), it seems likely that the ARTR is a downstream structure in the sensorimotor process, close to the motor output, receiving inputs from upstream integrative structures which more robustly encode the direction of a stereovisual contrast.

Chapter 6

Conclusions and perspectives

Be what you would seem to be – or, if you’d like it put more simply – Never imagine yourself not to be otherwise than what it might appear to others that what you were or might have been was not otherwise than what you had been would have appeared to them to be otherwise.

The Duchess.¹

We have seen that (i) the zebrafish larva has intrinsic persistent exploratory navigational dynamics which are biased in the presence of a smooth spatial or temporal light gradient. It is able to use two complementary strategies for climbing either of these orientational light gradients. (ii) This light-seeking behavior is reproducible in head-fixed conditions with a closed-loop virtual reality system which retroacts on the animal’s tail movements and continuously updates its surrounding illumination according to its angular distance to a source. The two strategies are used in combination when both spatial and temporal informations on the direction of the light gradient are available. (iii) An underlying neural circuit controls the persistent exploratory locomotion in zebrafish. During a motor event, its activity predominantly encodes the direction of a tail-bout. Independently from a motor event, its activity can be modulated by phototactic stimuli, promoting an increased persistence in the presence of an ipsiversive contrast.

6.1 Zebrafish and light

In the behavioral description of the larval zebrafish’s propensity to swim towards illuminated regions that I drew here, in the existing literature to which we contributed, the terms phototaxis and light-seeking behavior are used interchangeably. Its ability

¹*Alice’s Adventures in Wonderland*, L. Carroll.

to extract instantaneously the direction of the light gradient from the contrast by comparing intensities it receives on left and right eye puts this strategy undoubtedly in the category of tropo-phototaxis, strategy also termed stereo-visual comparison.

How to term the second temporal strategy, on the other hand, is less clear. In our study, building on previous ones, this strategy of climbing temporal gradients is sometimes termed “klino(photo)taxis”. But if we look back at the strict definition of klinotaxis, it is supposed to be a method of inferring the direction of a gradient by sampling cues in a temporal fashion, which implies a directional bias of $\langle \delta\theta \rangle$ after several sampling events. Yet, in our assay, unlike the previous results on the behavioral algorithm of temporal light-seeking behavior (X. Chen & Engert, 2014) we do not observe this bias. The steady-state orientational bias of θ we observe is possible through a higher frequency of turns and their increased amplitude, which makes this strategy closer to klinokinesis in which the rate of turning varies with the stimulus. This divergence in results might be explained by the difference of applied stimuli: Chen et al. used an abrupt light transition from a lit environment to complete darkness and vice-versa, where we tried to avoid abrupt transitions. We hypothesized that these huge differences of intensity might trigger escape responses (as it could resemble a very fast looming stimulus) or responses such as the visuo-motor reflex (VMR) of overall heightened locomotor activity, both different from a smooth exploratory behavior slightly biased by light. Behaviors such as VMR do contribute to staying or returning to illuminated regions, as observed by Fernandes et al. (2012), in which case the speed of movement participates to it, making it an orthokinesis (see figure 1.3).

So if we were to be completely rigorous in our terminology, “light-seeking behavior” would be a general term encompassing different strategies including tropophototaxis, klinophototaxis, klinophotokinesis or orthophotokinesis. But old habits die hard, and as we still speak of bacterial chemotaxis, phototaxis has probably just become a generic and common term to describe light-seeking behavior.

For the sake of clarity, we tried to limit ourself to a very limited and narrow aspect of how light can influence and bias zebrafish behavior. Yet, in a naturalistic environment, all stimuli would be highly intricate, act in concert and probably provide a much more complex behavioral response to all parameters at play. We know for example, that since the zebrafish is a diurnal animal, it is subject to circadian rhythmicity, the larva displaying diel vertical migration where it swims upward or downward in the water column, depending on the luminosity conditions (time scale of minutes). This behavior is not mediated by the visual system and is induced specifically by blue light. It has been shown to involve melatonin production in the pineal, as well as the thalamo-habenular pathway (Lin & Jesuthasan, 2017). Though it is impossible to completely separate contributions of potentially different pathways a stimulus can follow, it is important to bear it in mind for an accurate view of the observed process.

6.2 Structures implicated in zebrafish light-seeking behavior

Though I sing the praises of large-scale functional imaging, by lack of time I only focused on the description of a small subpart -the HBO or ARTR - of the data I had access to. Still the dynamics of this small subpart in the presence of a biasing stimulus are not completely deciphered. In response to a visual contrast, the motor output is immediately and directionally but stochastically biased by the spatial gradient. In response to whole-field illumination changes, in a temporal light-seeking strategy where a directional motor output is not necessary, the role of the ARTR is unclear, if at all it plays a role. A subsidiary question concerns the adaptations of the ARTR dynamics (its intrinsic pseudo-oscillation) to long-term environmental changes, namely illumination changes. It has been speculated, that the pseudo-period of left-right alternations of the ARTR might be influenced by ambient light levels. If the bout frequency is not affected in parallel, this might give rise to behaviors with more or less motor persistency in turning events, generating more localized or on the contrary more exploratory-like trajectories. This could be seen as a modulation of the 2D diffusion coefficient of the larva for adaptive navigation of its surroundings.

There are other known regions involved in light responsiveness. For example the habenula: being an anatomically and functionally asymmetrical structure, it is specifically the left habenula, which receives indirect inputs from ganglion cells, that mediates light-preference (Dreosti et al., 2014; Zhang et al., 2017). This light-preference does not seem to be a directional taxis, but participates in confining the animal to illuminated regions in the horizontal plane and in the diel vertical migration mentioned above (Cheng et al., 2017; Lin & Jesuthasan, 2017). Also receiving indirect inputs from the pineal, the habenula is thus involved in circadian behaviors. On a more general side note, the habenula is a highly versatile region - described as a relay-station (Bianco & Wilson, 2009) with responses to visual and olfactory stimuli (Dreosti et al., 2014), mediating fear, anxiety or avoidance behaviors (Agetsuma et al., 2010; Amo et al., 2014; Jesuthasan, 2012), and also involved in behavioral state-transitions (Andalman et al., 2019; Marques et al., 2020) and decision-making (Cherng et al., 2020).

The example of the habenula as a “multi-modal hub” is not unique. Many regions are not uni-sensory, tuned to one specific stimulus or encoding only one single behavior. Thus constructing multi-sensory paradigms can get some important insight into the way the brain processes information. For example Chen et al. (2018), by testing different stimuli known to evoke specific responses, were able to construct maps of the intersection of tested stimuli determining regions involved in multi-stimuli convergence. This can give insight into how information is hierarchized when processed by the nervous system. An interesting region to keep in mind for further work on light-seeking (and other) behavior is the multi-sensory convergence regions in the anterior hindbrain described by Chen et al. (2018), which could be key for integrating directional stimuli

and them transferring them to the ARTR if need be.

6.3 Outlooks in neuroscience

Large-scale functional imaging can bring about some interesting insights into how a cognitive system processes information, but also about functionally characterized global behavioral states, like sleep (Leung et al., 2019), exploration or exploitation (Marques et al., 2020) or even consciousness (Goldman et al., 2019). And though this work was solely focused on neurons, assuming they are, within their network, the most important part of the information processing system, evidence points to important regulatory functions of another matrix surrounding the neurons, and which can drastically influence their activity: the glia. It has recently been shown, that glia encode the futility of an attempted movement in zebrafish (Mu et al., 2019) and more generally respond to locomotion and sensory stimuli, regulate learning or state transitions, etc (Jurisch-Yaksi et al., 2020).

All in all, when looking at brain dynamics “naively”, a huge level of complexity arises from the neural activity, even when the animal performs “simple”, hard-wired innate behaviors. Thus some call for the need of thorough descriptions of behavior (a complete behavioral algorithm) before trying to explain them at a neuronal level (Krakauer et al., 2017). Indeed, some analysis tools, if used with lack of hypotheses, may give only partial or even wrong results. This has been illustrated in an interesting parallel drawn by Jonas & Kording (2017), who tried to understand how a microprocessor works with the tools of systems neuroscience. And did not exactly succeed. One could argue the brain is not and does not work as a microprocessor does, but both are considered information-processing systems, so common tools should be able to describe both at a certain level.

At least, the brain as a computational system is the current metaphor used for trying to understand it. Some speculate that, as former metaphors (like the brain as a hydraulic automata by Descartes, or the brain as a telegraph by von Helmholtz) we are reaching its limits. Arguing that this comparison has had its day, as it has not born much conceptual understanding of fundamental questions in neuroscience these past few decades (Gomez-Marin (2020) commenting on the last part of the book *The Idea of the Brain* by Matthew Cobb, available at this link: <https://www.theguardian.com/science/2020/feb/27/why-your-brain-is-not-a-computer-neuroscience-neural-networks-consciousness>). As Cobb highlights it, relying solely on “emergence” to explain the complexity of brain function may actually indicate a problem with the theoretical framework. As Richard Gregory stated it already back in 1981:

“The appearance of ‘emergence’ may well be a sign that a more general (or at least different) conceptual scheme is needed ... It is the role of good

theories to remove the appearance of emergence. (So explanations in terms of emergence are bogus.)”

But new possibilities for metaphors emerge, namely around the critical question of a neural code: does a representation of the external world exist in the brain? György Buzsáki for example asserts that instead of passively representing external stimuli, an organism actively searches for external clues and *constructs* information. Or Romain Brette who points out the limitations of a neural code metaphor, and suggests a more systemic (the brain within its organism within its environment) and dynamical approach (studying the sensorimotor loop).

In any case, much of today’s neuroscience research endeavor is at least partially motivated by finding links between what we may call the microscopical scale of the brain (the neuron) and the macroscopical one (network dynamics, or even behavior), which is the (big) missing step to explain the emergent properties of the nervous system. Whether it be through an experimental focus on simple (or less simple) processes, finding new theoretical or computational approaches or through the building of a completely new paradigm to explain brain function.

Bibliography

- Adler, J., & Tso, W.-W. (1974). "Decision" -Making in Bacteria : Chemotactic Response of *Escherichia coli* to Conflicting Stimuli. *American Association for the Advancement of Science*, 184(4143), 1292–1294.
- Agetsuma, M., Aizawa, H., Aoki, T., Nakayama, R., Takahoko, M., Goto, M., Sassa, T., Amo, R., Shiraki, T., Kawakami, K., Hosoya, T., Higashijima, S.-i., & Okamoto, H. (2010). The habenula is crucial for experience-dependent modification of fear responses in zebrafish. *Nature Neuroscience*, 13(11), 1354–1356. <https://doi.org/10.1038/nn.2654>
- Ahrens, M. B., Huang, K. H., Narayan, S., Mensh, B. D., & Engert, F. (2013). Two-photon calcium imaging during fictive navigation in virtual environments. *Frontiers in Neural Circuits*, 7(June). <https://doi.org/10.3389/fncir.2013.00104>
- Ahrens, M. B., Li, J. M., Orger, M. B., Robson, D. N., Schier, A. F., Engert, F., & Portugues, R. (2012). Brain-wide neuronal dynamics during motor adaptation in zebrafish. *Nature*, 485(7399), 471–477. <https://doi.org/10.1038/nature11057>
- Ahrens, M. B., Orger, M. B., Robson, D. N., Li, J. M., & Keller, P. J. (2013a). Whole-brain functional imaging at cellular resolution using light-sheet microscopy. *Nature Methods*, 10(5), 413–420. <https://doi.org/10.1038/nmeth.2434>
- Ahrens, M. B., Orger, M. B., Robson, D. N., Li, J. M., & Keller, P. J. (2013b). Whole-brain functional imaging at cellular resolution using light-sheet microscopy. *Nature Methods*, 10(5), 413–420. <https://doi.org/10.1038/nmeth.2434>
- Amo, R., Fredes, F., Kinoshita, M., Aoki, R., Aizawa, H., Agetsuma, M., Aoki, T., Shiraki, T., Kakinuma, H., Matsuda, M., Yamazaki, M., Takahoko, M., Tsuboi, T., Higashijima, S.-i., Miyasaka, N., Koide, T., Yabuki, Y., Yoshihara, Y., Fukai, T., & Okamoto, H. (2014). The habenulo-raphe serotonergic circuit encodes an aversive expectation value essential for adaptive active avoidance of danger. *Neuron*, 84(5), 1034–1048. <https://doi.org/10.1016/j.neuron.2014.10.035>
- Andalman, A. S., Burns, V. M., Lovett-Barron, M., Broxton, M., Poole, B., Yang, S. J., Grosenick, L., Lerner, T. N., Chen, R., Benster, T., Mourrain, P., Levoy, M., Rajan, K., & Deisseroth, K. (2019). Neuronal Dynamics Regulating Brain and

- Behavioral State Transitions. *Cell*, 177(4), 970–985.e20. <https://doi.org/10.1016/j.cell.2019.02.037>
- Angueyra, J. M., & Kindt, K. S. (2018). Leveraging zebrafish to study retinal degenerations. *Frontiers in Cell and Developmental Biology*, 6(SEP), 1–19. <https://doi.org/10.3389/fcell.2018.00110>
- Bahl, A., & Engert, F. (2019). Neural circuits for evidence accumulation and decision making in larval zebrafish. *Nature Neuroscience*. <https://doi.org/10.1038/s41593-019-0534-9>
- Benninger, R. K. P., & Piston, D. W. (2013). Two-photon excitation microscopy for unit 4.11 the study of living cells and tissues. *Current Protocols in Cell Biology*, SUPPL.59, 1–24. <https://doi.org/10.1002/0471143030.cb0411s59>
- Berens, P., Freeman, J., Deneux, T., Chenkov, N., McColgan, T., Speiser, A., Macke, J. H., Turaga, S. C., Mineault, P., Rupprecht, P., Gerhard, S., Friedrich, R. W., Friedrich, J., Paninski, L., Pachitariu, M., Harris, K. D., Bolte, B., Machado, T. A., Ringach, D., ... Bethge, M. (2018). Community-based benchmarking improves spike rate inference from two-photon calcium imaging data. *PLoS Computational Biology*, 14(5), 1–13. <https://doi.org/10.1371/journal.pcbi.1006157>
- Berg, H. C., & Brown, D. A. (1972). Chemotaxis in E coli analysed by 3D tracking. *Nature*, 239, 500–504.
- Bernardo, A. (2017). Virtual Reality and Simulation in Neurosurgical Training. *World Neurosurgery*, 106, 1015–1029. <https://doi.org/10.1016/j.wneu.2017.06.140>
- Bianco, I. H., Kampff, A. R., & Engert, F. (2011). Prey capture behavior evoked by simple visual stimuli in larval zebrafish. *Frontiers in Systems Neuroscience*, 5(December 2011), 1–13. <https://doi.org/10.3389/fnsys.2011.00101>
- Bianco, I. H., & Wilson, S. W. (2009). The habenular nuclei: a conserved asymmetric relay station in the vertebrate brain. *Philosophical Transactions of the Royal Society of London. Series B, Biological Sciences*, 364(1519), 1005–1020. <https://doi.org/10.1098/rstb.2008.0213>
- Bishop, B. H., Spence-Chorman, N., & Gahtan, E. (2016). Three-dimensional motion tracking reveals a diving component to visual and auditory escape swims in zebrafish larvae. *Journal of Experimental Biology*, 219(24), 3981–3987. <https://doi.org/10.1242/jeb.147124>
- Bohil, C. J., Alicea, B., & Biocca, F. A. (2011). Virtual reality in neuroscience research and therapy. *Nature Reviews Neuroscience*, 12(12). <https://doi.org/10.1038/nrn3122>
- Brini, M., Cali, T., Ottolini, D., & Carafoli, E. (2014). Neuronal calcium signaling : function and dysfunction. *Cellular and Molecular Life Sciences*. <https://doi.org/>

10.1007/s00018-013-1550-7

- Brockerhoff, S. E., Hurley, J. B., Janssen-Bienhold, U., Neuhauss, S. C., Driever, W., & Dowling, J. E. (1995). A behavioral screen for isolating zebrafish mutants with visual system defects. *Proceedings of the National Academy of Sciences*, *92*(23), 10545–10549. <https://doi.org/10.1073/pnas.92.23.10545>
- Brysch, C., Leyden, C., & Arrenberg, A. B. (2019). Functional architecture underlying binocular coordination of eye position and velocity in the larval zebrafish hindbrain. *BMC Biology*, *17*(1), 1–22. <https://doi.org/10.1186/s12915-019-0720-y>
- Budick, S. A., & O'Malley, D. M. (2000). Locomotor repertoire of the larval zebrafish: swimming, turning and prey capture. *The Journal of Experimental Biology*, *203*(Pt 17), 2565–2579. <https://doi.org/10.1242/jeb.01529>
- Burgess, H. A., & Granato, M. (2007). Modulation of locomotor activity in larval zebrafish during light adaptation. *Journal of Experimental Biology*, *210*(14), 2526–2539. <https://doi.org/10.1242/jeb.003939>
- Burgess, H. A., Schoch, H., & Granato, M. (2010). Distinct Retinal Pathways Drive Spatial Orientation Behaviors in Zebrafish Navigation. *Current Biology*, *20*(4), 381–386. <https://doi.org/10.1016/j.cub.2010.01.022>
- Celani, A., & Vergassola, M. (2010). Bacterial strategies for chemotaxis response. *Proceedings of the National Academy of Sciences*, *107*(4), 1391–1396. <https://doi.org/10.1073/pnas.0909673107>
- Chen, B. C., Legant, W. R., Wang, K., Shao, L., Milkie, D. E., Davidson, M. W., Janetopoulos, C., Wu, X. S., Hammer, J. A., Liu, Z., English, B. P., Mimori-Kiyosue, Y., Romero, D. P., Ritter, A. T., Lippincott-Schwartz, J., Fritz-Laylin, L., Mullins, R. D., Mitchell, D. M., Bembenek, J. N., ... Betzig, E. (2014). Lattice light-sheet microscopy: Imaging molecules to embryos at high spatiotemporal resolution. *Science*, *346*(6208). <https://doi.org/10.1126/science.1257998>
- Chen, T. W., Wardill, T. J., Sun, Y., Pulver, S. R., Renninger, S. L., Baohan, A., Schreiter, E. R., Kerr, R. A., Orger, M. B., Jayaraman, V., Looger, L. L., Svoboda, K., & Kim, D. S. (2013). Ultrasensitive fluorescent proteins for imaging neuronal activity. *Nature*, *499*(7458), 295–300. <https://doi.org/10.1038/nature12354>
- Chen, X., & Engert, F. (2014). Navigational strategies underlying phototaxis in larval zebrafish. *Frontiers in Systems Neuroscience*, *8*(March), 1–13. <https://doi.org/10.3389/fnsys.2014.00039>
- Chen, X., Mu, Y., Hu, Y., Kuan, A. T., Nikitchenko, M., Randlett, O., Chen, A. B., Gavornik, J. P., Sompolinsky, H., Engert, F., & Ahrens, M. B. (2018). Brain-wide Organization of Neuronal Activity and Convergent Sensorimotor Transformations in Larval Zebrafish. *Neuron*, *100*(4), 876–890.e5. <https://doi.org/10.1016/j.neuron.2018.09.042>

- Cheng, R. K., Krishnan, S., Lin, Q., Kibat, C., & Jesuthasan, S. (2017). Characterization of a thalamic nucleus mediating habenula responses to changes in ambient illumination. *BMC Biology*, *15*(1), 1–21. <https://doi.org/10.1186/s12915-017-0431-1>
- Chen, A. B., Deb, D., Bahl, A., & Engert, F. (2020). Algorithms underlying flexible phototaxis in larval zebrafish. *bioRxiv*, 2020.07.18.210260. <https://doi.org/10.1101/2020.07.18.210260>
- Cherng, B. W., Islam, T., Torigoe, M., Tsuboi, T., & Okamoto, H. (2020). The Dorsal Lateral Habenula-Interpeduncular Nucleus Pathway Is Essential for Left-Right-Dependent Decision Making in Zebrafish. *Cell Reports*, *32*(11), 108143. <https://doi.org/10.1016/j.celrep.2020.108143>
- Crevecœur, F., & Kording, K. P. (2017). Saccadic suppression as a perceptual consequence of efficient sensorimotor estimation. *eLife*, *6*, 1–15. <https://doi.org/10.7554/eLife.25073>
- Currier, T. A., & Nagel, K. I. (2018). Multisensory Control of Orientation in Tethered Flying *Drosophila*. *Current Biology*, *28*(22), 3533–3546.e6. <https://doi.org/10.1016/j.cub.2018.09.020>
- Dacke, M., Baird, E., Byrne, M., Scholtz, C. H., & Warrant, E. J. (2013). Dung beetles use the milky way for orientation. *Current Biology*, *23*(4), 298–300. <https://doi.org/10.1016/j.cub.2012.12.034>
- Dahmen, H., Wahl, V. L., Pfeffer, S. E., Mallot, H. A., & Wittlinger, M. (2017). Naturalistic path integration of *Cataglyphis* desert ants on an air-cushioned lightweight spherical treadmill. *Journal of Experimental Biology*, *220*(4), 634–644. <https://doi.org/10.1242/jeb.148213>
- Dehmelt, F. A., Meier, R., Hinz, J., Yoshimatsu, T., Simacek, C. A., Wang, K., Baden, T., & Arrenberg, A. B. (2019). Spherical arena reveals optokinetic response tuning to stimulus location, size and frequency across entire visual field of larval zebrafish. *bioRxiv*, 754408. <https://doi.org/10.1101/754408>
- Deneux, T., Kaszas, A., Szalay, G., Katona, G., Lakner, T., Grinvald, A., Rozsa, B., & Vanzetta, I. (2016). Accurate spike estimation from noisy calcium signals for ultrafast three-dimensional imaging of large neuronal populations in vivo. *Nature Communications*, *7*. <https://doi.org/10.1038/ncomms12190>
- Deo, C., & Lavis, L. D. (2018). Synthetic and genetically encoded fluorescent neural activity indicators. *Current Opinion in Neurobiology*, *50*(Table 1), 101–108. <https://doi.org/10.1016/j.conb.2018.01.003>
- Dombeck, D. A., Harvey, C. D., Tian, L., Looger, L. L., & Tank, D. W. (2010). Functional imaging of hippocampal place cells at cellular resolution during virtual navigation. *Nature Neuroscience*, *13*(11), 1433–1440. <https://doi.org/10.1038/nn.2648>

- Dombeck, D. A., & Reiser, M. B. (2012). Real neuroscience in virtual worlds. *Current Opinion in Neurobiology*, *22*(1), 3–10. <https://doi.org/10.1016/j.conb.2011.10.015>
- Dragomir, E. I., Štih, V., & Portugues, R. (2019). Evidence accumulation during a sensorimotor decision task revealed by whole-brain imaging. *Nature Neuroscience*. <https://doi.org/10.1038/s41593-019-0535-8>
- Dreosti, E., Vendrell Llopis, N., Carl, M., Yaksi, E., & Wilson, S. W. (2014). Left-right asymmetry is required for the habenulae to respond to both visual and olfactory stimuli. *Current Biology*, *24*(4), 440–445. <https://doi.org/10.1016/j.cub.2014.01.016>
- Dunn, T. W., Mu, Y., Narayan, S., Randlett, O., Naumann, E. A., Yang, C. T., Schier, A. F., Freeman, J., Engert, F., & Ahrens, M. B. (2016). Brain-wide mapping of neural activity controlling zebrafish exploratory locomotion. *eLife*, *5*(March 2016), 1–29. <https://doi.org/10.7554/eLife.12741>
- Easter, S. S., & Nicola, G. N. (1997). The Development of Eye Movements in the Zebrafish (*Danio rerio*). *Developmental Psychobiology*, *31*(4), 267–276. [https://doi.org/10.1002/\(SICI\)1098-2302\(199712\)31:4%3C267::AID-DEV4%3E3.0.CO;2-P](https://doi.org/10.1002/(SICI)1098-2302(199712)31:4%3C267::AID-DEV4%3E3.0.CO;2-P)
- Easter Jr, S. S., & Nicola, G. N. (1996). The Development of Vision in the Zebrafish. *Developmental Biology*, *180*(2), 646–663. https://ac.els-cdn.com/S0012160696903358/1-s2.0-S0012160696903358-main.pdf?%7B/_%7Dtid=5127746c-bbc2-4d6b-99ba-76814082f1d5%7B/&%7Dacdnat=1549017063%7B/_%7De3b9adb656fb244c4fe9fc5d7a0f7c72%7B/%7D0Ahttp://www.sciencedirect.com/science/article/pii/S0012160696903358
- El Beheiry, M., Doutreligne, S., Caporal, C., Ostertag, C., Dahan, M., & Masson, J. B. (2019). Virtual Reality: Beyond Visualization. *Journal of Molecular Biology*, *431*(7), 1315–1321. <https://doi.org/10.1016/j.jmb.2019.01.033>
- Emran, F., Rihel, J., Adolph, A. R., & Dowling, J. E. (2009). Zebrafish larvae lose vision at night. *Proceedings of the National Academy of Sciences*, *107*(13), 6034–6039. <https://doi.org/10.1073/pnas.0914718107>
- Emran, F., Rihel, J., Adolph, A. R., Wong, K. Y., Kraves, S., & Dowling, J. E. (2007). OFF ganglion cells cannot drive the optokinetic reflex in zebrafish. *Proceedings of the National Academy of Sciences*, *104*(48), 19126–19131.
- Engeszer, R. E., Patterson, L. B., Rao, A. A., & Parichy, D. M. (2007). Zebrafish in the wild: A review of natural history and new notes from the field. *Zebrafish*, *4*(1), 21–40. <https://doi.org/10.1089/zeb.2006.9997>
- Fahrbach, F. O., & Rohrbach, A. (2010). A line scanned light-sheet microscope with phase shaped self-reconstructing beams. *Optics Express*, *18*(23), 24229. <https://doi.org/10.1364/oe.18.024229>

- Fernandes, A. M., Fero, K., Arrenberg, A. B., Bergeron, S. A., Driever, W., & Burgess, H. A. (2012). Deep brain photoreceptors control light-seeking behavior in zebrafish larvae. *Current Biology*, *22*(21), 2042–2047. <https://doi.org/10.1016/j.cub.2012.08.016>
- Fisher, Y. E., Lu, J., D'Alessandro, I., & Wilson, R. I. (2019). Sensorimotor experience remaps visual input to a heading-direction network. *Nature*, *576*(7785), 121–125. <https://doi.org/10.1038/s41586-019-1772-4>
- Fleisch, V. C., & Neuhauss, S. C. F. (2006). Visual Behavior in Zebrafish. *Zebrafish*, *3*(2), 1–15. <https://doi.org/10.1016/B978-0-323-03675-7.50005-6>
- Foo, H., & Mason, P. (2005). Sensory suppression during feeding. *Proceedings of the National Academy of Sciences of the United States of America*, *102*(46), 16865–16869. <https://doi.org/10.1073/pnas.0506226102>
- Fraenkel, G. S., & Gunn, D. L. (1961). *The Orientation of Animals, Kinesis, Taxes and Compass Reactions*. <https://doi.org/10.1093/aesa/34.3.690a>
- Franco-Restrepo, J. E., Forero, D. A., & Vargas, R. A. (2019). A Review of Freely Available, Open-Source Software for the Automated Analysis of the Behavior of Adult Zebrafish. *Zebrafish*, *16*(3), 223–232. <https://doi.org/10.1089/zeb.2018.1662>
- Gebhardt, C., Auer, T. O., Henriques, P. M., Rajan, G., Durore, K., Bianco, I. H., & Del Bene, F. (2019). An interhemispheric neural circuit allowing binocular integration in the optic tectum. *Nature Communications*, *10*(1), 5471. <https://doi.org/10.1038/s41467-019-13484-9>
- Gerlai, R., Lahav, M., Guo, S., & Rosenthal, A. (2000). Drinks like a fish: Zebra fish (*Danio rerio*) as a behavior genetic model to study alcohol effects. *Pharmacology Biochemistry and Behavior*, *67*(4), 773–782. [https://doi.org/10.1016/S0091-3057\(00\)00422-6](https://doi.org/10.1016/S0091-3057(00)00422-6)
- Goldman, J. S., Tort-Colet, N., Volo, M. di, Susin, E., Bouté, J., Dali, M., Carlu, M., Nghiem, T. A., Górski, T., & Destexhe, A. (2019). Bridging Single Neuron Dynamics to Global Brain States. *Frontiers in Systems Neuroscience*, *13*(December), 1–9. <https://doi.org/10.3389/fnsys.2019.00075>
- Gomez-Marin, A. (2020). A history of the metaphorical brain. *Science*, *368*(6489). <https://doi.org/10.1126/science.abc0421>
- Gomez-Marin, A., & Louis, M. (2012). Active sensation during orientation behavior in the *Drosophila* larva: More sense than luck. *Current Opinion in Neurobiology*, *22*(2), 208–215. <https://doi.org/10.1016/j.conb.2011.11.008>
- Göppert-Mayer, M. (1931). *Über Elementarakte mit zwei Quantumsprüngen* (pp. 273–294) [PhD thesis]. John Hopkins.

- Götz, K. G. (1968). Flight control in *Drosophila* by visual perception of motion. *Kybernetik*, 4(6), 199–208. <https://doi.org/10.1007/BF00272517>
- Gray, J. R., Pawlowski, V., & Willis, M. A. (2002). A method for recording behavior and multineuronal CNS activity from tethered insects flying in virtual space. *Journal of Neuroscience Methods*, 120(2), 211–223. [https://doi.org/10.1016/S0165-0270\(02\)00223-6](https://doi.org/10.1016/S0165-0270(02)00223-6)
- Grienberger, C., & Konnerth, A. (2012). Imaging Calcium in Neurons. *Neuron*, 73(5), 862–885. <https://doi.org/10.1016/j.neuron.2012.02.011>
- Guggiana-Nilo, D. A., & Engert, F. (2016). Properties of the Visible Light Phototaxis and UV Avoidance Behaviors in the Larval Zebrafish. *Frontiers in Behavioral Neuroscience*, 10(August), 1–10. <https://doi.org/10.3389/fnbeh.2016.00160>
- Haber Kern, H., Basnak, M. A., Ahanonu, B., Schauder, D., Cohen, J. D., Bolstad, M., Bruns, C., & Jayaraman, V. (2019). Visually Guided Behavior and Optogenetically Induced Learning in Head-Fixed Flies Exploring a Virtual Landscape. *Current Biology*, 29(10), 1647–1659.e8. <https://doi.org/10.1016/j.cub.2019.04.033>
- Harris, D. J., Buckingham, G., Wilson, M. R., & Vine, S. J. (2019). Virtually the same? How impaired sensory information in virtual reality may disrupt vision for action. *Experimental Brain Research*, 237(11), 2761–2766. <https://doi.org/10.1007/s00221-019-05642-8>
- Hartmann, S., Vogt, R., Kunze, J., Rauschert, A., Kuhnert, K. D., Wanzenböck, J., Lamatsch, D. K., & Witte, K. (2018). Zebrafish larvae show negative phototaxis to near-infrared light. *PLoS ONE*, 13(11), 1–16. <https://doi.org/10.1371/journal.pone.0207264>
- Harvey, C. D., Collman, F., Dombeck, D. A., & Tank, D. W. (2009). Intracellular dynamics of hippocampal place cells during virtual navigation. *Nature*, 461(7266), 941–946. <https://doi.org/10.1038/nature08499>
- Haug, M. F., Biehlmaier, O., Mueller, K. P., & Neuhauss, S. C. F. (2010). Visual acuity in larval zebrafish: Behavior and histology. *Frontiers in Zoology*, 7, 1–7. <https://doi.org/10.1186/1742-9994-7-8>
- Heisenberg, M., & Wolf, R. (1988). Reafferent control of optomotor yaw torque in *Drosophila melanogaster*. *J. Comp. Physiol.*, 163, 373–388.
- Heyers, D., Manns, M., Luksch, H., Güntürkün, O., & Mouritsen, H. (2007). A visual pathway links brain structures active during magnetic compass orientation in migratory birds. *PLoS ONE*, 2(9). <https://doi.org/10.1371/journal.pone.0000937>
- Higashijima, S. I., Masino, M. A., Mandel, G., & Fetcho, J. R. (2003). Imaging Neuronal Activity during Zebrafish Behavior with a Genetically Encoded Calcium

- Indicator. *Journal of Neurophysiology*, 90(6), 3986–3997. <https://doi.org/10.1152/jn.00576.2003>
- Hires, S. A., Tian, L., & Looger, L. L. (2008). Reporting neural activity with genetically encoded calcium indicators. *Brain Cell Biology*, 36(1-4), 69–86. <https://doi.org/10.1007/s11068-008-9029-4>
- Horstick, E. J., Bayleyen, Y., Sinclair, J. L., & Burgess, H. A. (2017). Search strategy is regulated by somatostatin signaling and deep brain photoreceptors in zebrafish. *BMC Biology*, 15(1), 1–16. <https://doi.org/10.1186/s12915-016-0346-2>
- Hölscher, C., Schnee, A., Dahmen, H., Setia, L., & Mallot, H. A. (2005). Rats are able to navigate in virtual environments. *Journal of Experimental Biology*, 208(3), 561–569. <https://doi.org/10.1242/jeb.01371>
- Hsiao, H. S. (1973). Flight paths of night-flying moths to light. *Journal of Insect Physiology*, 19(10), 1971–1976. [https://doi.org/10.1016/0022-1910\(73\)90191-1](https://doi.org/10.1016/0022-1910(73)90191-1)
- Huang, K. H., Ahrens, M. B., Dunn, T. W., & Engert, F. (2013). Spinal projection neurons control turning behaviors in zebrafish. *Current Biology*, 23(16), 1566–1573. <https://doi.org/10.1016/j.cub.2013.06.044>
- Huang, K. H., Rupprecht, P., Frank, T., Kawakami, K., Bouwmeester, T., & Friedrich, R. W. (2020). A virtual reality system to analyze neural activity and behavior in adult zebrafish. *Nature Methods*. <https://doi.org/10.1038/s41592-020-0759-2>
- Huisken, J., & Stainier, D. Y. R. (2007). Even fluorescence excitation by multidirectional selective plane illumination microscopy (mSPIM). *Optics Letters*, 32(17), 2608. <https://doi.org/10.1364/ol.32.002608>
- Huisken, J., Swoger, J., Del Bene, F., Wittbrodt, J., & Stelzer, E. H. K. (2004). Optical sectioning deep inside live embryos by selective plane illumination microscopy. *Science*, 305(5686), 1007–1009. <https://doi.org/10.1126/science.1100035>
- Izard, S. G., Juanes, J. A., Peñalvo, F. J. G., Estella, J. M. G., Ledesma, M. J. S., & Ruisoto, P. (2018). Virtual Reality as an Educational and Training Tool for Medicine. *Journal of Medical Systems*, 42–50. https://doi.org/10.1007/978-3-030-55374-6_26
- Jeffery, K. J. (2007). Integration of the Sensory Inputs to Place Cells: What, Where, Why, and How? *Hippocampus*, 17, 775–785. <https://doi.org/10.1002/hipo>
- Jesuthasan, S. (2012). Fear, anxiety, and control in the zebrafish. *Developmental Neurobiology*, 72(3), 395–403. <https://doi.org/10.1002/dneu.20873>
- Jékely, G. (2009). Evolution of phototaxis. *Philosophical Transactions of the Royal Society B: Biological Sciences*, 364(1531), 2795–2808. <https://doi.org/10.1098/rstb.2009.0072>

- Jiao, Z.-F., Shang, C.-F., Wang, Y.-F., Yang, Z., Yang, C., Li, F.-N., Xie, J.-Z., Pan, J.-W., Fu, L., & Du, J.-L. (2018). All-optical imaging and manipulation of whole-brain neuronal activities in behaving larval zebrafish. *Biomedical Optics Express*, *9*(12), 6154. <https://doi.org/10.1364/boe.9.006154>
- Johnson, R. E., Linderman, S., Panier, T., Wee, C. L., Song, E., Herrera, K. J., Miller, A., & Engert, F. (2020). Probabilistic Models of Larval Zebrafish Behavior: Structure on Many Scales. *Current Biology*, *30*(1), 672246. <https://doi.org/10.1016/672246>
- Jonas, E., & Kording, K. P. (2017). Could a Neuroscientist Understand a Microprocessor? *PLoS Computational Biology*, *13*(1), 1–24. <https://doi.org/10.1371/journal.pcbi.1005268>
- Jouary, A., Haudrechy, M., Candelier, R., & Sumbre, G. (2016). A 2D virtual reality system for visual goal-driven navigation in zebrafish larvae. *Scientific Reports*, *6*(March), 1–13. <https://doi.org/10.1038/srep34015>
- Jurisch-Yaksi, N., Yaksi, E., & Kizil, C. (2020). Radial glia in the zebrafish brain: Functional, structural, and physiological comparison with the mammalian glia. *Glia*, *April*, 1–20. <https://doi.org/10.1002/glia.23849>
- Kaiser, W., & Garrett, C. G. B. (1961). Two-photon excitation in CaF₂: Eu²⁺. *Physical Review Letters*, *7*(6), 229–231. <https://doi.org/10.1103/PhysRevLett.7.229>
- Kalueff, A. V., Gebhardt, M., Stewart, A. M., Cachat, J. M., Brimmer, M., Chawla, J. S., Craddock, C., Kyzar, E. J., Roth, A., Landsman, S., Gaikwad, S., Robinson, K., Baatrup, E., Tierney, K., Shamchuk, A., Norton, W., Miller, N., Nicolson, T., Braubach, O., ... Schneider, and the Zebrafish Neuros, H. (2013). Towards a Comprehensive Catalog of Zebrafish Behavior 1.0 and Beyond. *Zebrafish*, *10*(1), 70–86. <https://doi.org/10.1089/zeb.2012.0861>
- Karpenko, S., Wolf, S., Lafaye, J., Le Goc, G., Panier, T., Bormuth, V., Candelier, R., & Debrégeas, G. (2020). From behavior to circuit modeling of light-seeking navigation in zebrafish larvae. *eLife*, *9*, 1–24. <https://doi.org/10.7554/eLife.52882>
- Keller, P. J., Schmidt, A. D., Wittbrodt, J., & Stelzer, E. H. K. (2008). *Reconstruction of Zebrafish Early Light Sheet Microscopy*. *322*(November), 1065–1069.
- Kim, D. H., Kim, J., Marques, J. C., Grama, A., Hildebrand, D. G. C., Gu, W., Li, J. M., & Robson, D. N. (2017). Pan-neuronal calcium imaging with cellular resolution in freely swimming zebrafish. *Nature Methods*, *14*(11), 1107–1114. <https://doi.org/10.1038/nmeth.4429>
- Kist, A. M., & Portugues, R. (2019). Optomotor Swimming in Larval Zebrafish Is Driven by Global Whole-Field Visual Motion and Local Light-Dark Transitions. *Cell Reports*, *29*(3), 659–670.e3. <https://doi.org/10.1016/j.celrep.2019.09.024>

- Krakauer, J. W., Ghazanfar, A. A., Gomez-Marin, A., MacIver, M. A., & Poeppel, D. (2017). Neuroscience Needs Behavior: Correcting a Reductionist Bias. *Neuron*, *93*(3), 480–490. <https://doi.org/10.1016/j.neuron.2016.12.041>
- Leung, L. C., Wang, G. X., Madelaine, R., Skariah, G., Kawakami, K., Deisseroth, K., Urban, A. E., & Mourrain, P. (2019). Neural signatures of sleep in zebrafish. *Nature*, *571*(7764), 198–204. <https://doi.org/10.1038/s41586-019-1336-7>
- Lin, M. Z., & Schnitzer, M. J. (2016). Genetically encoded indicators of neuronal activity. *Nature Neuroscience*, *19*(9). <https://doi.org/10.1038/nn.4359>
- Lin, Q., & Jesuthasan, S. (2017). Masking of a circadian behavior in larval zebrafish involves the thalamo-habenula pathway. *Scientific Reports*, *7*(1), 1–11. <https://doi.org/10.1038/s41598-017-04205-7>
- Lister, J. A., Robertson, C. P., Lepage, T., Johnson, S. L., & Raible, D. W. (1999). Nacre Encodes a Zebrafish Microphthalmia-Related Protein That Regulates Neural-Crest-Derived Pigment Cell Fate. *Development*, *126*(17), 3757–3767.
- Liu, T. L., Upadhyayula, S., Milkie, D. E., Singh, V., Wang, K., Swinburne, I. A., Mosaliganti, K. R., Collins, Z. M., Hiscock, T. W., Shea, J., Kohrman, A. Q., Medwig, T. N., Dambournet, D., Forster, R., Cunniff, B., Ruan, Y., Yashiro, H., Scholpp, S., Meyerowitz, E. M., ... Betzig, E. (2018). Observing the cell in its native state: Imaging subcellular dynamics in multicellular organisms. *Science*, *360*(6386). <https://doi.org/10.1126/science.aag1392>
- Liu, Y., Carmer, R., Zhang, G., Venkatraman, P., Brown, S. A., Pang, C. P., Zhang, M., Ma, P., & Leung, Y. F. (2015). Statistical analysis of zebrafish locomotor response. *PLoS ONE*, *10*(10), 1–25. <https://doi.org/10.1371/journal.pone.0139521>
- Lungarella, M., & Sporns, O. (2005). Information self-structuring: Key principle for learning and development. *Proceedings of 2005 4th IEEE International Conference on Development and Learning, 2005*, 25–30. <https://doi.org/10.1109/DEVLRN.2005.1490938>
- Ma, M., Ramirez, A. D., Wang, T., Roberts, R. L., Harmon, K. E., Schoppik, D., Sharma, A., Kuang, C., Goei, S. L., Gagnon, J. A., Zimmerman, S., Tsai, S. Q., Reyon, D., Keith Joung, J., Aksay, E. R. F., Schier, A. F., & Albert Pan, Y. (2020). Zebrafish *dscaml1* deficiency impairs retinal patterning and oculomotor function. *Journal of Neuroscience*, *40*(1), 143–158. <https://doi.org/10.1523/JNEUROSCI.1783-19.2019>
- Macnab, R. M., & Koshland, D. E. (1972). The Gradient-Sensing Mechanism in Bacterial Chemotaxis. *Proceedings of the National Academy of Sciences*, *69*(9), 2509–2512. <https://doi.org/10.1073/pnas.69.9.2509>
- Maimon, G., Straw, A. D., & Dickinson, M. H. (2010). Active flight increases the gain of visual motion processing in *Drosophila*. *Nature Neuroscience*, *13*(3), 393–399.

<https://doi.org/10.1038/nn.2492>

- Major, G., Baker, R., Aksay, E., Mensh, B., Seung, H. S., & Tank, D. W. (2004). Plasticity and tuning by visual feedback of the stability of a neural integrator. *Proceedings of the National Academy of Sciences of the United States of America*, *101*(20), 7739–7744. <https://doi.org/10.1073/pnas.0401970101>
- Marques, J. C., Lackner, S., Félix, R., & Orger, M. B. (2018). Structure of the Zebrafish Locomotor Repertoire Revealed with Unsupervised Behavioral Clustering. *Current Biology*, 181–195. <https://doi.org/10.1016/j.cub.2017.12.002>
- Marques, J. C., Li, M., Schaak, D., Robson, D. N., & Li, J. M. (2020). Internal state dynamics shape brainwide activity and foraging behaviour. *Nature*, *577*(7789), 239–243. <https://doi.org/10.1038/s41586-019-1858-z>
- Marr, D. (1982). *Vision*.
- Martinez-Conde, S., & Macknik, S. L. (2008). Fixational eye movements across vertebrates: Comparative dynamics, physiology, and perception. *Journal of Vision*, *8*(14), 1–16. <https://doi.org/10.1167/8.14.28>
- Maximino, C., Brito, T. M. de, Colmanetti, R., Pontes, A. A. A., Castro, H. M. de, Lacerda, R. I. T. de, Morato, S., & Gouveia, A. (2010). Parametric analyses of anxiety in zebrafish scototaxis. *Behavioural Brain Research*, *210*(1), 1–7. <https://doi.org/10.1016/j.bbr.2010.01.031>
- McClenahan, P., Troup, M., & Scott, E. K. (2012). Fin-tail coordination during escape and predatory behavior in larval zebrafish. *PLoS ONE*, *7*(2), 1–11. <https://doi.org/10.1371/journal.pone.0032295>
- Mearns, D. S., Donovan, J. C., Fernandes, A. M., Semmelhack, J. L., & Baier, H. (2020). Deconstructing Hunting Behavior Reveals a Tightly Coupled Stimulus-Response Loop. *Current Biology*, *30*(1), 54–69.e9. <https://doi.org/10.1016/j.cub.2019.11.022>
- Mello, B. A., & Tu, Y. (2007). Effects of adaptation in maintaining high sensitivity over a wide range of backgrounds for *Escherichia coli* chemotaxis. *Biophysical Journal*, *92*(7), 2329–2337. <https://doi.org/10.1529/biophysj.106.097808>
- Migault, G., Plas, T. L. van der, Trentesaux, H., Panier, T., Candelier, R., Proville, R., Englitz, B., Debrégeas, G., & Bormuth, V. (2018). Whole-Brain Calcium Imaging during Physiological Vestibular Stimulation in Larval Zebrafish. *Current Biology*, *28*(23), 3723–3735.e6. <https://doi.org/10.1016/j.cub.2018.10.017>
- Minderer, M., Harvey, C. D., Donato, F., & Moser, E. I. (2016). Neuroscience: Virtual reality explored. *Nature*, *533*, 324–325. <https://doi.org/10.1038/nature17899>
- Miri, A., Daie, K., Burdine, R. D., Aksay, E., & Tank, D. W. (2011). Regression-Based Identification of Behavior-Encoding Neurons During Large-Scale Optical Imaging

- of Neural Activity at Cellular Resolution. *Journal of Neurophysiology*, 105(2), 964–980. <https://doi.org/10.1152/jn.00702.2010>
- Mon-Williams, M., Warm, J. P., & Rushton, S. (1993). Binocular vision in a virtual world: visual deficits following the wearing of a head-mounted display. *Ophthalmic and Physiological Optics*, 13(4), 387–391. <https://doi.org/10.1111/j.1475-1313.1993.tb00496.x>
- Mouritsen, H. (2018). Long-distance navigation and magnetoreception in migratory animals. *Nature*, 558(7708), 50–59. <https://doi.org/10.1038/s41586-018-0176-1>
- Mu, Y., Bennett, D. V., Rubinov, M., Narayan, S., Yang, C.-T., Tanimoto, M., Mensh, B. D., Looger, L. L., & Ahrens, M. B. (2019). Glia Accumulate Evidence that Actions Are Futile and Suppress Unsuccessful Behavior. *Cell*, 1–17. <https://doi.org/10.1016/j.cell.2019.05.050>
- Muto, A., Ohkura, M., Kotani, T., Higashijima, S. I., Nakai, J., & Kawakami, K. (2011). Genetic visualization with an improved GCaMP calcium indicator reveals spatiotemporal activation of the spinal motor neurons in zebrafish. *Proceedings of the National Academy of Sciences of the United States of America*, 108(13), 5425–5430. <https://doi.org/10.1073/pnas.1000887108>
- Nakai, J., Ohkura, M., & Imoto, K. (2001). A high signal-to-noise Ca²⁺ probe composed of a single green fluorescent protein. *Nature Biotechnology*, 19, 137–141. [https://doi.org/10.1016/s0091-679x\(02\)70014-9](https://doi.org/10.1016/s0091-679x(02)70014-9)
- Nakazawa, H., & Murphy, T. H. (1999). Activation of nuclear calcium dynamics by synaptic stimulation in cultured cortical neurons. *Journal of Neurochemistry*, 73(3), 1075–1083. <https://doi.org/10.1046/j.1471-4159.1999.0731075.x>
- Naumann, E. A., Fitzgerald, J. E., Dunn, T. W., Rihel, J., Sompolinsky, H., & Engert, F. (2016). From Whole-Brain Data to Functional Circuit Models: The Zebrafish Optomotor Response. *Cell*, 167(4), 947–960.e20. <https://doi.org/10.1016/j.cell.2016.10.019>
- Neuhauss, S. C. F. (2010). *Zebrafish vision* (Vol. 29, pp. 81–122). Elsevier. [https://doi.org/10.1016/S1546-5098\(10\)02903-1](https://doi.org/10.1016/S1546-5098(10)02903-1)
- Niell, C. M., & Stryker, M. P. (2010). Modulation of Visual Responses by Behavioral State in Mouse Visual Cortex. *Neuron*, 65(4), 472–479. <https://doi.org/10.1016/j.neuron.2010.01.033>
- Nilsson, D. E. (2009). The evolution of eyes and visually guided behaviour. *Philosophical Transactions of the Royal Society B: Biological Sciences*, 364(1531), 2833–2847. <https://doi.org/10.1098/rstb.2009.0083>
- O’Keefe, J., Dostrovsky, J., & J. O’Keefe, J. D. (1971). The hippocampus as a spatial map . Preliminary evidence from unit activity in the freely-moving rat. *Brain*

- Research*, 34(1), 171–175. <http://www.ncbi.nlm.nih.gov/pubmed/5124915>
- Oliveira, J., Silveira, M., Chacon, D., & Luchiani, A. (2015). The Zebrafish World of Colors and Shapes: Preference and Discrimination. *Zebrafish*, 12(2), 166–173. <https://doi.org/10.1089/zeb.2014.1019>
- Orger, M. B. (2016). The Cellular Organization of Zebrafish Visuomotor Circuits. *Current Biology*, 26(9), R377–R385. <https://doi.org/10.1016/j.cub.2016.03.054>
- Orger, M. B., & Baier, H. (2005). Channeling of red and green cone inputs to the zebrafish optomotor response. *Visual Neuroscience*, 22(3), 275–281. <https://doi.org/10.1017/s0952523805223039>
- Orger, M. B., Kampff, A. R., Severi, K. E., Bollmann, J. H., & Engert, F. (2008). Control of visually guided behavior by distinct populations of spinal projection neurons. *Nature Neuroscience*, 11(3), 327–333. <https://doi.org/10.1038/nn2048>
- Orger, M. B., Smear, M. C., Anstis, S. M., & Baier, H. (2000). Perception of Fourier and non-Fourier motion by larval zebrafish. *Nature Neuroscience*, 3(11), 1128–1133. <https://doi.org/10.1038/80649>
- Pachitariu, M., Stringer, C., & Harris, K. D. (2018). Robustness of spike deconvolution for neuronal calcium imaging. *Journal of Neuroscience*, 38(37), 7976–7985. <https://doi.org/10.1523/JNEUROSCI.3339-17.2018>
- Pahl, M., Zhu, H., Tautz, J., & Zhang, S. (2011). Large scale homing in honeybees. *PLoS ONE*, 6(5), 1–7. <https://doi.org/10.1371/journal.pone.0019669>
- Panier, T., Romano, S. A., Olive, R., Pietri, T., Sumbre, G., Candelier, R., & Debrégeas, G. (2013). Fast functional imaging of multiple brain regions in intact zebrafish larvae using Selective Plane Illumination Microscopy. *Frontiers in Neural Circuits*, 7(April), 1–11. <https://doi.org/10.3389/fncir.2013.00065>
- Pfeifer, R., Lungarella, M., & Iida, F. (2007). Self-organization, embodiment, and biologically inspired robotics. *Science*, 318(5853), 1088–1093. <https://doi.org/10.1126/science.1145803>
- Planchon, T. A., Gao, L., Milkie, D. E., Davidson, M. W., Galbraith, J. A., Galbraith, C. G., & Betzig, E. (2011). Rapid three-dimensional isotropic imaging of living cells using Bessel beam plane illumination. *Nature Methods*, 8(5), 417–423. <https://doi.org/10.1038/nmeth.1586>
- Portugues, R., & Engert, F. (2011). Adaptive locomotor behavior in larval zebrafish. *Frontiers in Systems Neuroscience*, 5(AUGUST 2011), 1–11. <https://doi.org/10.3389/fnsys.2011.00072>
- Portugues, R., Feierstein, C. E., Engert, F., & Orger, M. B. (2014). Whole-brain activity maps reveal stereotyped, distributed networks for visuomotor behavior. *Neuron*, 81(6), 1328–1343. <https://doi.org/10.1016/j.neuron.2014.01.019>

- Privat, M., Romano, S. A., Pietri, T., Jouary, A., Boulanger-Weill, J., Elbaz, N., Duchemin, A., Soares, D., & Sumbre, G. (2019). Sensorimotor Transformations in the Zebrafish Auditory System. *Current Biology*, *29*(23), 4010–4023.e4. <https://doi.org/10.1016/j.cub.2019.10.020>
- Randlett, O., Wee, C. L., Naumann, E. A., Nnaemeka, O., Schoppik, D., Fitzgerald, J. E., Portugues, R., Lacoste, A. M. B., Riegler, C., Engert, F., & Schier, A. F. (2015). Whole-brain activity mapping onto a zebrafish brain atlas. *Nature Methods*, *12*(11), 1039–1046. <https://doi.org/10.1038/nmeth.3581>
- Raymond, P. A., Barthel, L. K., & Curran, G. A. (1995). Developmental patterning of rod and cone photoreceptors in embryonic zebrafish. *Journal of Comparative Neurology*, *359*(4), 537–550. <https://doi.org/10.1002/cne.903590403>
- Regan, C. (1995). An investigation into nausea and other side-effects of head-coupled immersive virtual reality. *Virtual Reality*, *1*(1), 17–31. <https://doi.org/10.1007/BF02009710>
- Renz, M. (2013). Fluorescence microscopy-A historical and technical perspective. *Cytometry Part A*, *83*(9), 767–779. <https://doi.org/10.1002/cyto.a.22295>
- Rinner, O., Rick, J. M., & Neuhauss, S. C. F. (2005). Contrast sensitivity, spatial and temporal tuning of the larval zebrafish optokinetic response. *Investigative Ophthalmology and Visual Science*, *46*(1), 137–142. <https://doi.org/10.1167/iovs.04-0682>
- Risner, M. L., Lemerise, E., Vukmanic, E. V., & Moore, A. (2006). Behavioral spectral sensitivity of the zebrafish (*Danio rerio*). *Vision Research*, *46*(17), 2625–2635. <https://doi.org/10.1016/j.visres.2005.12.014>
- Riva, G., Wiederhold, B. K., & Mantovani, F. (2019). Neuroscience of Virtual Reality: From Virtual Exposure to Embodied Medicine. *Cyberpsychology, Behavior, and Social Networking*, *22*(1), 82–96. <https://doi.org/10.1089/cyber.2017.29099.gri>
- Robson, D. N. (2013). *Thermal navigation in larval zebrafish* (p. 106) [PhD thesis].
- Roeser, T., & Baier, H. (2003). Visuomotor behaviors in larval zebrafish after GFP-guided laser ablation of the optic tectum. *Journal of Neuroscience*, *23*(9), 3726–3734. <https://doi.org/10.1523/jneurosci.23-09-03726.2003>
- Saleem, A. B., Ayaz, A. I., Jeffery, K. J., Harris, K. D., & Carandini, M. (2013). Integration of visual motion and locomotion in mouse visual cortex. *Nature Neuroscience*, *16*(12), 1864–1869. <https://doi.org/10.1038/nn.3567>
- Saszik, S., & Bilotta, J. (1999). ERG assessment of zebrafish retinal development. *Visual Neuroscience*, *16*(5), 881–888. <https://doi.org/10.1017/S0952523899165076>
- Scholz, M., Dinner, A. R., Levine, E., & Biron, D. (2017). Stochastic feeding dynamics arise from the need for information and energy. *Proceedings of the National*

- Academy of Sciences*, 114(35), 9261–9266. <https://doi.org/10.1073/pnas.1703958114>
- Schoonheim, P. J., Arrenberg, A. B., Del Bene, F., & Baier, H. (2010). Optogenetic Localization and Genetic Perturbation of Saccade-Generating Neurons in Zebrafish. *Journal of Neuroscience*, 30(20), 7111–7120. <https://doi.org/10.1523/JNEUROSCI.15193-09.2010>
- Serra, E. L., Medalha, C. C., & Mattioli, R. (1999). Natural preference of zebrafish (*Danio rerio*) for a dark environment. *Brazilian Journal of Medical and Biological Research*, 32(12), 1551–1553. <https://doi.org/10.1590/S0100-879X1999001200016>
- Shepherd, G. M. (2015). *Foundations of the neuron doctrine*.
- Shiozaki, H. M., Ohta, K., & Kazama, H. (2020). A Multi-regional Network Encoding Heading and Steering Maneuvers in *Drosophila*. *Neuron*, 106(1), 126–141.e5. <https://doi.org/10.1016/j.neuron.2020.01.009>
- Sims, D. W., Humphries, N. E., Hu, N., Medan, V., & Berni, J. (2019). Optimal searching behaviour generated intrinsically by the central pattern generator for locomotion. *eLife*, 8, 1–31. <https://doi.org/10.7554/eLife.50316>
- Spillmann, L. (2014). Receptive fields of visual neurons: The early years. *Perception*, 43(11), 1145–1176. <https://doi.org/10.1068/p7721>
- Stewart, A. M., Braubach, O., Spitsbergen, J., Gerlai, R., & Kalueff, A. V. (2014). Zebrafish models for translational neuroscience research: from tank to bedside. *Trends in Neurosciences*. <https://doi.org/10.1016/j.tins.2014.02.011>
- Stowers, J. R., Hofbauer, M., Bastien, R., Griessner, J., Higgins, P., Farooqui, S., Fischer, R. M., Nowikovsky, K., Haubensak, W., Couzin, I. D., Tessmar-Raible, K., & Straw, A. D. (2017). Virtual reality for freely moving animals. *Nature Methods*, 14(10), 995–1002. <https://doi.org/10.1038/nmeth.4399>
- Theis, L., Berens, P., Froudarakis, E., Reimer, J., Román Rosón, M., Baden, T., Euler, T., Tolias, A. S., & Bethge, M. (2016). Benchmarking Spike Rate Inference in Population Calcium Imaging. *Neuron*, 90(3), 471–482. <https://doi.org/10.1016/j.neuron.2016.04.014>
- Thurley, K., & Ayaz, A. (2017). Virtual reality systems for rodents. *Current Zoology*, 63(1), 109–119. <https://doi.org/10.1093/cz/zow070>
- Tsai, K.-T., & Chou, Y.-H. (2019). Random Walk Revisited: Quantification and Comparative Analysis of *Drosophila* Walking Trajectories. *iScience*, 19, 1145–1159. <https://doi.org/10.1016/j.isci.2019.08.054>
- Tubiana, J., Wolf, S., & Debrégeas, G. (2017). *Blind sparse deconvolution for inferring spike trains from fluorescence recordings*. 1–30. <http://biorxiv.org/lookup/doi/10.1101/156364> <https://pubmed.ncbi.nlm.nih.gov/3111101/>

- Venkatraman, P., Mills-Henry, I., Ramaswamy, K., Pascuzzi, P., Hassan, M., Zhang, J., Zhang, X., Ma, P., Dowling, J., Pang, C. P., Zhang, M., & Leung, Y. F. (2020). Rods contribute to Visual Behaviour in Larval Zebrafish (In Revision). *Investigative Ophthalmology & Visual Science*, 10–12.
- Vishniakou, I., Plöger, P. G., & Seelig, J. D. (2019). Virtual reality for animal navigation with camera-based optical flow tracking. *Journal of Neuroscience Methods*, 327(August), 108403. <https://doi.org/10.1016/j.jneumeth.2019.108403>
- Viswanathan, G. M., Buldyrev, S. V., Havlin, S., Da Luz, M. G. E., Raposo, E. P., & Stanley, H. E. (1999). Optimizing the success of random searches. *Nature*, 401(6756), 911–914. <https://doi.org/10.1038/44831>
- Vladimirov, N., Mu, Y., Kawashima, T., Bennett, D. V., Yang, C. T., Looger, L. L., Keller, P. J., Freeman, J., & Ahrens, M. B. (2014). Light-sheet functional imaging in fictively behaving zebrafish. *Nature Methods*, 11(9), 883–884. <https://doi.org/10.1038/nmeth.3040>
- Vogelstein, J. T., Packer, A. M., Machado, T. A., Sippy, T., Babadi, B., Yuste, R., & Paninski, L. (2010). Fast nonnegative deconvolution for spike train inference from population calcium imaging. *Journal of Neurophysiology*, 104(6), 3691–3704. <https://doi.org/10.1152/jn.01073.2009>
- Wang, K., Hinz, J., Haikala, V., Reiff, D. F., & Arrenberg, A. B. (2019). Selective processing of all rotational and translational optic flow directions in the zebrafish pretectum and tectum. *BMC Biology*, 17(1), 1–18. <https://doi.org/10.1186/s12915-019-0648-2>
- Wiener, J., Shettleworth, S., Bingman, V., Cheng, K., Healy, S., Jacobs, L., Mallot, H., Menzel, R., & Newcombe, N. (2010). *Animal Navigation – A Synthesis*. 1–33. <https://pdfs.semanticscholar.org/e6c4/b58604fc26ea31af79f6dbd2063902135a05.pdf>
- Wiltschko, R., & Wiltschko, W. (2019). Magnetoreception in birds. *Journal of the Royal Society Interface*, 16(158), 0–3. <https://doi.org/10.1098/rsif.2019.0295>
- Wolf, S., Dubreuil, A. M., Bertoni, T., Böhm, U. L., Bormuth, V., Candelier, R., Karpenko, S., Hildebrand, D. G. C., Bianco, I. H., Monasson, R., & Debrégeas, G. (2017). Sensorimotor computation underlying phototaxis in zebrafish. *Nature Communications*, 8(1), 1–12. <https://doi.org/10.1038/s41467-017-00310-3>
- Wolf, S., Supatto, W., Debrégeas, G., Mahou, P., Kruglik, S. G., Sintes, J. M., Beaupaire, E., & Candelier, R. (2015). Whole-brain functional imaging with two-photon light-sheet microscopy. *Nature Methods*, 12(5), 379–380. <https://doi.org/10.1038/nmeth.3371>
- Wolpert, D. M., Ghahramani, Z., & Jordan, M. 1. (1995). An internal model for sensorimotor integration - Wolpert et al. (1995).pdf. *Science*, 269, 1880–1882. <http://dx.doi.org/10.1038/nphys2178>

- Wright, P. W., Brier, L. M., Bauer, A. Q., Baxter, G. A., Kraft, A. W., Reisman, M. D., Bice, A. R., Snyder, A. Z., Lee, J. M., & Culver, J. P. (2017). Functional connectivity structure of cortical calcium dynamics in anesthetized and awake mice. *PLoS ONE*, *12*(10), 1–27. <https://doi.org/10.1371/journal.pone.0185759>
- Yang, H. H., & St-Pierre, F. (2016). Genetically encoded voltage indicators: Opportunities and challenges. *Journal of Neuroscience*, *36*(39), 9977–9989. <https://doi.org/10.1523/JNEUROSCI.1095-16.2016>
- Yuan, J., Fahrner, K. A., Turner, L., & Berg, H. C. (2010). Asymmetry in the clockwise and counterclockwise rotation of the bacterial flagellar motor. *Proceedings of the National Academy of Sciences*, *107*(29), 12846–12849. <https://doi.org/10.1073/pnas.1007333107>
- Zeil, J., Boeddeker, N., & Hemmi, J. M. (2008). Vision and the organization of behaviour. *Current Biology*, *18*(8), 320–323. <https://doi.org/10.1016/j.cub.2008.02.017>
- Zhang, B. bing, Yao, Y. yuan, Zhang, H. fei, Kawakami, K., & Du, J. lin. (2017). Left Habenula Mediates Light-Preference Behavior in Zebrafish via an Asymmetrical Visual Pathway. *Neuron*, *93*(4), 914–928.e4. <https://doi.org/10.1016/j.neuron.2017.01.011>
- Zhou, M., Bear, J., Roberts, P. A., Janiak, F. K., Semmelhack, J., Yoshimatsu, T., & Baden, T. (2020). Zebrafish Retinal Ganglion Cells Asymmetrically Encode Spectral and Temporal Information across Visual Space. *Current Biology*, *30*(15), 2927–2942.e7. <https://doi.org/10.1016/j.cub.2020.05.055>
- Zimmermann, M. J. Y., Nevala, N. E., Yoshimatsu, T., Osorio, D., Nilsson, D. E., Berens, P., & Baden, T. (2018). Zebrafish Differentially Process Color across Visual Space to Match Natural Scenes. *Current Biology*, *28*(13), 2018–2032.e5. <https://doi.org/10.1016/j.cub.2018.04.075>

Afin de survivre et de se développer, les organismes motiles utilisent les signaux sensoriels de leur environnement pour naviguer vers les environnements où ils sont les plus susceptibles d'éviter les prédateurs, trouver de la nourriture ou rencontrer des partenaires. Cette navigation exige que la perception sensorielle et l'action motrice soient coordonnées au sein d'une même boucle de rétroaction. Celle-ci est mise en œuvre chez nombre d'organismes - des bactéries aux nématodes, en passant par les insectes, ainsi que chez les vertébrés.

Comprendre la relation entre comportement à l'échelle de l'organisme et dynamique des circuits à l'échelle d'un cerveau chez les vertébrés est un défi central dans les neurosciences, auquel ce travail vise à contribuer. La larve de poisson-zèbre, ayant une accessibilité unique pour l'imagerie fonctionnelle à l'échelle du cerveau entier ainsi qu'une large palette de comportements innés, est un organisme idéal pour aborder ce sujet. Je m'intéresse plus particulièrement à la navigation biaisée par la lumière -aussi appelée phototaxie - chez la larve de poisson-zèbre : j'étudie comment une telle tâche sensorimotrice est mise en œuvre sur le plan comportemental, et quelle est la dynamique du réseau neuronal sous-jacent.

La première section (i) de cette thèse vise à caractériser la façon dont les séquences de stimulation motrice et visuelle régissent la sélection d'événements de nage discrets qui font la navigation du poisson, en présence d'une source lumineuse distante. En utilisant une expérience de réalité virtuelle, deux stratégies différentes de phototaxie sont étudiées : l'une basée sur le contraste spatial perçu, l'autre sur le changement d'intensité lumineuse totale perçu lors d'un événement de nage. Les séquences de nage sont décrites à l'aide d'un modèle de chaînes de Markov qui prédit quantitativement la distribution stationnaire de l'orientation du poisson sous un profil d'illumination donné.

Une deuxième partie (ii) se concentre sur la transposition de l'expérience de phototaxie développée dans la section (i) d'un animal en nage libre à un animal partiellement immobilisé. Le suivi des mouvements de la queue permet de calculer une orientation virtuelle, utilisée pour mettre à jour l'environnement visuel. Cette approche permet d'émuler une navigation virtuelle en présence d'une source de lumière distante.

La dernière partie du projet (iii) se concentre sur le circuit neuronal qui sous-tend ce comportement. Spécifiquement un circuit nommé ARTR, connu pour être impliqué dans la sélection de l'orientation à chaque mouvement de nage. La technique développée dans la section (ii) est utilisée en combinaison avec un microscope à feuille de lumière 2 photons, permettant d'interroger expérimentalement les circuits d'intérêt, en utilisant des stimuli visuels simples, soit délivrés lors d'un mouvement de la queue, soit de manière aléatoire. Cela permet de démêler les contributions du stimulus visuel et de l'efférence motrice.

Dans son ensemble, cette contribution pourrait permettre de mieux comprendre comment un stimulus peut biaiser la dynamique neurale interne d'un animal qui navigue, afin de déclencher une réponse appropriée à changement de l'environnement abrupt.

MOTS CLÉS

processus sensorimoteur, rétroaction, phototaxie, poisson zèbre, microscopie par nappe laser, 2-photon

ABSTRACT

In order to survive and thrive, motile organisms use sensory cues to navigate towards environments where they are most likely to avoid predators, obtain food or find mates. This sensory-guided navigation requires sensory perception and motor action to be coordinated in a feedback loop which is implemented by number of organisms - ranging from bacteria to nematodes or insects, and also by vertebrates.

Bridging brain-scale circuit dynamics and organism-scale behaviour in a model vertebrate is a central challenge in neuroscience, to which this work aims to contribute. Zebrafish larva, for its unique accessibility to brain-wide functional imaging and wide display of innate behaviours is an ideal organism to tackle this topic. I specifically focus on light-seeking navigation of larval zebrafish: I investigate how such a sensorimotor task is behaviourally implemented, and what the underlying neural dynamics are.

The first section (i) of this thesis is aimed at the characterisation of how motor and visual stimulation sequences govern the selection of discrete swim-bout events that sub-serve the fish navigation in the presence and absence of a distant light source. Using a virtual reality assay, two different light-seeking strategies are tested: either based on spatial contrast or on global intensity modulation according to the fish's body orientation. The swim bout sequences are described using a comprehensive Markov-chain model of navigation that quantitatively predicts the stationary distribution of the fish's orientation under any given illumination profile.

A second part (ii) focuses on the transposition of the virtual assay developed in section (i) from a freely swimming onto a partially tethered animal. Recording its eye and tail movements in order to compute a virtual orientation and thus updating the visual environment enables the emulation of a navigation with respect to a distant light source, using spatial contrast cues.

And the final part (iii) targets the neural circuit that sub-serves this behaviour. The behavioural description of section (i) is mapped on a neuronal model of the ARTR, a small neural circuit involved in the orientation-selection of swim bouts, which can capture the statistics of both spontaneous and contrast-driven navigation. Using the assay developed in section (ii) added onto a 2-photon light-sheet microscope, this neural circuit is experimentally interrogated using illumination changes upon an attempted swim bout or uncorrelated from a swim event. This enables to disentangle the contributions of the visual stimulus and motor efference in biasing global neural dynamics.

All in all, this work might participate to a better understanding of how a stimulus may bias the internal neural dynamics of a navigating animal in order to trigger an appropriate response to an acute sensible environmental fluctuation.

KEYWORDS

sensorimotor process, closed-loop, phototaxis, zebrafish larva, light-sheet microscopy, 2-photon